NASA/CR-1999-208725

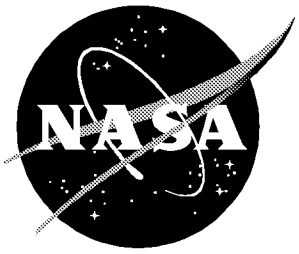

Analysis of Wind Tunnel Oscillatory Data of the X-31A Aircraft

Mark S. Smith
The George Washington University
Joint Institute for Advancement of Flight Sciences
Langley Research Center, Hampton, Virginia

February 1999

The NASA STI Program Office . . . in Profile

Since its founding, NASA has been dedicated to the advancement of aeronautics and space science. The NASA Scientific and Technical Information (STI) Program Office plays a key part in helping NASA maintain this important role.

The NASA STI Program Office is operated by Langley Research Center, the lead center for NASA's scientific and technical information. The NASA STI Program Office provides access to the NASA STI Database, the largest collection of aeronautical and space science STI in the world. The Program Office is also NASA's institutional mechanism for disseminating the results of its research and development activities. These results are published by NASA in the NASA STI Report Series, which includes the following report types:

- TECHNICAL PUBLICATION. Reports of completed research or a major significant phase of research that present the results of NASA programs and include extensive data or theoretical analysis. Includes compilations of significant scientific and technical data and information deemed to be of continuing reference value. NASA counterpart or peer-reviewed formal professional papers, but having less stringent limitations on manuscript length and extent of graphic presentations.

- TECHNICAL MEMORANDUM. Scientific and technical findings that are preliminary or of specialized interest, e.g., quick release reports, working papers, and bibliographies that contain minimal annotation. Does not contain extensive analysis.

- CONTRACTOR REPORT. Scientific and technical findings by NASA-sponsored contractors and grantees.

- CONFERENCE PUBLICATION. Collected papers from scientific and technical conferences, symposia, seminars, or other meetings sponsored or co-sponsored by NASA.

- SPECIAL PUBLICATION. Scientific, technical, or historical information from NASA programs, projects, and missions, often concerned with subjects having substantial public interest.

- TECHNICAL TRANSLATION. English-language translations of foreign scientific and technical material pertinent to NASA's mission.

Specialized services that complement the STI Program Office's diverse offerings include creating custom thesauri, building customized databases, organizing and publishing research results . . . even providing videos.

For more information about the NASA STI Program Office, see the following:

- Access the NASA STI Program Home Page at *http://www.sti.nasa.gov*

- Email your question via the Internet to help@sti.nasa.gov

- Fax your question to the NASA STI Help Desk at (301) 621-0134

- Telephone the NASA STI Help Desk at (301) 621-0390

- Write to:
  NASA STI Help Desk
  NASA Center for AeroSpace Information
  7121 Standard Drive
  Hanover, MD 21076-1320

NASA/CR-1999-208725

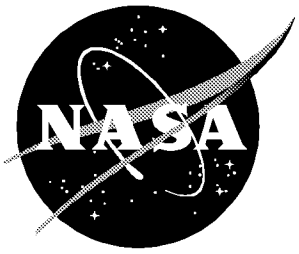

Analysis of Wind Tunnel Oscillatory Data of the X-31A Aircraft

Mark S. Smith
The George Washington University
Joint Institute for Advancement of Flight Sciences
Langley Research Center, Hampton, Virginia

National Aeronautics and
Space Administration

Langley Research Center
Hampton, Virginia 23681-2199

Prepared for Langley Research Center
under Cooperative Agreement NCC1-24

February 1999

Available from:

NASA Center for AeroSpace Information (CASI)
7121 Standard Drive
Hanover, MD 21076-1320
(301) 621-0390

National Technical Information Service (NTIS)
5285 Port Royal Road
Springfield, VA 22161-2171
(703) 605-6000

ABSTRACT

Wind tunnel oscillatory tests in pitch, roll, and yaw were performed on a 19%-scale model of the X-31A aircraft. These tests were used to study the aerodynamic characteristics of the X-31 in response to harmonic oscillations at six frequencies. In-phase and out-of-phase components of the aerodynamic coefficients were obtained over a range of angles of attack from 0° to 90°. To account for the effect of frequency on the data, mathematical models with unsteady terms were formulated by use of two different indicial functions. Data from a reduced set of frequencies were used to estimate model parameters, including steady-state static and dynamic stability derivatives. Both models showed good prediction capability and the ability to accurately fit the measured data. Estimated static stability derivatives compared well with those obtained from static wind tunnel tests. The roll and yaw rate derivative estimates were compared with rotary-balance wind tunnel data and theoretical predictions. The estimates and theoretical predictions were in agreement at small angles of attack. The rotary-balance data showed, in general, acceptable agreement with the steady-state derivative estimates.

ACKNOWLEDGMENTS

The author would like to thank everyone at NASA Langley Research Center that made this thesis possible, especially those who were involved in gathering the data used in this study, and those whose work laid the foundation that it is built on. In particular, thanks go to Mark Croom, for his work in obtaining the data, as well as for his assistance. Also, my thanks to Dr. Vladislav Klein, who served as my academic advisor. I would also like to thank Bihrle Applied Research for supplying the rotary-balance data, and Sue Grafton for allowing me to commandeer a large portion of her office to do my work.

TABLE OF CONTENTS

LIST OF FIGURES

LIST OF TABLES

LIST OF SYMBOLS

a,b_1	indicial function parameters
b	wingspan, ft
$\bar{c}$	wing mean aerodynamic chord, ft
c	indicial function parameter in Model I, eq. (12)
c_1,c_2	indicial function parameters in Model II, eq. (24)
C_N,C_A,C_m	normal-force, axial-force, and pitching-moment coefficients
C_Y,C_l,C_n	side-force, rolling-moment, and yawing-moment coefficients
f	frequency, Hz
f_u,f_v	mathematical model parameters
J	cost function
k	reduced frequency, $k = \omega\ell / V$
ℓ	characteristic length, either $\ell = \bar{c} / 2$ or $\ell = b / 2$
m	number of frequencies
n	number of angles of attack
n_c	number of cycles
n_p	number of unknown parameters in mathematical model
p	rolling velocity, rad/sec
q	pitching velocity, rad/sec
r	yawing velocity, rad/sec
s	a.) standard error
	b.) parameter in Laplace transform (used in Chapter 3)
t	time, sec
T	period, sec
T_1	time constant, $T_1 = \tau_1\ell / V$, sec

u,v	steady-state aerodynamic derivatives as in mathematical models
V	airspeed, ft/sec
w_u,w_v	terms in Model II, eq. (32)
z_u,z_v	mathematical model parameters, eq. (23)
α	angle of attack, rad or deg
β	sideslip angle, rad or deg
Δ	increment
ϕ	roll angle, rad or deg
ψ	yaw angle, rad or deg
θ	pitch angle, rad or deg
ω	angular frequency, rad/sec
τ_1	nondimensional time constant, $\tau_1=V / \ell b_1$
Ω	rotation rate about freestream velocity vector, rad/sec

Subscript:

A	amplitude

Superscript:

^	estimated value

Superscript over aerodynamic derivative:

___	oscillatory data

Aerodynamic Derivatives:

$$C_{\xi_x}(\infty) \equiv C_{\xi_x} = \frac{\partial C_\xi}{\partial x} \quad \text{for } \xi = N, A, Y, m, l, n$$

$$\text{where } x = \alpha, \beta, \frac{\dot{\alpha}\bar{c}}{2V}, \frac{\dot{\beta}b}{2V}, \frac{q\bar{c}}{2V}, \frac{\dot{q}\bar{c}^2}{4V^2}, \frac{pb}{2V}, \frac{\dot{p}b^2}{4V^2}, \frac{rb}{2V}, or\ \frac{\dot{r}b^2}{4V^2}$$

Rotary Derivatives:

$$C_{l_\Omega} = \left.\frac{\partial C_l}{\partial \frac{\Omega b}{2V}}\right|_{\Omega=0} \quad \text{and} \quad C_{n_\Omega} = \left.\frac{\partial C_n}{\partial \frac{\Omega b}{2V}}\right|_{\Omega=0}$$

1. INTRODUCTION

Wind tunnel tests have long been used as a means of analyzing the aerodynamic characteristics of aircraft. These tests are necessary not only to validate theory, but also to extend it where it is incomplete.[1] Even with advancements in computational fluid dynamics, wind tunnels remain prominent in the effort to obtain accurate aerodynamic data for aircraft. Various methods of wind tunnel testing are currently in use, each with its own focus. Through these different kinds of tests, an overall survey of an aircraft's aerodynamic characteristics can be pieced together. While the different wind tunnel test methods provide data for a variety of conditions, they can create difficulty in comparing results. As test methods continue to evolve, so must the methodologies by which their data are analyzed.

The simplest wind tunnel test method is static testing, where the model remains fixed at selected angles of orientation. The resulting measured data are aerodynamic force and moment coefficients that are functions of angle of attack and sideslip, and are independent of time. From these data, angle-of-attack and sideslip stability derivatives typically are estimated. Derivatives related to control surface deflections can also be found using static tests. The angle-of-attack derivatives are usually determined by numerical differentiation of the measured data. The sideslip derivatives are found using data measured at different sideslip angles. The angle-of-attack and sideslip derivatives are sometimes referred to as *static* derivatives.

While the derivatives measured using static wind tunnel tests are important, they provide no information about the aircraft's response to motion. To compensate for this deficiency, dynamic wind tunnel test methods have been developed. Dynamic tests are used to validate the static test results and provide information about an aircraft in flight regimes where static data are no longer sufficient to describe its characteristics.[2] Typically, the model is moved

through a specific kind of motion that depends on the desired type of data. In contrast to static tests, the resulting data are often not only dependent on the model's orientation, but also on how it reached that orientation. As with static testing, the measured data are analyzed to find aerodynamic derivatives. In this case, however, the results include *dynamic* derivatives, such as translation or rotation rate derivatives.

One type of dynamic wind tunnel testing is rotary-balance testing. In the most common type of rotary-balance test, the model rotates at a constant rate about the freestream velocity vector. Such a test could be used, for example, to determine an aircraft's aerodynamic characteristics during a spin. The measured aerodynamic coefficients are functions of the model's rotation rate. The derivatives of these data with respect to rotation rate are then computed and used for analysis.

Another dynamic wind tunnel test method is forced-oscillation testing. While different types of oscillatory tests are used, the most common consists of harmonic one-degree-of-freedom motion about either the pitch, roll, or yaw axis. The measured data from forced-oscillation tests are time histories of the aerodynamic force and moment coefficients. These data are used to determine aerodynamic coefficients described by in-phase and out-of-phase components.[3] Typically, the in-phase component is comprised of a static derivative and a rotational derivative, while the out-of-phase component features a rotary derivative combined with a translation acceleration derivative.[3] The equations for the in-phase components explicitly account for frequency effects, while the out-of-phase equations used to determine damping rate derivatives do not. As a result, the estimated stability derivatives are determined as functions of frequency.

Traditionally, it is assumed that the effect of frequency on the forced-oscillation data is negligible. This assumption is valid in some cases, but not for modern fighter aircraft, as demonstrated by the strong frequency dependence of forced-oscillation data that is noted in references 3 and 4. Modern fighters are designed to routinely operate at high angles of attack, where this frequency effect is more pronounced. The frequency dependence makes

forced-oscillation data difficult to compare with other types of data, such as data from static or rotary-balance tests. It also is in conflict with the assumption that the values of the stability derivatives do not change with time.[3]

Various methods for dealing with the frequency effect on oscillatory data have been suggested. One approach implemented in references 3 and 4 uses indicial functions to account for the unsteady behavior of the aerodynamic stability coefficients. From postulated forms of the indicial functions, mathematical models are developed and used to fit the measured data. The resulting estimated model parameters can be used to predict in-phase and out-of-phase data for a given frequency. More importantly, they provide a means of obtaining steady-state (time and frequency independent) static and rate stability derivatives from forced-oscillation data. By removing the dependence on frequency, the estimated static derivatives are easier to compare with static wind tunnel test data. Estimated pitch, roll, and yaw rate derivatives can then also be compared more easily with other kinds of dynamic test data, when available.

The purpose of this report is to present the stability derivatives estimated from wind tunnel oscillatory data for the X-31A aircraft and evaluate the mathematical models that were used. First, a brief description of the X-31A is given. This is followed by a description of the wind tunnel tests used to obtain data for this study. The data from forced oscillations in pitch, roll, and yaw are presented, along with data measured using static and rotary-balance tests. The traditional, steady model for analyzing oscillatory data is developed. Two indicial functions are then introduced and used to develop mathematical models with unsteady terms. Next, the parameter estimation procedure used in this study is described. Following that, the results from using the mathematical models are presented and discussed. This includes the fit and prediction capabilities of both models, as well as the individual model parameters. Comparisons are drawn between the two models. The accuracy of the estimated angle-of-attack and sideslip derivatives are assessed through comparisons with the static wind tunnel test data. The estimated pitch, roll, and yaw rate

derivatives are presented, as well. As a means of evaluating their accuracy, comparisons with rotary-balance data are made. Rate derivatives predicted using two theoretical methods are included to provide another means of comparison. The presented information is then summarized, followed by some recommendations for future work.

2. WIND TUNNEL MODEL AND EXPERIMENT

2.1 X-31A Description

The X-31A is a single-seat experimental fighter developed for the Enhanced Fighter Maneuverability program.[5] It features all-moving canards and a double-delta wing planform. The wing is equipped with leading and trailing-edge flaps for control purposes. Control can also be provided by thrust vectoring. The aircraft has no horizontal tail, and a single vertical tail. It also features leading-edge, nose, and aft-mounted strakes. Figure 1 shows a three-view of the X-31 from reference 5. Geometric parameters for the X-31 (also from ref. 5) can be found in Table 1. The wing area, S, of the full-scale aircraft is 226.3 ft^2 (21.0 m^2). The wing span, b, is 22.83 ft (6.96 m). The full-scale aircraft's mean aerodynamic chord, $\bar{c}$, is 12.35 ft (3.76 m).

The numerous control surfaces of the X-31 provide many possibilities for controlling the aircraft. For this study, however, only one configuration was analyzed. All data presented in this thesis are for a symmetrical canard deflection of -40° (i.e., 40° canard leading-edge downward). The leading edge flaps were set at 40° down inboard and 32° down outboard. There was no trailing edge flap deflection. Also, all data are for a sideslip angle of zero and are referred to body axes.

2.2 Wind Tunnel Test Setups

2.2.1 Forced-Oscillation Testing

Oscillatory data were gathered using a one-degree-of-freedom forced-oscillation rig in NASA Langley Research Center's 30 x 60-Foot wind tunnel. For the testing, a 19%-scale model of the X-31A was used. Three separate experiments were done for oscillations in

pitch, roll, and yaw. Figure 2 shows the model mounted on the forced-oscillation rig. (Although the figure shows the model with its vertical tail removed, all of the data presented in this thesis were obtained with the vertical tail attached.) The tests were run at a dynamic pressure of 10 pounds per square foot (psf), which corresponds at sea level to a velocity of approximately 91.7 ft/s (28 m/s), a Mach number of about 0.08, and a Reynolds number of 1.37×10^6, based on the $\bar{c}$ of the 19%-scale model. The amplitude of the oscillations was ±5° about an offset angle of zero. For the aforementioned control surface deflections, measurements were taken at six different oscillation frequencies. These frequencies were nondimensionalized for analysis purposes. Tables 2 and 3 show the relationship between the frequencies, f (Hz), and the reduced frequencies, k, given by the equation:

$$k = \frac{\ell}{V}\omega = 2\pi f \frac{\ell}{V} \tag{1}$$

where ℓ is the characteristic length and V is the wind velocity. For the longitudinal case, the characteristic length is half of the mean aerodynamic chord of the wing. For the lateral case, the characteristic length is the semi-span of the wing, $b/2$.

When analyzing the oscillatory data it is assumed that the longitudinal aerodynamic coefficients are linearly dependent on angle of attack, pitching velocity, and their rates of change for a small change from a reference condition.[4] Following the development in reference 4, the change in the normal-force coefficient with respect to its mean value is written as

$$\Delta C_N = C_{N_\alpha}\Delta\alpha + \frac{\ell}{V}C_{N_{\dot\alpha}}\dot\alpha + \frac{\ell}{V}C_{N_q}q + \left(\frac{\ell}{V}\right)^2 C_{N_{\dot q}}\dot q \tag{2}$$

where

$$\begin{aligned} \Delta\alpha &= \alpha_A \sin\omega t \\ \dot\alpha = q &= \omega\alpha_A \cos\omega t \\ \ddot\alpha = \dot q &= -\omega^2\alpha_A \sin\omega t \end{aligned} \tag{3}$$

From this, it can be found that

$$\begin{aligned}\Delta C_N &= \alpha_A\left(C_{N_\alpha} - k^2 C_{N_{\dot{q}}}\right)\sin\omega t + \alpha_A k\left(C_{N_{\dot{\alpha}}} + C_{N_q}\right)\cos\omega t \\ &= \alpha_A\left(\overline{C}_{N_\alpha}\sin\omega t + k\overline{C}_{N_q}\cos\omega t\right)\end{aligned} \tag{4}$$

where the in-phase and out-of-phase components of the normal-force coefficient are given by the equations

$$\overline{C}_{N_\alpha} = C_{N_\alpha} - k^2 C_{N_{\dot{q}}} \tag{5}$$

$$\overline{C}_{N_q} = C_{N_q} + C_{N_{\dot{\alpha}}} \tag{6}$$

These parameters can be determined using the orthogonality condition to integrate the measured time histories of the aerodynamic coefficients over n_c cycles. The resulting integrals are written as

$$\overline{C}_{N_\alpha} = \frac{2}{\alpha_A n_c T}\int_0^{n_c T}\Delta C_N(t)\sin\omega t\, dt \tag{7}$$

$$\overline{C}_{N_q} = \frac{2}{k\alpha_A n_c T}\int_0^{n_c T}\Delta C_N(t)\cos\omega t\, dt \tag{8}$$

For pitch-axis oscillations, this development can also be used for lift, drag, pitching moment, and axial force.

A similar analysis can be used for the roll and yaw-axis oscillations. The resulting out-of-phase equations used for the roll axis are of the form

$$\overline{C}_{l_p} = C_{l_p} + C_{l_{\dot{\beta}}}\sin\alpha \tag{9}$$

with similar equations for the yawing-moment and side-force coefficients. For the yaw-axis oscillations, the out-of-phase equations are of the form

$$\overline{C}_{l_r} = C_{l_r} - C_{l_{\dot{\beta}}}\cos\alpha \tag{10}$$

All of the remaining expressions for this type of analysis can be found in Table 4.[7] While the equations account for some frequency dependence, they do not model any time-dependent (or *unsteady*) effects.

The measured time histories of the aerodynamic coefficients of the X-31A were integrated using eqs. (7) and (8) and similar equations for other coefficients. The computed in-phase and out-of-phase data are contained in Tables 5-13. These data can also be seen in Figures 3-11. For clarity, only four frequencies were included in each graph. Typically, the frequencies omitted from the graphs were the third and fifth. For the yawing moment calculated from yaw oscillations, however, the third and fourth frequencies were not included. This was due to bad data for k=0.1186 (f=0.8 Hz). It can be seen from the figures that, in some cases, the data are independent of frequency at angles of attack less than approximately 20°. This trend is shown more often by the in-phase components. Overall, however, the figures show that the aerodynamic coefficients are very dependent on frequency.

2.2.2 Static Testing

Static wind tunnel tests on the X-31A configuration were done using a 13.3%-scale model in NASA Langley's 12-Ft. wind tunnel. The control surface deflections were the same as those used in the forced-oscillation tests, as was the dynamic pressure of the tunnel (10 psf). The measured normal-force, axial-force, and pitching-moment coefficients can be found in Figure 12. These curves were numerically differentiated to determine the angle of attack derivatives shown in Figure 13. Lateral stability derivatives were determined using runs at $\beta=\pm5°$. These parameters are shown in Figure 14.

2.2.3 Rotary-Balance Testing

To determine the high-angle-of-attack rotational aerodynamic behavior of the X-31A, another 13.3%-scale model was tested in Langley's 20-Ft Spin Tunnel using the rotary-balance technique.[8] The control surface deflections were the same as those used in the other wind tunnel tests. Various types of rotary-balance setups are currently in use, including some that allow the inclusion of oscillatory motion.[9] Reference 9 contains an in-

depth look at rotary-balance testing. The rig used for the X-31 tests generates a steady roll about the wind axis, which is the most common type of rotary-balance test. A thorough description of the test procedure used for the X-31A can be found in reference 8. The tests were done at a freestream velocity of 25 ft/sec (7.62 m/s), which corresponds to a dynamic pressure of only 0.74 psf. Figure 15 shows the measured rolling and yawing-moment coefficients at zero sideslip as a function of the spin coefficient (or *nondimensional rotation rate*), $\Omega b/2V$, where Ω is the rotation rate in radians per second.[8] Using these data, the rotation rate (also known as *rotary*) derivatives were determined. Since the moment coefficients are typically non-linear functions of the rotation rate, it is necessary to linearize them over a small range approaching a rotation rate of zero.[10] Figure 16 shows that the estimated rotary derivatives are very dependent on the range that is used to calculate them. The smallest range was selected, using data for $\Omega b/2V=\pm 0.05$.[10] For this study, only the rolling and yawing moment data were considered. It is possible, however, to predict pitch damping using measured pitching-moment coefficients from different sideslip settings.[11]

3. MATHEMATICAL MODELS FOR OSCILLATORY DATA

3.1 Model I

Data from forced-oscillation tests demonstrate a frequency dependence, which contradicts the assumption that the stability derivatives are time-invariant.[3] This frequency effect for the X-31A was demonstrated by Figures 3-11. To account for the frequency dependence, aerodynamic models have been proposed that include unsteady terms. By using these terms, the frequency effect can be extracted from the data and steady-state stability derivatives can be estimated. The in-phase and out-of-phase components of the aerodynamic coefficients are then represented as the sum of a steady-state (either static or rotational) stability derivative and a term containing the unsteady effects.[11] Such unsteady mathematical models are developed through the use of indicial functions.[12] These functions are characterized by a response that damps to a steady-state value as time increases. Some applications of indicial functions are discussed by Tobak in reference 13.

Reference 4 presents the development of a mathematical model for oscillatory data where, for pitch oscillations, the equation for the normal-force coefficient can be written as

$$C_N(t) = \int_0^t C_{N\alpha}(t-\tau)\frac{\mathrm{d}}{\mathrm{d}\tau}\alpha(\tau)\,\mathrm{d}\tau + \frac{\ell}{V}\int_0^t C_{Nq}(t-\tau)\frac{\mathrm{d}}{\mathrm{d}\tau}q(\tau)d\tau \qquad (11)$$

where q represents the angular pitching velocity in radians per second. The indicial functions are represented by $C_{N_\alpha}(t)$ and $C_{N_q}(t)$. In reference 4, the effect of $\dot{q}(t)$ on the lift is neglected. In the analysis presented here, its effect on the normal force will similarly be neglected. Though indicial functions have been studied extensively in aerodynamics, their proper analytical forms are not obvious.[12] To achieve a model with a small number of parameters, one form of indicial function can be postulated as[4]

$$C_{N_\alpha}(t) = a\left(1 - e^{-b_1 t}\right) + c \tag{12}$$

which can be rewritten as

$$C_{N_\alpha}(t) = C_{N_\alpha}(\infty) - ae^{-b_1 t} \tag{13}$$

Using the Laplace transform on equation (11), a set of steady-state equations can be determined, as is done in reference 12. Using this approach, the resulting mathematical model is found to be

$$\overline{C}_{N_\alpha} = C_{N_\alpha}(\infty) - a\frac{\tau_1^2 k^2}{1 + \tau_1^2 k^2} \tag{14}$$

$$\overline{C}_{N_q} = C_{N_q}(\infty) - a\frac{\tau_1}{1 + \tau_1^2 k^2} \tag{15}$$

where k is the reduced frequency and τ_1 is a nondimensional parameter given by the equation

$$\tau_1 = \frac{V}{\ell b_1} \tag{16}$$

For pitch oscillations, the same form will apply to the equations for lift, drag, axial force, and pitching moment. The value of τ_1, however, will generally differ for each aerodynamic coefficient.

This model, which will be called Model I, can also be extended to roll and yaw oscillations. A detailed description can also be found in reference 12. For oscillations in roll, the rolling-moment coefficient is considered to be a function of only the roll angle, ϕ, and the angular rolling velocity, p.[12] From reference 12, the resulting equations can be written as

$$\overline{C}_{l_\beta} = C_{l_\beta}(\infty)\sin\alpha - a\frac{\tau_1^2 k^2}{1 + \tau_1^2 k^2}\sin\alpha \tag{17}$$

$$\overline{C}_{l_p} = C_{l_p}(\infty) - a\frac{\tau_1}{1 + \tau_1^2 k^2}\sin\alpha \tag{18}$$

The sinα terms in equations (17) and (18) come from the relationship between sideslip angle and rolling velocity.[12] The equations for side-force and yawing-moment coefficients are of a similar form. The rolling-moment equations for yaw oscillations are determined to be

$$\overline{C}_{l_\beta} = C_{l_\beta}(\infty)\cos\alpha - a\frac{\tau_1^2 k^2}{1+\tau_1^2 k^2}\cos\alpha \tag{19}$$

$$\overline{C}_{l_r} = C_{l_r}(\infty) + a\frac{\tau_1}{1+\tau_1^2 k^2}\cos\alpha \tag{20}$$

where the cosα terms are from the relationship between sideslip angle and the angular yawing velocity, r.[12] As before, the side-force and yawing-moment equations follow the same form. All of the expressions for this model can be found in Table 14.

To simplify the notation, the in-phase and out-of-phase equations of Model I can be rewritten in the form

$$\overline{u}_{ji} = u_i f_{u_i} - a_i z_{u_j} f_{u_i} \tag{21}$$

$$\overline{v}_{ji} = v_i - a_i z_{v_j} f_{v_i} \tag{22}$$

where u_i and v_i represent the steady-state static and rate derivatives. These are time-independent coefficients that are functions of angle of attack. In the case of pitch oscillations, for the normal force:

$$u_i = C_{N_\alpha}(\infty, \alpha_i) \qquad v_i = C_{N_q}(\infty, \alpha_i)$$

In all oscillation cases, the functions z_u and z_v represent the frequency-dependent terms

$$z_{u_j} = \frac{\tau_1^2 k_j^2}{1+\tau_1^2 k_j^2} \qquad z_{v_j} = \frac{\tau_1}{1+\tau_1^2 k_j^2} \tag{23}$$

The functions f_u and f_v in equations (21) and (22) are dependent on the type of oscillations that the model represents. For oscillations in pitch, both are equal to one for all values of angle of attack. For roll oscillations,

$$f_{u_i} = \sin\alpha = f_{v_i}$$

and for yaw

$$f_{u_i} = \cos\alpha = -f_{v_i}$$

In all of these equations, $i=1,2,...n$ and $j=1,2,...m$, where n is the number of values of angle of attack and m is the number of frequencies to be used for analysis.

3.2 Model II

As mentioned before, the proper forms for indicial functions are not readily known. Using different indicial functions to develop other mathematical models provides a way to determine the best form. The response of the indicial function used in Model I is bounded by its steady-state value; that is, the response curve never crosses the steady-state value. The indicial responses presented by Tobak in reference 13 demonstrate a tendency to overshoot the steady-state value before returning to it as time approaches infinity. The inability of the Model I indicial function to account for this type of behavior could potentially affect the accuracy of the model. A more accurate model can possibly be created by using an indicial function with a response that resembles those of reference 13.

One way of developing a new model would be to add another time-dependent term to the indicial function used for Model I. This extra term should be bounded with time so that the response will reach a steady-state value as time approaches infinity. A suitable new indicial function would then be

$$C_{N_\alpha}(t) = a\left(1 - e^{-b_1 t}\right) + c_1 - c_2\left(\frac{V}{\ell}\right)^2 t^2 e^{-b_1 t} \tag{24}$$

which can be rewritten in the form

$$C_{N_\alpha}(t) = C_{N_\alpha}(\infty) - ae^{-b_1 t} - c_2\left(\frac{V}{\ell}\right)^2 t^2 e^{-b_1 t} \tag{25}$$

where the c term in the previous model has been renamed c_1. The parameter c_2 is a function of angle of attack similar to a. The t^2 term needs to be multiplied by the $(V/\ell)^2$ term so that

the vector c_2 will be nondimensional. This form of indicial function will allow the value of the aerodynamic derivative to cross the steady-state value, though it will not always do so. The shape of the indicial response will depend on the aerodynamic parameter it describes, and the angle of attack. The mathematical model based on the indicial function of equation (25) will be called Model II.[†]

Using the indicial function of equation (25), a steady-state set of equations can be derived, as was done for Model I. Following the development in reference 12, the Laplace transform of equation (11) for the new model becomes

$$C_N(s) = \left[C_{N_\alpha}(\infty) - a\frac{s}{s+b_1} - c_2\left(\frac{V}{\ell}\right)^2 \frac{2s}{(s+b_1)^2} + \frac{\ell}{V} C_{N_q} s \right] \alpha(s) \tag{26}$$

where $q(s)$ was replaced by $s\alpha(s)$. As in reference 12, the expression for $\alpha(t)$ can be written in complex form as

$$\alpha(t) = \alpha_A e^{i\omega t} = \alpha_A(\cos(\omega t) + i\sin(\omega t)) \tag{27}$$

and by replacing s with $i\omega$, the steady-state solution for the in-phase and out-of-phase equations is found to be

$$\overline{C}_{N_\alpha} = C_{N_\alpha}(\infty) - \left(a\frac{1}{1+\tau_1^2 k^2} + 2c_2 \frac{\tau_1^2(3-\tau_1^2 k^2)}{(1+\tau_1^2 k^2)^3} \right) \tau_1^2 k^2 \tag{28}$$

$$\overline{C}_{N_q} = C_{N_q}(\infty) - \left(a\frac{1}{1+\tau_1^2 k^2} + 2c_2 \frac{\tau_1^2(1-3\tau_1^2 k^2)}{(1+\tau_1^2 k^2)^3} \right) \tau_1 \tag{29}$$

The equations for the other aerodynamic coefficients follow a similar derivation. As with Model I, the roll and yaw-axis equations will include sine and cosine terms. All the equations for Model II can be found in Table 15. The two models are somewhat similar, but the extra time-dependent term in the second indicial function causes the steady-state solution to be more complex.

[†] Note: The Model II presented here is different than the one presented in reference 4.

The equations for Model II can be represented in a simplified form as were those of Model I. The in-phase and out-of-phase equations are now

$$\overline{u}_{ji} = u_i f_{u_i} - a_i z_{u_j} f_{u_i} - c_{2_i} w_{u_j} f_{u_i} \tag{30}$$

$$\overline{v}_{ji} = v_i - a_i z_{v_j} f_{v_i} - c_{2_i} w_{v_j} f_{v_i} \tag{31}$$

where the u, v, a, and f represent the same terms as in Model I. Also, the frequency-dependent terms z_u and z_v remain the same. The only change in the new model is the addition of the w_u and w_v terms, where

$$w_{u_j} = \frac{2\tau_1^4 k_j^2 \left(3 - \tau_1^2 k_j^2\right)}{\left(1 + \tau_1^2 k_j^2\right)^3} \qquad w_{v_j} = \frac{2\tau_1^3 \left(1 - 3\tau_1^2 k_j^2\right)}{\left(1 + \tau_1^2 k_j^2\right)^3} \tag{32}$$

While the nomenclature used by Models I and II is similar, the unknown model parameters will take on different values due to the different model structures.

4. PARAMETER ESTIMATION METHOD

To determine the values for the unknown model parameters, the nonlinear estimation technique of reference 3 was used. Due to the different structure of the two mathematical models, the application of the estimation method differed slightly. For data at n angles of attack, Model I has $3n+1$ unknown parameters: u_i, v_i, a_i, and τ_1. The addition of the extra term in Model II adds n unknowns to this in the form of c_{2_i}. For both models, a cost function was defined that describes the sum of the squared differences between the measured and estimated in-phase and out-of-phase data. The cost function used in Model I was

$$J_I = \sum_{j=1}^{m} \sum_{i=1}^{n} \left\{ \left[\overline{u}_{ji} - f_{u_i}\left(u_i - a_i z_{u_j}\right) \right]^2 + \left[\overline{v}_{ji} - \left(v_i - a_i z_{v_j} f_{v_i}\right) \right]^2 \right\} \tag{33}$$

and that of Model II was

$$J_{II} = \sum_{j=1}^{m} \sum_{i=1}^{n} \left\{ \left[\overline{u}_{ji} - f_{u_i}\left(u_i - a_i z_{u_j} - c_{2_i} w_{u_j}\right) \right]^2 + \left[\overline{v}_{ji} - \left(v_i - f_{v_i}\left(a_i z_{v_j} + c_{2_i} w_{v_j}\right)\right) \right]^2 \right\} \tag{34}$$

Using the appropriate cost function, a linearized least-squares approach was initially used to determine the value of τ_1 that generates the lowest cost.[3] Once this value was found, a Modified Newton-Raphson method was used to find the final parameter estimates based on the initial, least-squares values. The standard errors of the parameters were also computed. The variance estimate for this problem is given by the equation[3]

$$s^2 = \frac{J(\theta)}{2nm - n_p} \tag{35}$$

where θ is the set of parameter estimates, m is the number of reduced frequencies used, and n_p is the number of unknown model parameters. The $2nm$ represents the total number of data points used, as there were nm points for each set of in-phase and out-of-phase data.

Estimation using the mathematical models for roll and yaw-axis oscillations is complicated by their trigonometric terms. For angles of attack that cause these terms to be zero, the in-phase component will be zero for all frequencies. Also, the out-of-phase part will be frequency independent at these angles of attack. Considering measurement error, the data from the X-31 tests indicate that these conditions may be physically accurate. During the estimation procedure, however, they cause the system of equations used in the linearized least-squares approach to be ill-defined. In other words, there will be more unknown parameters than equations, and the estimation technique will not work. To eliminate this problem, data at $\alpha=0°$ were not used for analyzing roll-axis oscillations. For yaw-axis oscillations, data at $\alpha=90°$ were not used.

During the estimation process, data were omitted at one frequency (f=0.6 Hz) and reserved for checking the ability of the model to predict frequency-dependent in-phase and out-of-phase data. For the yawing-moment coefficient measured using oscillations in yaw, one additional frequency (f=0.8 Hz) was eliminated due to irregular data. The four frequencies that remained were sufficient for the estimation process. Equation (35) indicates that the number of measured data points must be greater than or equal to the number of unknowns.[3] Using only four frequencies will satisfy this requirement, but the smaller number of points may negatively affect the estimation accuracy.

5. RESULTS AND DISCUSSION

5.1 Fit to the Measured Data and Prediction Capability

Before analyzing the estimated model parameters themselves, it is necessary to assess the ability of the mathematical models to fit the measured data. Both mathematical models were used to fit data from three different experiments: oscillations in roll, yaw, or pitch. Figures 17-22 compare the results of the estimation with the measured data for key aerodynamic coefficients at selected frequencies. Results were similar for the coefficients that are not shown in the figures. This can be seen in Table 16, which shows the estimated variances and costs of both models for all of the aerodynamic coefficients. This information is also presented, in graphical form, in Figures 23 and 24. From the cost comparisons and the graphs, it can be seen that the estimated in-phase and out-of-phase components of the aerodynamic coefficients agreed well with the experimental data for both mathematical models.

From Figures 17-22, it can be seen that the in-phase estimates of Model II were very similar to those of Model I, and it is not apparent whether either model was more accurate in modeling in-phase data. Model II, however, demonstrated better accuracy in modeling out-of-phase data. This is shown most clearly by the oscillatory roll damping results shown in Figure 20. According to equation (35), the estimated variances of the models will be dependent on the number of unknown parameters. Since Model II consists of n more unknowns than Model I, it will produce higher variances for the same cost. Therefore, a comparison of the final costs of each model is useful. The table shows that Model II produced smaller costs and standard errors for all aerodynamic coefficients when fitting the measured data.

After the parameter estimation, the mathematical models were used to predict in-phase and out-of-phase data for a frequency of 0.6 Hz, for which measured data were omitted during the estimation procedure. These predictions are shown for three selected cases in Figures 25-27. Comparisons between Models I and II in this case are difficult to make using the graphs, as both showed the ability to accurately predict the oscillatory force and moment coefficients. In some cases, Model I showed superior prediction capabilities. Other times, however, the second model appeared to be better suited to predict the extreme nonlinearity of the data. Table 17 shows a comparison of the sum of the squared differences (residuals) between the measured and predicted in-phase and out-of-phase data at f=0.6 Hz for both models. The squared residuals, r^2, were found using the equation

$$r^2 = \sum_{i=1}^{n} \left(\bar{y}_i - \hat{\bar{y}}_i \right)^2 \tag{36}$$

where $\bar{y}_i$ represents either the in-phase or out-of-phase component and, as before, n is the number of angles-of-attack. In most cases, the predictions of Model I produced slightly smaller residuals than those of Model II.

The minor increase in prediction error for Model II may be indicative of a more substantial problem. It is possible that the extra term in Model II improved the accuracy of the fit to the data, but its high-order frequency dependence created some errors in prediction. This notion is supported by Figures 28 and 29, which show an example of predicted in-phase and out-of-phase data over a range of frequencies just beyond the values that were used experimentally. The in-phase components predicted by both models were in agreement with each other, and appeared well behaved over the entire frequency range. These characteristics did not hold true for the out-of-phase component predictions shown in Figure 29. The out-of-phase components predicted by Model II were somewhat inconsistent with those of Model I as the reduced frequency approaches zero, and seemed to be erratic.

The prediction results suggest that Model I is a parsimonious model and should be used when more conservative predictions are desired, particularly at very small values of reduced frequency. To improve the overall prediction quality of Model II, it would likely be necessary to measure data at more frequencies. The oscillation frequencies would also need to be spaced closely to reduce the tendency of Model II to overpredict in regions where there is no measured data. While these two changes might improve Model II's prediction capability, they may do so at the cost of losing some of the improvement in fit accuracy. Gathering data at the additional frequencies would also increase the time (and, therefore, money) spent on the wind tunnel test itself.

5.2 Estimated Parameters

The individual parameters that comprise the mathematical models provide information about the aircraft's aerodynamic behavior. The most important of these are the estimates of the static and dynamic stability derivatives, the *u* and *v* terms in the models, but it is also of interest to study the other unknown parameters in the models. Tables 18-19 show the estimated values of τ_1 and calculated time constants for each model along with their standard errors. It can be seen that the values of τ_1 differed between the models, sometimes significantly. Their values also were very dependent on the aerodynamic coefficient for which they were used. Also, neither model produced consistently lower standard errors than the other.

The effect of indicial function form on estimated parameters is evident in the differences between their predicted indicial response curves. These responses can be determined by substituting the estimated model parameters into the indicial function definitions. For example, Figure 30 shows a comparison of indicial response curves predicted for C_{m_α} at different values of angle of attack. Here, the influence of the extra time term is apparent,

especially at α=80°. There did not appear to be a discernible trend describing the shape of the indicial response for either model, however.

Key to the shape of the aerodynamic derivative indicial response curves are the a vectors in both models, and the c_2 vector in Model II. These parameters are related to the unsteady effects on the aerodynamic coefficients, but their physical significance is not evident.[12] Plots of these parameters are shown in Figures 31-36. Included are the 2s confidence intervals for the estimates of a from Model I, and the c_2 estimates of Model II. As can be seen, the shape and values of these parameters varied depending on the particular aerodynamic coefficient the model described. In most cases, there was not a large difference between the estimated a vectors of Models I and II. The difference in the time response of the two models was due to the inclusion of c_2 in Model II. It is important to note that the c_2 term in the model is multiplied by $(V/\ell)^2$, which is typically much greater than one. This is why c_2 is significant even though its values are very small. It is not evident whether the small size of the c_2 parameters had any adverse effects on the estimation procedure.

The estimated steady-state static derivatives were compared to those determined experimentally through static wind tunnel tests. These are the stability derivatives with respect to angle of attack and sideslip. The comparison between the static data and the estimates from the two models are shown in Figures 37-39. For simplicity, only the standard errors for the Model I estimates are included. The static derivatives estimated by both models were very similar. The angle-of-attack derivatives estimated from pitch oscillation data agreed well overall with the static test data, particularly for the normal-force coefficient. The estimated values of C_{m_α} showed the largest discrepancy from the measured data.

The sideslip derivative estimates also showed, in general, good agreement with the static test data. The estimates of C_{Y_β}, in particular, correlated well with the measured values.

The estimates of C_{n_β} differed substantially from the measured data at angles of attack between 50° and 70° in the roll case. Due to the form of the mathematical models, either roll or yaw oscillatory data can be used to estimate the sideslip derivatives. Figures 40 and 41 show comparisons between the yaw-axis and roll-axis estimates for Models I and II. Both oscillation cases produced similar derivative estimates.

Many factors contribute to the discrepancies between the stability derivatives estimated from forced-oscillation tests with those of static tests. Some of these are related to the experimental procedures. Though for identical configurations, a different X-31 model was used for each kind of test, which can create differences in their results. Some discrepancies may be due to the use of different wind tunnels. Also, a potential source of error is the measured forced-oscillation data itself. No statement can be made regarding the accuracy or repeatability of the data. Error may also be induced by the time history integration used to calculate the in-phase and out-of-phase data used in this study.

Estimates of the pitch, roll, and yaw rate derivatives (e.g., C_{m_q}, C_{l_p}, C_{l_r}) from each model are shown in Figures 42-44. Again, the standard error bars have been shown for only the Model I estimates. As opposed to the static case, no experimental data were available for a direct comparison, which made it difficult to assess the accuracy of the estimates. Though in agreement, there was more of a difference between the two models' estimated dynamic derivatives than was shown with the static derivatives. Rate derivatives are closely related to the out-of-phase component of the oscillatory data. The differences between the results of the two models indicate that the extra term in Model II primarily influenced the modeling of out-of-phase phenomena, which is also suggested by the fit to the measured data.

The influence of the f_u and f_v terms in the mathematical models can be seen by the behavior of the standard errors of the estimated stability derivatives. As shown before, the roll-axis equations feature the $\sin\alpha$ terms. Consequently, data at α=0° were not used in the

estimation process because the model would not be valid at that angle of attack. For the static derivatives, the standard errors were largest near α=0° for the roll-axis case and decreased as angle of attack increased. The opposite was true for the yaw-axis case, where the sine terms are replaced by cosine terms. Here, data at α=90° were not used, and the standard errors increased with α for the sideslip derivative estimates. The behavior of the standard errors suggests that roll and yaw estimates be used together in a way to neutralize the problems at α=0° and 90°. This would mean emphasizing the yaw-axis predictions for small angles of attack, and the roll-axis predictions for large angles of attack. The standard error trends shown for the sideslip derivative estimates did not extend to the roll and yaw rate derivatives. The standard errors for the angle-of-attack derivatives were nearly independent of angle of attack, especially for the normal and axial-force coefficients. As with the results from the other two oscillation axes, this trend did not extend to the rate derivatives.

In addition to the error bars included in the graphs, the minimum and maximum standard errors for the estimated parameters can be found in Tables 20 and 21. The tables show that the extrema of Model II's standard errors were often smaller than those of Model I. The errors for the a vectors varied between the two models, but comparisons are skewed slightly by the different model forms. For Model II, the standard errors for the c_2 vectors were very small, as were the values of c_2 themselves.

5.3 Comparison with Rotary-Balance Data

To help evaluate the estimated rate derivatives, comparisons were made with data measured using the rotary-balance test method. Due to the differences in the two techniques, however, such comparisons are suspect. As with the comparison between forced-oscillation and static testing, differences in the X-31 wind tunnel models and the

wind tunnels themselves can lead to some discrepancies. Also, the rotary-balance tests were done at a much lower dynamic pressure than the forced-oscillation tests, which could also change the results. One main difference between the two methods is that rotary-balance data are measured at a constant rotation rate, as opposed to the harmonic motion of forced-oscillation testing. A result of this is that the two tests model different flow phenomena. Therefore, comparisons with rotary-balance data can provide a general assessment of the forced-oscillation results, but not any significant conclusions about their accuracy.

Traditional comparisons between rotary-balance and oscillatory data have also been complicated by the oscillatory derivatives' frequency dependence. This problem can be reduced by using the steady-state roll and yaw rate derivative estimates: $C_{l_p}(\infty)$, $C_{n_p}(\infty)$, $C_{l_r}(\infty)$, and $C_{n_r}(\infty)$. Though this makes for a truer comparison, it does not compensate for the substantial differences in test methods. Since the derivatives from rotary-balance testing are based the rate of rotation about the wind axis, it is necessary to convert the derivatives estimated from the oscillatory data. The relationship between the two is given by the equations

$$C_{l_\Omega} = C_{l_p}(\infty)\cos\alpha + C_{l_r}(\infty)\sin\alpha \tag{37}$$

$$C_{n_\Omega} = C_{n_p}(\infty)\cos\alpha + C_{n_r}(\infty)\sin\alpha \tag{38}$$

where C_{l_Ω} and C_{n_Ω} are the rotary derivatives.

The comparison between the estimated derivatives from rotary-balance data and the steady-state estimates from forced-oscillation data is shown in Figure 45. The figure shows that the two types of data do not correlate well overall. The estimated rotary rolling-moment derivative, C_{l_Ω}, varied from the rotary-balance data the most at angles of attack between approximately 35° and 60°, but showed good agreement at small angles of attack. The estimated rotary yawing-moment derivatives followed the same trend as the measured data, but individual data points did not agree as well as in the rolling-moment case. Due to

the limitations of this comparison, these discrepancies do not necessarily mean that the estimated derivatives from oscillatory data were in error.

5.4 Comparison with Theoretical Predictions

There are several methods available for the analytical prediction of an aircraft's aerodynamic qualities. These can be limited in their ability to model aircraft such as the X-31, but provide a way to quickly estimate desired parameters. One commonly used tool for stability derivative prediction is the USAF Datcom handbook, reference 14, which has been integrated into a computer program called Digital Datcom.[15] The normal limitations of Datcom's analytical methods are accentuated by the configuration of the X-31. The canard must be input as a wing and the wing as a horizontal tail, which the program neglects when computing the lateral-directional dynamic derivatives.[16] The methods used by the program allow for the superposition of the results, so the final predictions for canard configurations must be assembled from separate runs.[16] Digital Datcom does not have the ability to precisely match the leading and trailing-edge flap configuration of the X-31. It also does not take into account the effect of strakes. These problems can be offset by the input of experimental data when it is available.

Another way to predict an aircraft's stability and control characteristics is the use of strip theory. One computer program that predominantly uses strip theory to determine pitch, roll, and yaw rate derivatives is called DYNAMIC.[17] For this program, experimental data are required for all surfaces. The load distributions for the lifting surfaces are to be input, as well as the normal and axial-force coefficients as a function of angle of attack. It is sufficient to use panel methods to generate the input when experimental data are not available.[17] The program has the capability to approximate the normal force curve for the fuselage, as well as its C_{Y_β} curve. It can also approximate the aerodynamic characteristics of the vertical tail. The output from DYNAMIC is primarily the roll and yaw rate

derivatives for C_n and C_l. The computed static derivatives for the fuselage and vertical tail can also be output.

For the prediction of the X-31's dynamic derivatives, the geometry input data were scaled to 19% to match the wind tunnel model used in forced-oscillation tests. The fore and aft strakes were neglected due to the limits of the programs. To account for the wing strakes and control surface deflections, a panel method was used to predict the lift curve of the wing. This prediction was then used as input for the programs in lieu of experimental data. The flight conditions input for the theoretical predictions were the same as those of the oscillatory tests, as well.

It is also possible to predict the lateral-directional stability derivatives using a combined method using rotary-balance and theoretical data.[10] Here, the spin rate derivatives from rotary-balance testing are used in conjunction with analytical predictions, such as Datcom or DYNAMIC. To make these predictions, the relationship between the rotary and body-axis roll and yaw rate derivatives is manipulated to give the following equations[10]

$$C_{l_{p,pred}} = \frac{C_{l_{\Omega,rb}} - C_{l_r} \sin\alpha}{\cos\alpha} \tag{39}$$

$$C_{n_{p,pred}} = \frac{C_{n_{\Omega,rb}} - C_{n_r} \sin\alpha}{\cos\alpha} \tag{40}$$

$$C_{l_{r,pred}} = \frac{C_{l_{\Omega,rb}} - C_{l_p} \cos\alpha}{\sin\alpha} \tag{41}$$

$$C_{n_{r,pred}} = \frac{C_{n_{\Omega,rb}} - C_{n_p} \cos\alpha}{\sin\alpha} \tag{42}$$

The results are roll and yaw rate derivatives that can be compared with the analytical or forced-oscillation predictions. The inclusion of rotary-balance data may improve the results by accounting for nonlinear behavior.[10]

A comparison of the predictions from Digital Datcom and DYNAMIC with the estimated derivatives from oscillatory data can be found in Figures 46 and 47. It can be seen that the estimated derivatives agreed well with the theoretical predictions for small angles of attack.

The X-31's aerodynamic parameters are highly nonlinear, particularly at angles of attack greater than approximately 25°. The theoretical predictions are not capable of modeling such nonlinearities. The predictions of C_{l_p}, however, showed good agreement at slightly larger angles of attack, while the other predicted derivatives did not. Combining the predictions with rotary-balance data improved the results for higher angles of attack, as was also noted for a different study in reference 10. The results for the X-31 are shown by Figures 48 and 49. Figure 50 shows a comparison of the theoretical predictions with rotary-balance data and the oscillatory estimates in the form of the rotary derivatives. As before, theory provides results that concurred with the wind tunnel data estimates for moderate angles of attack. The predicted values of C_{l_Ω} tended to be in better agreement with the estimated data. At small angles of attack, the theoretical predictions indicated, in general, that the oscillatory estimates were reasonable with respect to theory. Due to their limitations, however, the theoretical predictions cannot be used to draw any major conclusions about the accuracy of estimated derivatives from oscillatory data.

6. CONCLUDING REMARKS

Three types of wind tunnel tests--static, rotary-balance, and forced-oscillation--were performed on models of the X-31A configuration. Three separate forced-oscillation tests were performed, one each for oscillations in pitch, roll, and yaw. The resulting data were shown to be dependent on the frequency of the motion. Two unsteady models developed using indicial functions were used to account for this frequency effect. Both functions were formulated so that the estimated aerodynamic coefficient would approach a steady-state value as time increases. The second function featured an added term that made it possible for the value of the coefficient to cross its steady-state value.

The unsteady models were used to fit the measured data and estimate the X-31's static and dynamic stability derivatives. Both models showed good accuracy in fitting the measured data. Model II produced a closer fit, especially for the out-of-phase data. The two models also showed good prediction capability. In comparison to the experimental data, the predictions for both models were similar, with Model I appearing to have produced a more accurate prediction overall. Results based on a range of frequencies indicated that Model II is likely to overpredict in-phase and out-of-phase data.

Both models were used to estimate steady-state stability derivatives, which were compared with static and rotary-balance wind tunnel data. The estimated static derivatives showed good agreement, in general, with those from the static test data. No experimental data were available for direct comparison with the estimated rate derivatives. For a general assessment of the results, the estimated roll and yaw rate derivatives from oscillatory data were compared with rotary-balance data. The estimated derivatives followed the overall trend of the rotary-balance data, but showed substantial disagreement in some areas, likely due to differences in the wind tunnel test methods.

Two analytical methods were also used for comparison of roll and yaw rate derivatives. Though the configuration of the X-31 limited their effectiveness, the analytical methods provided useful theoretical predictions of stability parameters at small angles of attack. The accuracy of these predictions was improved slightly by combining them with rotary-balance data. Overall, the theoretical predictions indicate that the estimated rate derivatives have reasonable values at small angles of attack. Due to their limitations, however, no conclusive statements could be made regarding the accuracy of the oscillatory data estimates.

There were many potential sources for error in the comparisons used in this study. The three wind tunnel test methods described different flow phenomena, which influenced the results even though the estimated derivatives from oscillatory data were frequency independent. Also, while the unsteady mathematical models showed the ability to accurately fit the measured data, no statement can be made as to the accuracy of the data. Inaccuracies in the measured data might have lead to inaccurate derivative estimates. Also, the in-phase and out-of-phase data used for this study were not measured directly, but computed from the measured data. This also could have introduced error into the results.

The formulation of the indicial function used in the mathematical models was shown to have an influence on the parameter estimates. The inclusion of another term into the indicial function slightly improved the overall accuracy of the model in fitting the experimental data. The prediction problems shown by Model II, especially when predicting out-of-phase data at certain frequencies, might have been due to its high-order frequency terms. In general, Model II seemed to have poorer prediction capabilities than Model I. Both of the models produced similar results when estimating the angle of attack and sideslip derivatives. The standard errors produced by Model II, however, were typically smaller. This held true even in some areas where the estimates of Model I were closer to the static test data, which may be related to the accuracy of the measured data. The dynamic stability derivatives estimated with both models agreed overall, but sometimes

differed notably. It is possible that the extra term in Model II provided better modeling of out-of-phase effects, which are related to the rate derivatives. The improved fit accuracy of Model II was offset by its increased complexity and possible prediction errors, and could not be directly linked to more accurate steady-state stability derivative estimates. Overall, the results suggested that Model I was the better unsteady mathematical model.

7. RECOMMENDATIONS FOR FUTURE RESEARCH

While the use of models with unsteady terms to analyze oscillatory data is effective, it is possible that some improvements can be made. Not neglecting the effect of $C_{N_{\dot{q}}}$ (or the comparable terms for the other coefficients) in the mathematical model derivation may improve the estimation results. While the criteria used to justify its omission were valid, conditions may exist where the term's influence is substantial. Taking this effect into account could make the stability derivative estimates more accurate. Inclusion of the $C_{N_{\dot{q}}}$ term may also alleviate the problems caused by the sine and cosine terms for the roll and yaw axis oscillation models. The trigonometric terms might not apply to the new term when the model is derived. Also, the type of indicial function may be studied further to determine what is the best form to use.

Another item to be studied is the extension of the indicial function approach to other types of dynamic wind tunnel testing. For example, reference 9 describes a rotary-balance test rig that features the addition of oscillatory motion. Other different types of oscillatory testing are also in use. It may be possible to extend the indicial function approach to these test methods. This potentially could provide more accurate stability derivative estimates or estimates of parameters not included in the models for one-degree-of-freedom oscillatory motion.

REFERENCES

1. Pankhurst, R. C.; and Holder, D. W.: Wind-Tunnel Technique. London: Pitman, 1952, Revised 1965.
2. Chambers, J. R.; DiCarlo, D. J.; and Johnson, J. L., Jr.: Applications of Dynamic Stability Parameters to Problems in Aircraft Dynamics. AGARD-LS-114, pp. 17-1 to 17-12. 1981.
3. Klein, V.; and Noderer, K. D.: Modeling of Aircraft Unsteady Aerodynamic Characteristics. Part 2--Parameters Estimated From Wind Tunnel Data. NASA TM 110161. April 1995.
4. Klein, V.; Murphy, P.C.; Curry, T. J.; and Brandon, J. M.: Analysis of Wind Tunnel Longitudinal Static and Oscillatory Data of the F-16XL Aircraft. NASA TM-97-206276. Dec. 1997.
5. Whiting, M. R.: Differential Canard Deflection for Generation of Yawing Moment on the X-31 With and Without the Vertical Tail. M. S. Thesis. George Washington University. Jan. 1996.
6. Villeta, J. R.: Lateral-Directional Static and Dynamic Stability Analysis at High Angles of Attack for the X-31 Configuration. M. S. Thesis. George Washington University. Aug. 1992.
7. Grafton, S. B.; and Libbey, C. E.: Dynamic Stability Derivatives of a Twin-Jet Fighter Model for Angles of Attack From -10° to 110°. NASA TN D-6091. Jan. 1971.
8. Dickes, E.; Barnhart, B.; and Bihrle, W., Jr.: Analysis of Static and Rotational Aerodynamics at High Angles of Attack for Rockwell X-31A. BAR 91-7. Oct. 1991.
9. Rotary-Balance Testing for Aircraft Dynamics. AGARD-AR-265. Dec. 1990.
10. Simon, J. M.: Dynamic Derivative Data for High Angle of Attack Simulation. AIAA-92-4355-CP. Aug. 1992.

11. Blake, W. B.: A Study of the Rotary Balance Technique for Predicting Pitch Damping. AIAA-93-3619-CP. Aug. 1993.

12. Klein, V.; and Noderer, K. D.: Modeling of Aircraft Unsteady Aerodynamic Characteristics. Part I--Postulated Models. NASA TM 109120. May 1994.

13. Tobak, M.: On the Use of the Indicial Function Concept in the Analysis of Unsteady Motions of Wings and Wing-Tail Combinations. NACA Report 1188. 1954.

14. Finck, R. D.: USAF Stability and Control Datcom. AFWAL-TR-83-3048. Oct. 1960, Revised 1978.

15. Vukelich, S. R.; and Williams, J. E.: The USAF Stability and Control Digital Datcom. AFFDL-TR-79-3032. April 1979.

16. Blake, W. B.: Prediction of Fighter Aircraft Dynamic Derivatives Using Digital Datcom. AIAA-85-4070. Oct. 1985.

17. Thomas, R. W.: Analysis of Aircraft Stability and Control Design Methods. AFWAL-TR-84-3038. May 1984.

Table 1. Basic geometric characteristics of the X-31A. (Ref. 5)

	Full Scale	19%	13.3%
Center of Gravity:			
FS (inches)	269.2	51.0	35.8
BL (inches)	0.0	0.0	0.0
WL (inches)	-2.0	-0.38	-0.267
Wing:			
Span (ft)	22.83	4.34	3.04
Mean Aerodynamic Chord (ft)	12.35	2.35	1.65
Reference Area (sq. ft)	226.30	8.17	4.02
Aspect Ratio	2.30	2.3	2.3
Sweep, inboard (deg)	57	57	57
Sweep, outboard (deg)	45	45	45
Vertical Tail:			
Height (ft)	6.81	1.29	0.908
Reference Area (sq. ft)	37.55	1.35	0.668
Sweep (deg)	50	50	50
Volume Coefficient	0.0925	0.0925	0.0925
Fuselage:			
Length (ft)	43.33	8.23	5.78
Canard:			
Span (ft)	8.64	1.64	1.15
Reference Area, Total (sq. ft)	23.6	0.852	0.420
Aspect Ratio	3.18	3.18	3.18
Sweep (deg)	45	45	45

Table 2. Frequencies used in analysis for longitudinal cases.

f, hz	ω, rad/sec	k
0.25	1.5708	0.0201
0.40	2.5133	0.0322
0.60	3.7699	0.0483
0.80	5.0265	0.0643
1.00	6.2832	0.0804
1.19	7.4770	0.0957

Table 3. Frequencies used in analysis for lateral-directional cases.

f, hz	ω, rad/sec	k
0.25	1.5708	0.0371
0.40	2.5133	0.0593
0.60	3.7699	0.0890
0.80	5.0265	0.1186
1.00	6.2832	0.1483
1.20	7.5398	0.1779

Table 4. Expressions for aerodynamic coefficients with no unsteady terms.

In-phase	Out-of-phase
Pitching	
$C_{m_\alpha} - k^2 C_{m_{\dot{q}}}$	$C_{m_q} + C_{m_{\dot{\alpha}}}$
$C_{N_\alpha} - k^2 C_{N_{\dot{q}}}$	$C_{N_q} + C_{N_{\dot{\alpha}}}$
$C_{A_\alpha} - k^2 C_{A_{\dot{q}}}$	$C_{A_q} + C_{A_{\dot{\alpha}}}$
Rolling	
$C_{Y_\beta} \sin\alpha - k^2 C_{Y_{\dot{p}}}$	$C_{Y_p} + C_{Y_{\dot{\beta}}} \sin\alpha$
$C_{n_\beta} \sin\alpha - k^2 C_{n_{\dot{p}}}$	$C_{n_p} + C_{n_{\dot{\beta}}} \sin\alpha$
$C_{l_\beta} \sin\alpha - k^2 C_{l_{\dot{p}}}$	$C_{l_p} + C_{l_{\dot{\beta}}} \sin\alpha$
Yawing	
$C_{Y_\beta} \cos\alpha + k^2 C_{Y_{\dot{r}}}$	$C_{Y_r} - C_{Y_{\dot{\beta}}} \cos\alpha$
$C_{n_\beta} \cos\alpha + k^2 C_{n_{\dot{r}}}$	$C_{n_r} - C_{n_{\dot{\beta}}} \cos\alpha$
$C_{l_\beta} \cos\alpha + k^2 C_{l_{\dot{r}}}$	$C_{l_r} - C_{l_{\dot{\beta}}} \cos\alpha$

Table 5a. Measured in-phase components of normal-force coefficient. Pitch-axis oscillations.

Component	α, deg	k=0.0201	k=0.0322	k=0.0483	k=0.0643	k=0.0804	k=0.0957
$\overline{C}_{N_\alpha}$	0.0	2.9644	3.0093	3.0388	3.0308	3.0675	3.0679
	10.0	3.0490	3.0784	3.0853	3.1155	3.1086	3.1656
	15.0	3.0512	3.0192	3.0459	3.0456	3.0631	3.0755
	20.0	2.9015	2.9257	2.9651	2.9853	2.9931	2.9935
	25.0	2.2512	2.3124	2.4025	2.4988	2.5567	2.6446
	27.5	1.5669	1.7588	2.0242	2.2276	2.4063	2.5900
	30.0	1.0503	1.2950	1.6580	2.0583	2.3847	2.5579
	32.5	0.7645	1.0451	1.4478	1.8572	2.1304	2.4222
	35.0	0.8624	1.1175	1.4762	1.8220	2.1189	2.3325
	37.5	1.1976	1.3905	1.6922	2.0048	2.2077	2.3455
	40.0	1.3744	1.5706	1.8226	2.0318	2.2169	2.3848
	42.5	1.4045	1.6117	1.8757	2.1219	2.2684	2.4686
	45.0	1.5323	1.7273	1.9445	2.1456	2.2837	2.4480
	47.5	1.6601	1.8429	2.0133	2.1694	2.2989	2.4273
	50.0	1.5299	1.6314	1.8398	1.9920	2.1101	2.1813
	55.0	1.0131	1.2205	1.4974	1.7007	1.8115	1.8694
	60.0	0.5689	0.8753	1.1776	1.4707	1.6047	1.6987
	65.0	0.4255	0.7035	0.9406	1.1898	1.3275	1.4235
	70.0	0.3566	0.5232	0.7302	0.9407	1.0250	1.2002
	75.0	0.2487	0.3801	0.5411	0.6791	0.7615	0.8197
	80.0	0.2082	0.2219	0.3848	0.4526	0.5065	0.6488
	85.0	0.1377	0.2112	0.2306	0.3070	0.3176	0.3969
	88.0	0.0485	0.1537	0.1425	0.1899	0.2449	0.2600

Table 5b. Measured out-of-phase component of normal-force coefficient. Pitch-axis oscillations.

Component	α, deg	k=0.0201	k=0.0322	k=0.0483	k=0.0643	k=0.0804	k=0.0957
$\overline{C}_{N_q}$	0.0	7.3819	7.2324	6.4397	5.7717	5.2901	4.9654
	10.0	3.5563	4.7111	4.5399	4.5419	4.7022	4.6821
	15.0	4.1972	4.2075	4.4031	4.4406	4.3294	4.3789
	20.0	4.8884	5.9337	5.2135	4.8264	4.8108	4.6280
	25.0	12.3860	11.8060	11.4250	9.9515	9.4749	8.8731
	27.5	28.3080	23.0710	19.5670	16.4900	14.6790	12.5730
	30.0	37.9760	34.8380	29.1800	22.9610	19.1410	16.4260
	32.5	43.5530	39.3970	33.0350	27.5990	22.8270	18.9270
	35.0	37.8140	33.6610	27.2840	22.0400	19.0870	16.3390
	37.5	29.5150	25.5790	21.0190	18.0890	15.3390	13.4850
	40.0	25.7460	24.4820	19.3410	16.7250	14.3390	11.9340
	42.5	26.7710	23.3050	19.1120	15.1560	12.6090	10.8170
	45.0	23.9680	20.5280	16.9760	13.5630	11.4260	9.6863
	47.5	21.1640	17.7510	14.8400	11.9700	10.2430	8.5554
	50.0	18.4510	16.7520	14.0670	11.8780	10.5180	9.2547
	55.0	28.2390	22.9380	17.9190	13.3160	11.3750	10.1080
	60.0	36.1080	27.9480	21.6920	15.8220	12.9350	10.5460
	65.0	28.9460	25.5880	19.4510	15.1780	12.2360	10.0320
	70.0	25.7800	20.3700	16.3080	12.9660	10.4530	8.8396
	75.0	16.0550	15.3680	12.1220	9.7379	8.8626	7.5955
	80.0	9.1150	10.7460	9.4733	7.8003	6.9229	6.4940
	85.0	5.8386	6.6643	5.8922	5.0492	5.2447	4.2496
	88.0	7.5967	5.9899	5.5013	4.5757	3.6865	3.8332

Table 6a. Measured in-phase component of axial-force coefficient. Pitch-axis oscillations.

Component	α, deg	k=0.0201	k=0.0322	k=0.0483	k=0.0643	k=0.0804	k=0.0957
$\overline{C}_{A_\alpha}$	0.0	-0.2795	-0.2746	-0.2849	-0.2762	-0.2862	-0.2848
	10.0	-0.5876	-0.5936	-0.5937	-0.5980	-0.5970	-0.6121
	15.0	-0.6041	-0.5968	-0.6055	-0.6011	-0.6067	-0.6092
	20.0	-0.5488	-0.5526	-0.5593	-0.5639	-0.5665	-0.5711
	25.0	-0.3228	-0.3394	-0.3539	-0.3729	-0.3914	-0.4197
	27.5	-0.1274	-0.1595	-0.2051	-0.2429	-0.2852	-0.3264
	30.0	0.0014	-0.0398	-0.0922	-0.1672	-0.2316	-0.2701
	32.5	0.0498	0.0074	-0.0593	-0.1195	-0.1711	-0.2281
	35.0	0.0072	-0.0269	-0.0701	-0.1169	-0.1628	-0.1949
	37.5	0.0304	0.0021	-0.0546	-0.0919	-0.1206	-0.1402
	40.0	0.0668	0.0258	-0.0202	-0.0506	-0.0877	-0.1177
	42.5	0.0644	0.0223	-0.0284	-0.0735	-0.1076	-0.1487
	45.0	-0.0019	-0.0381	-0.0938	-0.1492	-0.1914	-0.2346
	47.5	-0.0682	-0.0985	-0.1592	-0.2249	-0.2751	-0.3205
	50.0	-0.1617	-0.1839	-0.2166	-0.2739	-0.2945	-0.3143
	55.0	-0.2576	-0.2957	-0.3348	-0.3761	-0.4129	-0.4089
	60.0	-0.1808	-0.2437	-0.3071	-0.3972	-0.4028	-0.4289
	65.0	-0.0745	-0.1645	-0.1965	-0.3171	-0.3077	-0.3165
	70.0	-0.0336	-0.0724	-0.1309	-0.1820	-0.2308	-0.2731
	75.0	-0.0377	-0.0660	-0.1169	-0.1708	-0.2095	-0.2248
	80.0	-0.1320	-0.1487	-0.1878	-0.2056	-0.2217	-0.2473
	85.0	-0.1280	-0.1429	-0.1456	-0.1519	-0.1644	-0.1893
	88.0	-0.0984	-0.1155	-0.1057	-0.1137	-0.1138	-0.1145

Table 6b. Measured out-of-phase component of axial-force coefficient. Pitch-axis oscillations.

Component	α, deg	k=0.0201	k=0.0322	k=0.0483	k=0.0643	k=0.0804	k=0.0957
$\overline{C}_{A_q}$	0.0	-0.9875	-0.9834	-0.8656	-0.7448	-0.7206	-0.6713
	10.0	-0.4132	-0.5735	-0.5488	-0.6012	-0.5803	-0.5987
	15.0	-0.6099	-0.5959	-0.5128	-0.5913	-0.5528	-0.5624
	20.0	-0.8181	-0.9397	-0.7487	-0.6911	-0.6851	-0.6618
	25.0	-2.6108	-2.3402	-2.3286	-2.0070	-1.8101	-1.6532
	27.5	-5.3939	-4.6436	-4.0475	-3.4463	-3.0479	-2.5955
	30.0	-6.8789	-6.3442	-5.3223	-4.3288	-3.6972	-3.1630
	32.5	-7.1502	-6.4088	-5.2353	-4.4113	-3.4749	-2.8161
	35.0	-5.4894	-4.6579	-3.6305	-2.9303	-2.5670	-2.1387
	37.5	-4.7378	-4.1495	-3.2195	-2.6751	-2.1803	-1.8402
	40.0	-5.3772	-4.7622	-3.6626	-2.9736	-2.4837	-2.1142
	42.5	-5.6872	-4.9292	-3.9794	-3.0719	-2.5298	-2.1806
	45.0	-5.5565	-4.7180	-3.9154	-2.8889	-2.3280	-1.8982
	47.5	-5.4259	-4.5068	-3.8513	-2.7060	-2.1261	-1.6159
	50.0	-2.9475	-2.6133	-2.1813	-1.6834	-1.4784	-1.2031
	55.0	-2.9148	-2.1853	-1.3904	-0.6488	-0.3670	-0.3806
	60.0	-4.8699	-3.8305	-2.6422	-1.5768	-1.1129	-0.6621
	65.0	-4.8362	-4.4163	-3.2913	-2.1396	-1.7411	-1.2413
	70.0	-4.5385	-3.4046	-2.7931	-2.1076	-1.5282	-1.2472
	75.0	-3.4333	-3.3004	-2.4056	-1.8296	-1.5997	-1.3912
	80.0	-1.5134	-1.5978	-1.3987	-0.8530	-0.7322	-0.5955
	85.0	-0.4405	-0.5961	-0.6032	-0.5116	-0.4688	-0.4299
	88.0	-0.8655	-0.8608	-0.8479	-0.6208	-0.6558	-0.6157

Table 7a. Measured in-phase component of pitching-moment coefficient. Pitch-axis oscillations.

Component	α, deg	k=0.0201	k=0.0322	k=0.0483	k=0.0643	k=0.0804	k=0.0957
$\overline{C}_{m_\alpha}$	0.0	-0.0805	-0.0712	-0.0743	-0.0836	-0.0468	-0.0661
	10.0	-0.0105	-0.0190	-0.0086	-0.0151	0.0222	-0.0026
	15.0	0.1116	0.1101	0.1077	0.1047	0.1381	0.1116
	20.0	0.2564	0.2455	0.2363	0.2345	0.2633	0.2399
	25.0	0.2046	0.2078	0.1921	0.1763	0.1932	0.1593
	27.5	0.1063	0.1095	0.0929	0.0736	0.0903	0.0637
	30.0	0.0521	0.0598	0.0353	0.0092	0.0283	-0.0164
	32.5	0.0827	0.0797	0.0688	0.0332	0.0432	-0.0015
	35.0	0.1043	0.0889	0.0579	0.0189	0.0149	-0.0432
	37.5	0.0938	0.0661	0.0321	-0.0235	-0.0319	-0.0735
	40.0	0.0698	0.0492	-0.0021	-0.0506	-0.0490	-0.1055
	42.5	0.0662	0.0310	-0.0291	-0.0974	-0.0982	-0.1714
	45.0	-0.0199	-0.0476	-0.1063	-0.1537	-0.1607	-0.2117
	47.5	-0.1060	-0.1261	-0.1835	-0.2099	-0.2233	-0.2521
	50.0	-0.0546	-0.0808	-0.1308	-0.1590	-0.1887	-0.2153
	55.0	0.0846	0.0361	-0.0445	-0.0951	-0.1289	-0.1585
	60.0	0.0098	-0.0476	-0.1042	-0.1613	-0.1985	-0.2229
	65.0	-0.1508	-0.1814	-0.2210	-0.2589	-0.2937	-0.3072
	70.0	-0.3168	-0.3213	-0.3448	-0.3603	-0.3490	-0.3590
	75.0	-0.3905	-0.3987	-0.4062	-0.4004	-0.3851	-0.3655
	80.0	-0.3371	-0.3135	-0.3358	-0.3431	-0.3509	-0.3650
	85.0	-0.3841	-0.3929	-0.3932	-0.4122	-0.4148	-0.3996
	88.0	-0.4106	-0.4162	-0.4315	-0.4420	-0.4575	-0.4395

Table 7b. Measured out-of-phase component of pitching-moment coefficient. Pitch-axis oscillations.

Component	α, deg	k=0.0201	k=0.0322	k=0.0483	k=0.0643	k=0.0804	k=0.0957
$\overline{C}_{m_q}$	0.0	-1.3311	-1.3257	-1.2309	-1.3829	-1.3414	-1.3496
	10.0	-1.4057	-1.3000	-1.4350	-1.3010	-1.3959	-1.4256
	15.0	-2.2334	-1.9633	-1.8958	-1.8188	-1.8282	-1.8942
	20.0	-2.6677	-2.6009	-2.6323	-2.5487	-2.5324	-2.4871
	25.0	-3.4637	-3.1751	-3.0431	-2.9947	-2.8638	-2.8015
	27.5	-2.7033	-2.7150	-2.8446	-2.7941	-2.7511	-2.7952
	30.0	-3.4375	-3.5230	-3.2897	-3.1202	-2.8808	-2.8039
	32.5	-4.3033	-4.0930	-4.2917	-3.7993	-3.8028	-3.6685
	35.0	-5.3307	-5.0833	-4.7723	-4.3824	-4.1151	-3.9903
	37.5	-6.3114	-5.6738	-4.8771	-4.3377	-3.9514	-3.7483
	40.0	-6.6859	-6.1380	-5.3756	-5.0104	-4.5129	-4.0015
	42.5	-6.8577	-6.4663	-5.7257	-4.9542	-4.3354	-3.9234
	45.0	-6.3878	-5.8314	-4.9620	-4.3785	-3.9751	-3.5760
	47.5	-5.9178	-5.1965	-4.1984	-3.8029	-3.6149	-3.2286
	50.0	-6.0593	-5.7958	-5.0830	-4.3470	-3.9861	-3.6628
	55.0	-9.2338	-8.0336	-6.9525	-5.9864	-5.2790	-4.8483
	60.0	-9.4763	-7.5477	-6.2749	-5.2536	-4.6959	-4.1613
	65.0	-6.4440	-5.5953	-5.0093	-3.9720	-3.7720	-3.3335
	70.0	-4.3785	-3.9715	-3.1556	-2.9936	-2.6346	-2.6024
	75.0	-1.8598	-2.1815	-1.9029	-2.0292	-2.0935	-2.0749
	80.0	-2.3493	-3.2793	-2.9855	-2.9844	-2.9938	-3.1111
	85.0	-2.4780	-2.7302	-2.8948	-2.6485	-2.7628	-2.5395
	88.0	-3.5091	-2.6139	-2.7245	-2.4417	-2.2283	-2.2611

Table 8a. Measured in-phase component of rolling-moment coefficient. Roll-axis oscillations.

Component	α, deg	k=0.0371	k=0.0593	k=0.0890	k=0.1186	k=0.1483	k=0.1779
$\overline{C}_{l_\beta}$	0.0	-0.0003	0.0111	0.0005	-0.0020	0.0045	0.0009
	10.0	0.0094	0.0100	-0.0020	0.0023	-0.0020	-0.0074
	15.0	-0.0096	-0.0082	-0.0163	-0.0103	-0.0131	-0.0203
	20.0	-0.0275	-0.0242	-0.0273	-0.0293	-0.0300	-0.0329
	25.0	-0.0682	-0.0545	-0.0594	-0.0590	-0.0454	-0.0493
	27.5	-0.0272	-0.0237	-0.0276	-0.0208	-0.0189	-0.0129
	30.0	-0.0567	-0.0461	-0.0542	-0.0431	-0.0373	-0.0351
	32.5	-0.1485	-0.1118	-0.0981	-0.0705	-0.0703	-0.0740
	35.0	-0.1899	-0.1756	-0.1647	-0.1343	-0.1257	-0.1129
	37.5	-0.2003	-0.1724	-0.1578	-0.1350	-0.1132	-0.1024
	40.0	-0.1722	-0.1634	-0.1431	-0.1235	-0.1123	-0.0937
	42.5	-0.1005	-0.1022	-0.1149	-0.1178	-0.1140	-0.1102
	45.0	-0.0895	-0.0819	-0.0865	-0.0811	-0.0863	-0.0828
	47.5	-0.0761	-0.0695	-0.0806	-0.0726	-0.0651	-0.0703
	50.0	-0.0692	-0.0609	-0.0622	-0.0664	-0.0577	-0.0559
	55.0	-0.0742	-0.0760	-0.0669	-0.0750	-0.0688	-0.0613
	60.0	-0.0858	-0.0697	-0.0751	-0.0771	-0.0791	-0.0758
	65.0	-0.0725	-0.0679	-0.0801	-0.0801	-0.0823	-0.0794
	70.0	-0.0810	-0.0742	-0.0851	-0.0733	-0.0828	-0.0844
	80.0	-0.0978	-0.0918	-0.0965	-0.0954	-0.0928	-0.0887
	90.0	-0.1030	-0.1002	-0.1070	-0.1055	-0.1046	-0.1093

Table 8b. Measured out-of-phase component of rolling-moment coefficient. Roll-axis oscillations.

Component	α, deg	k=0.0371	k=0.0593	k=0.0890	k=0.1186	k=0.1483	k=0.1779
$\overline{C}_{l_p}$	0.0	-0.1783	-0.1344	-0.2939	-0.2711	-0.2319	-0.2205
	10.0	-0.3405	-0.1882	-0.3277	-0.3053	-0.2755	-0.2416
	15.0	-0.3075	-0.1498	-0.1880	-0.2643	-0.2049	-0.2347
	20.0	-0.0190	-0.1332	-0.2368	-0.1913	-0.2164	-0.2177
	25.0	0.0211	0.0145	-0.0650	-0.1395	-0.0997	-0.0959
	27.5	-0.0336	0.0850	-0.0506	-0.1414	-0.1461	-0.1817
	30.0	0.3584	0.2553	0.0670	0.0264	-0.0250	-0.0907
	32.5	1.3111	0.8771	0.6045	0.4370	0.2905	0.1561
	35.0	1.0869	1.0373	0.7485	0.6641	0.5410	0.4028
	37.5	1.4454	1.3413	0.9794	0.7022	0.5476	0.4890
	40.0	1.2772	0.9859	0.8215	0.5501	0.4889	0.4715
	42.5	-0.2458	-0.0548	0.0232	0.1746	0.2380	0.2241
	45.0	0.0829	0.1436	0.0532	0.0938	0.1147	0.1494
	47.5	0.2477	0.1610	0.1182	0.1300	0.1131	0.0907
	50.0	0.1679	0.0852	0.0199	0.0610	0.0372	-0.0546
	55.0	0.0468	0.0183	-0.1580	0.0532	0.0404	0.0035
	60.0	0.0981	0.1520	-0.0294	0.0468	-0.0940	-0.0377
	65.0	-0.0260	-0.1666	-0.0587	-0.1005	-0.1703	-0.1021
	70.0	-0.0542	-0.0051	-0.0881	-0.0987	-0.0981	-0.1070
	80.0	-0.0179	0.0308	0.0809	-0.1409	-0.1250	-0.1156
	90.0	-0.1670	-0.0884	-0.1284	-0.1718	-0.0578	-0.0660

Table 9a. Measured in-phase component of yawing-moment coefficient. Roll-axis oscillations.

Component	α, deg	k=0.0371	k=0.0593	k=0.0890	k=0.1186	k=0.1483	k=0.1779
$\overline{C}_{n_\beta}$	0.0	0.0028	0.0034	0.0022	0.0014	0.0010	0.0007
	10.0	0.0300	0.0303	0.0256	0.0331	0.0306	0.0217
	15.0	0.0254	0.0238	0.0210	0.0285	0.0245	0.0213
	20.0	-0.0012	-0.0004	0.0040	-0.0024	-0.0048	-0.0010
	25.0	-0.0156	-0.0155	-0.0212	-0.0124	-0.0180	-0.0228
	27.5	-0.0388	-0.0472	-0.0535	-0.0485	-0.0476	-0.0438
	30.0	-0.0170	-0.0322	-0.0476	-0.0607	-0.0486	-0.0362
	32.5	0.0529	0.0349	0.0031	-0.0110	-0.0095	0.0091
	35.0	0.1027	0.0883	0.0784	0.0614	0.0574	0.0543
	37.5	0.1235	0.1120	0.0814	0.0612	0.0567	0.0453
	40.0	0.1552	0.1402	0.1359	0.0908	0.0864	0.0593
	42.5	0.1226	0.1266	0.1284	0.1270	0.1052	0.1191
	45.0	0.0852	0.0876	0.0807	0.0763	0.0779	0.0672
	47.5	0.0591	0.0607	0.0586	0.0405	0.0429	0.0480
	50.0	0.0832	0.0819	0.0700	0.0675	0.0786	0.0794
	55.0	0.1511	0.1587	0.1420	0.1432	0.1362	0.1262
	60.0	0.1885	0.1866	0.1826	0.1704	0.1811	0.1491
	65.0	0.0429	0.0553	-0.0262	0.0477	0.1198	0.0003
	70.0	-0.2327	-0.2326	-0.2350	-0.2393	-0.2377	-0.2256
	80.0	-0.2377	-0.2342	-0.2224	-0.2253	-0.1962	-0.2217
	90.0	-0.0760	-0.0610	-0.0623	-0.0711	-0.0687	-0.0539

Table 9b. Measured out-of-phase component of yawing-moment coefficient. Roll-axis oscillations.

Component	α, deg	k=0.0371	k=0.0593	k=0.0890	k=0.1186	k=0.1483	k=0.1779
$\overline{C}_{n_p}$	0.0	0.0383	0.0699	0.0260	0.0082	0.0179	0.0056
	10.0	-0.0698	-0.0034	-0.0079	-0.0087	-0.0098	0.0073
	15.0	-0.0523	-0.0352	-0.1034	-0.0653	-0.0497	-0.0691
	20.0	-0.0522	-0.0493	-0.0754	-0.0116	-0.0597	-0.0719
	25.0	-0.2142	0.0117	-0.0492	-0.0324	-0.0089	0.0049
	27.5	-0.0014	-0.0975	-0.0676	0.0012	-0.0429	0.0222
	30.0	-0.4294	-0.3884	-0.1247	-0.0572	-0.0575	-0.0044
	32.5	-1.2851	-0.8479	-0.6237	-0.4568	-0.2925	-0.2671
	35.0	-1.0604	-0.8571	-0.7261	-0.6674	-0.5516	-0.5299
	37.5	-1.4513	-1.4141	-1.0624	-0.9252	-0.7200	-0.6794
	40.0	-2.0667	-1.6895	-1.4713	-1.1341	-1.0936	-0.9697
	42.5	0.2998	-0.0644	-0.3285	-0.4958	-0.8048	-0.6602
	45.0	-0.9418	-0.5928	-0.6890	-0.7208	-0.7447	-0.6437
	47.5	-0.4427	-0.6524	-0.5456	-0.4521	-0.4571	-0.4236
	50.0	-0.2813	-0.5183	-0.4425	-0.4725	-0.4357	-0.4101
	55.0	-0.7189	-0.8262	-0.7097	-0.8586	-0.7045	-0.7565
	60.0	-1.2318	-1.2808	-1.2629	-1.0405	-0.7069	-0.8855
	65.0	-0.6309	-0.8584	-0.6628	-0.8312	-0.5580	-0.7496
	70.0	-0.0168	-0.0628	-0.0628	-0.0362	-0.1187	-0.0365
	80.0	0.1713	0.3604	0.0200	0.2448	0.1940	0.1797
	90.0	-0.0734	-0.1218	-0.0325	-0.0953	0.0737	0.2000

Table 10a. Measured in-phase component of side-force coefficient. Roll-axis oscillations.

Component	α, deg	k=0.0371	k=0.0593	k=0.0890	k=0.1186	k=0.1483	k=0.1779
$\overline{C}_{Y_\beta}$	0.0	-0.0277	0.0014	0.0242	0.0027	-0.0149	-0.0164
	10.0	-0.2574	-0.2595	-0.2254	-0.2514	-0.2355	-0.2049
	15.0	-0.2988	-0.2785	-0.3038	-0.3120	-0.2887	-0.3063
	20.0	-0.3285	-0.3283	-0.3277	-0.3131	-0.3165	-0.3299
	25.0	-0.4019	-0.3663	-0.3802	-0.3819	-0.3908	-0.3745
	27.5	-0.4285	-0.3977	-0.3946	-0.3952	-0.4189	-0.4065
	30.0	-0.3945	-0.3909	-0.3821	-0.3809	-0.4072	-0.4200
	32.5	-0.2217	-0.2489	-0.2656	-0.2817	-0.3092	-0.3450
	35.0	-0.1525	-0.1540	-0.1803	-0.2387	-0.2651	-0.2700
	37.5	-0.0308	-0.0653	-0.1377	-0.1743	-0.2318	-0.2494
	40.0	-0.0420	-0.0728	-0.1366	-0.1720	-0.2098	-0.2480
	42.5	-0.2023	-0.1681	-0.1466	-0.1320	-0.1144	-0.1184
	45.0	-0.0072	-0.0226	0.0290	0.0367	0.0522	0.1221
	47.5	0.2368	0.2445	0.2914	0.3295	0.3378	0.3236
	50.0	0.4275	0.4521	0.4640	0.4584	0.4287	0.5053
	55.0	0.1839	0.2256	0.1881	0.3133	0.3044	0.3310
	60.0	0.2909	0.3691	0.4116	0.4608	0.4038	0.5307
	65.0	0.2953	0.3584	0.2844	0.4873	0.4188	0.5164
	70.0	0.1061	0.1440	0.1572	0.1770	0.1506	0.1372
	80.0	0.1232	0.1094	0.1039	0.0593	0.0213	0.0556
	90.0	0.0586	0.0404	0.0418	0.0140	-0.0198	-0.0046

Table 10b. Measured out-of-phase component of side-force coefficient. Roll-axis oscillations.

Component	α, deg	k=0.0371	k=0.0593	k=0.0890	k=0.1186	k=0.1483	k=0.1779
$\overline{C}_{Y_p}$	0.0	0.2293	-0.3053	0.0658	0.0759	0.1364	0.1447
	10.0	0.1480	0.1000	0.2558	0.0677	0.2342	0.1866
	15.0	0.4670	0.2649	0.4995	0.2518	0.2951	0.2616
	20.0	0.5192	0.0985	0.1672	0.1182	0.1526	0.1761
	25.0	0.1770	-0.1940	-0.0282	-0.0974	-0.0810	-0.0212
	27.5	0.1599	0.2469	0.2740	0.0501	0.1228	0.0408
	30.0	-0.5858	-0.1358	-0.2439	-0.1524	-0.0638	-0.1919
	32.5	-1.0657	-1.3661	-0.9983	-0.7950	-0.6163	-0.4033
	35.0	-1.5901	-1.0848	-1.2104	-0.9084	-0.7216	-0.6148
	37.5	-2.4393	-2.4381	-2.0775	-1.5656	-1.1642	-0.8205
	40.0	-2.3031	-1.9522	-2.0344	-1.3683	-0.8929	-0.7866
	42.5	0.5250	0.5444	0.3402	-0.1301	-0.0809	-0.0744
	45.0	1.4551	0.9332	0.6810	0.4220	0.3758	-0.0086
	47.5	-0.2069	0.3485	0.0101	-0.8433	-0.4764	-0.5636
	50.0	-0.6460	-0.0776	-1.2388	-1.2086	-1.4195	-1.0678
	55.0	1.1938	0.7093	0.4900	0.0150	-0.0336	0.0604
	60.0	0.7729	0.8654	0.2764	0.1047	-0.1630	-0.4845
	65.0	0.6884	1.2056	0.0519	-0.1131	-1.3147	-0.6338
	70.0	0.0819	-0.1974	-0.1726	-0.0998	-0.0748	-0.3628
	80.0	-0.7640	-1.4649	-1.1196	-1.2360	-0.9720	-1.0373
	90.0	-0.1028	-1.0847	-0.9980	-0.6591	-1.6847	-2.0007

Table 11a. Measured in-phase component of rolling-moment coefficient. Yaw-axis oscillations.

Component	α, deg	k=0.0371	k=0.0593	k=0.0890	k=0.1186	k=0.1483	k=0.1779
$\overline{C}_{l_\beta}$	0.0	0.0557	0.0571	0.0594	0.0542	0.0559	0.0527
	10.0	-0.0188	-0.0223	-0.0217	-0.0209	-0.0197	-0.0288
	15.0	-0.0967	-0.0993	-0.1069	-0.1036	-0.1070	-0.1083
	20.0	-0.1024	-0.1039	-0.1021	-0.1063	-0.1110	-0.1122
	25.0	-0.1283	-0.1293	-0.1299	-0.1365	-0.1393	-0.1480
	27.5	-0.1381	-0.1383	-0.1266	-0.1299	-0.1255	-0.1230
	30.0	-0.1614	-0.1310	-0.1072	-0.1049	-0.0957	-0.0942
	32.5	-0.1975	-0.1746	-0.1559	-0.1281	-0.1211	-0.1195
	35.0	-0.2748	-0.2586	-0.2381	-0.2196	-0.1992	-0.1789
	37.5	-0.2872	-0.2662	-0.2476	-0.2039	-0.1901	-0.1832
	40.0	-0.2696	-0.2743	-0.2355	-0.2185	-0.1939	-0.1882
	42.5	-0.1459	-0.1656	-0.1764	-0.1707	-0.1744	-0.1535
	45.0	-0.1222	-0.1296	-0.1318	-0.1336	-0.1343	-0.1215
	47.5	-0.0931	-0.1001	-0.1004	-0.1114	-0.1066	-0.1023
	50.0	-0.0795	-0.0850	-0.0888	-0.0849	-0.0889	-0.0894
	55.0	-0.0489	-0.0489	-0.0485	-0.0561	-0.0557	-0.0542
	60.0	-0.0517	-0.0483	-0.0473	-0.0533	-0.0457	-0.0450
	65.0	-0.0408	-0.0409	-0.0366	-0.0390	-0.0371	-0.0372
	70.0	-0.0276	-0.0284	-0.0291	-0.0329	-0.0302	-0.0351
	75.0	-0.0238	-0.0239	-0.0239	-0.0254	-0.0244	-0.0253
	80.0	-0.0170	-0.0178	-0.0183	-0.0169	-0.0118	-0.0120
	85.0	-0.0145	-0.0118	-0.0129	-0.0101	-0.0121	-0.0151
	90.0	-0.0051	-0.0074	-0.0009	-0.0007	0.0017	-0.0028

Table 11b. Measured out-of-phase component of rolling-moment coefficient. Yaw-axis oscillations.

Component	α, deg	k=0.0371	k=0.0593	k=0.0890	k=0.1186	k=0.1483	k=0.1779
$\overline{C}_{l_r}$	0.0	0.1038	0.0528	0.1009	0.1529	0.1248	0.0929
	10.0	0.2514	0.2463	0.2284	0.1923	0.2267	0.2573
	15.0	0.2275	0.1868	0.1560	0.1997	0.2096	0.2040
	20.0	0.2844	0.3813	0.3296	0.3901	0.3739	0.3842
	25.0	0.2547	0.2512	0.3751	0.3634	0.4274	0.3910
	27.5	0.0975	0.1210	0.2094	0.3197	0.3235	0.4137
	30.0	-1.2594	-0.7124	-0.1764	0.0339	0.2694	0.3344
	32.5	-1.1117	-0.9104	-0.3248	-0.1709	0.0107	0.2229
	35.0	-1.5339	-1.0524	-0.6853	-0.5322	-0.4036	-0.2989
	37.5	-1.2108	-1.2361	-0.9612	-0.6479	-0.4567	-0.2928
	40.0	-1.2149	-0.9945	-0.6646	-0.5499	-0.4130	-0.3221
	42.5	0.5155	0.1485	-0.0047	-0.1399	-0.2439	-0.2865
	45.0	0.3472	0.1234	0.0197	-0.0711	-0.1014	-0.1212
	47.5	0.0197	0.0755	0.0321	0.0135	-0.0084	-0.0374
	50.0	0.2216	0.2434	0.1267	0.1154	0.0560	0.0740
	55.0	0.0790	0.0676	0.2428	0.1899	0.1855	0.1428
	60.0	-0.0412	-0.0102	0.0441	0.0187	0.1092	0.0885
	65.0	0.0079	0.0378	0.0154	0.0197	0.0518	0.0351
	70.0	0.0555	0.0680	0.0803	0.0762	0.0764	0.0344
	75.0	0.0791	0.0449	0.0248	0.0230	0.0280	0.0393
	80.0	0.0677	0.0703	0.1038	0.0495	0.0421	0.0570
	85.0	0.0988	-0.0173	0.1675	0.0948	0.1335	0.0996
	90.0	0.1090	0.0351	0.0469	0.0407	0.0691	0.0613

Table 12a. Measured in-phase component of yawing-moment coefficient. Yaw-axis oscillations.

Component	α, deg	k=0.0371	k=0.0593	k=0.0890	k=0.1186	k=0.1483	k=0.1779
$\overline{C}_{n_\beta}$	0.0	0.0686	0.0756	0.0784	0.0817	0.0774	0.0971
	10.0	0.0957	0.0985	0.0997	0.1083	0.1059	0.1164
	15.0	0.0886	0.0928	0.0889	0.0991	0.0905	0.1104
	20.0	-0.0169	-0.0073	-0.0107	0.0015	-0.0033	0.0042
	25.0	-0.0738	-0.0685	-0.0575	-0.0611	-0.0404	-0.0295
	27.5	-0.0643	-0.0598	-0.0628	-0.0468	-0.0499	-0.0308
	30.0	-0.0379	-0.0682	-0.0789	-0.0901	-0.1089	-0.0932
	32.5	0.0485	0.0189	0.0026	-0.0286	-0.0604	-0.0455
	35.0	0.0955	0.0856	0.0575	0.0444	0.0217	0.0066
	37.5	0.0990	0.0842	0.0586	0.0166	-0.0197	-0.0247
	40.0	0.1347	0.1083	0.0900	0.0434	-0.0055	-0.0281
	42.5	0.1912	0.1802	0.1593	0.1347	0.0830	0.0428
	45.0	0.1262	0.1147	0.1032	0.2488	0.0597	0.0345
	47.5	0.0289	0.0064	0.0053	0.3196	-0.0165	-0.0299
	50.0	-0.0105	-0.0251	-0.0300	0.2350	-0.0514	-0.0336
	55.0	0.0064	0.0134	-0.0315	0.3081	-0.0133	0.0038
	60.0	0.0819	0.0871	0.0514	0.3763	0.0429	0.0262
	65.0	0.1167	0.0966	0.0823	0.4008	0.0639	0.0218
	70.0	-0.0631	-0.0562	-0.0592	0.2592	-0.0480	-0.0618
	75.0	-0.0833	-0.0851	-0.0831	0.2314	-0.0938	-0.0851
	80.0	-0.0524	-0.0446	-0.0617	0.2434	-0.0511	-0.0646
	85.0	-0.0260	-0.0398	-0.0385	0.2685	-0.0341	-0.0523
	90.0	0.0067	0.0074	-0.0002	0.3093	-0.0030	0.0084

Table 12b. Measured out-of-phase component of yawing-moment coefficient. Yaw-axis oscillations.

Component	α, deg	k=0.0371	k=0.0593	k=0.0890	k=0.1186	k=0.1483	k=0.1779
$\overline{C}_{n_r}$	0.0	-0.7696	-0.7513	-0.7474	-0.7478	-0.7580	-0.7660
	10.0	-0.7809	-0.7005	-0.7527	-0.7954	-0.7711	-0.7930
	15.0	-0.6904	-0.6840	-0.7701	-0.7778	-0.7800	-0.7777
	20.0	-1.0426	-0.8424	-0.9537	-0.9033	-0.9300	-0.9629
	25.0	-1.2447	-1.0885	-1.1340	-1.1171	-1.1045	-1.1303
	27.5	-1.0309	-1.0051	-1.1080	-1.0507	-1.0791	-1.1582
	30.0	0.7704	0.2054	-0.2155	-0.4894	-0.7030	-0.8039
	32.5	1.0242	0.7483	0.2443	-0.1156	-0.2741	-0.4265
	35.0	0.7701	0.6548	0.3935	0.2732	0.1909	0.1025
	37.5	1.2423	1.1722	1.0214	0.7486	0.6235	0.4700
	40.0	2.1476	1.7036	1.7573	1.3286	1.0983	0.9858
	42.5	1.5566	1.7716	1.3620	1.3903	1.5296	1.3853
	45.0	0.6779	0.8042	1.0254	1.1466	0.9245	1.0105
	47.5	0.3047	0.5082	0.6091	0.7292	0.5482	0.4807
	50.0	0.7284	0.5022	0.4884	0.2342	0.4258	0.6051
	55.0	0.7536	0.4378	0.5457	0.6687	0.7144	0.8218
	60.0	0.9760	0.8150	0.8129	0.6892	0.8533	0.7957
	65.0	1.6615	1.3927	1.3356	1.2085	1.0574	1.2092
	70.0	-0.2518	-0.3184	-0.3248	-0.1049	-0.1343	-0.1290
	75.0	-0.2207	-0.3465	-0.3335	-0.1851	-0.3241	-0.3004
	80.0	-0.3594	-0.3025	-0.2203	-0.0807	-0.1698	-0.3343
	85.0	-0.4654	-0.4997	-0.1424	-0.0324	-0.1964	-0.2423
	90.0	-0.0649	-0.1229	-0.2202	-0.2131	-0.2903	-0.2440

Table 13a. Measured in-phase component of side-force coefficient. Yaw-axis oscillations.

Component	α, deg	k=0.0371	k=0.0593	k=0.0890	k=0.1186	k=0.1483	k=0.1779
$\overline{C}_{Y_\beta}$	0.0	-1.2071	-1.2006	-1.2296	-1.2580	-1.2756	-1.2894
	10.0	-1.3089	-1.3130	-1.3061	-1.3237	-1.3518	-1.3503
	15.0	-1.1909	-1.2256	-1.2072	-1.2298	-1.2244	-1.2622
	20.0	-0.9923	-1.0209	-1.0236	-1.0474	-1.0626	-1.0953
	25.0	-0.8815	-0.8780	-0.8983	-0.9354	-0.9445	-0.9943
	27.5	-0.8716	-0.8775	-0.8916	-0.9543	-0.9531	-0.9940
	30.0	-0.6809	-0.7087	-0.7173	-0.7513	-0.7532	-0.7956
	32.5	-0.3937	-0.4307	-0.5104	-0.5390	-0.5669	-0.6307
	35.0	-0.1842	-0.2331	-0.2939	-0.3454	-0.3863	-0.4094
	37.5	-0.0391	-0.0744	-0.1464	-0.2134	-0.2477	-0.3028
	40.0	0.0200	-0.0036	-0.0931	-0.1306	-0.1547	-0.1717
	42.5	-0.2125	-0.1577	-0.1056	-0.0863	-0.0450	-0.0397
	45.0	-0.1393	-0.0936	-0.0327	0.0083	0.0725	0.1223
	47.5	0.0566	0.1150	0.1580	0.1699	0.2397	0.2796
	50.0	0.3130	0.3583	0.4227	0.4224	0.4653	0.4970
	55.0	0.0758	0.1087	0.2009	0.2052	0.2929	0.3268
	60.0	0.1056	0.1425	0.1678	0.1499	0.2317	0.3734
	65.0	0.1375	0.1685	0.2647	0.2849	0.3155	0.3322
	70.0	0.0416	0.0459	0.0674	0.0611	0.1194	0.1632
	75.0	0.0255	0.0558	0.0332	-0.0046	0.0428	0.0029
	80.0	0.0457	0.0205	0.0571	0.0339	0.0301	0.0449
	85.0	0.0368	0.0733	0.0894	0.0675	0.1224	0.1106
	90.0	0.0393	0.0338	0.0497	0.0021	0.0308	0.0502

Table 13b. Measured out-of-phase component of side-force coefficient. Yaw-axis oscillations.

Component	α, deg	k=0.0371	k=0.0593	k=0.0890	k=0.1186	k=0.1483	k=0.1779
$\overline{C}_{Y_r}$	0.0	0.7261	0.6392	0.8237	1.1890	1.3541	1.4379
	10.0	1.0827	0.3108	0.8036	1.1440	1.1683	1.3027
	15.0	0.8243	1.0339	1.0699	1.3983	1.3053	1.4407
	20.0	0.9669	1.0009	1.4554	1.4873	1.5582	1.6336
	25.0	1.4195	1.1909	1.9273	1.6202	1.9135	1.9351
	27.5	1.3266	1.5696	1.7907	1.5701	1.5969	1.7379
	30.0	1.9311	1.7005	1.9808	1.6946	1.8877	1.8956
	32.5	3.6799	3.2349	2.9141	2.5638	2.1983	2.3083
	35.0	3.7730	2.7103	2.6575	2.4252	2.1272	1.9476
	37.5	3.3288	3.2430	2.9257	2.2714	1.8962	1.7730
	40.0	2.3255	2.3049	1.9268	1.5337	1.1640	1.0708
	42.5	-2.6066	-1.9045	-1.0118	-0.9485	-0.5004	-0.2662
	45.0	-2.4425	-1.9047	-1.5228	-1.2635	-0.6128	-0.4561
	47.5	-1.2037	-1.1548	-0.8032	-0.5239	-0.0885	0.2458
	50.0	-1.4719	-0.7216	0.0742	0.5609	0.6286	0.4907
	55.0	-1.7574	-1.5515	-1.6808	-1.6010	-1.2863	-0.9604
	60.0	-1.5675	-1.8584	-1.6011	-0.8926	-1.2269	-0.8953
	65.0	-1.9387	-1.5712	-0.8955	-0.1233	0.1583	0.3807
	70.0	-0.5665	-0.3958	-0.5769	-0.6126	-0.6725	-0.0295
	75.0	-0.4481	-0.2195	-0.1820	-0.3372	-0.1956	-0.4398
	80.0	0.0507	-0.2337	-0.5623	-0.5267	-0.5402	-0.1111
	85.0	-0.4420	0.5036	-0.7752	-0.6032	-0.6948	-0.4142
	90.0	-0.7074	-0.5092	-0.0164	-0.1749	-0.4182	-0.1543

Table 14. Expressions for aerodynamic coefficients with unsteady terms. Model I.

In-phase	Out-of-phase
Pitching	
$C_{m_\alpha} - a\frac{\tau_1^2 k^2}{1+\tau_1^2 k^2}$	$C_{m_q} - a\frac{\tau_1}{1+\tau_1^2 k^2}$
$C_{N_\alpha} - a\frac{\tau_1^2 k^2}{1+\tau_1^2 k^2}$	$C_{N_q} - a\frac{\tau_1}{1+\tau_1^2 k^2}$
$C_{A_\alpha} - a\frac{\tau_1^2 k^2}{1+\tau_1^2 k^2}$	$C_{A_q} - a\frac{\tau_1}{1+\tau_1^2 k^2}$
Rolling	
$C_{Y_\beta}\sin\alpha - a\frac{\tau_1^2 k^2}{1+\tau_1^2 k^2}\sin\alpha$	$C_{Y_p} - a\frac{\tau_1}{1+\tau_1^2 k^2}\sin\alpha$
$C_{n_\beta}\sin\alpha - a\frac{\tau_1^2 k^2}{1+\tau_1^2 k^2}\sin\alpha$	$C_{n_p} - a\frac{\tau_1}{1+\tau_1^2 k^2}\sin\alpha$
$C_{l_\beta}\sin\alpha - a\frac{\tau_1^2 k^2}{1+\tau_1^2 k^2}\sin\alpha$	$C_{l_p} - a\frac{\tau_1}{1+\tau_1^2 k^2}\sin\alpha$
Yawing	
$C_{Y_\beta}\cos\alpha - a\frac{\tau_1^2 k^2}{1+\tau_1^2 k^2}\cos\alpha$	$C_{Y_r} + a\frac{\tau_1}{1+\tau_1^2 k^2}\cos\alpha$
$C_{n_\beta}\cos\alpha - a\frac{\tau_1^2 k^2}{1+\tau_1^2 k^2}\cos\alpha$	$C_{n_r} + a\frac{\tau_1}{1+\tau_1^2 k^2}\cos\alpha$
$C_{l_\beta}\cos\alpha - a\frac{\tau_1^2 k^2}{1+\tau_1^2 k^2}\cos\alpha$	$C_{l_r} + a\frac{\tau_1}{1+\tau_1^2 k^2}\cos\alpha$

Table 15. Expressions for aerodynamic coefficients with unsteady terms. Model II.

In-phase	Out-of-phase
Pitching	
$C_{m_\alpha} - a\frac{\tau_1^2k^2}{1+\tau_1^2k^2} - 2c_2\frac{\tau_1^4k^2\left(3-\tau_1^2k^2\right)}{\left(1+\tau_1^2k^2\right)^3}$	$C_{m_q} - a\frac{\tau_1}{1+\tau_1^2k^2} - 2c_2\frac{\tau_1^3\left(1-3\tau_1^2k^2\right)}{\left(1+\tau_1^2k^2\right)^3}$
$C_{N_\alpha} - a\frac{\tau_1^2k^2}{1+\tau_1^2k^2} - 2c_2\frac{\tau_1^4k^2\left(3-\tau_1^2k^2\right)}{\left(1+\tau_1^2k^2\right)^3}$	$C_{N_q} - a\frac{\tau_1}{1+\tau_1^2k^2} - 2c_2\frac{\tau_1^3\left(1-3\tau_1^2k^2\right)}{\left(1+\tau_1^2k^2\right)^3}$
$C_{A_\alpha} - a\frac{\tau_1^2k^2}{1+\tau_1^2k^2} - 2c_2\frac{\tau_1^4k^2\left(3-\tau_1^2k^2\right)}{\left(1+\tau_1^2k^2\right)^3}$	$C_{A_q} - a\frac{\tau_1}{1+\tau_1^2k^2} - 2c_2\frac{\tau_1^3\left(1-3\tau_1^2k^2\right)}{\left(1+\tau_1^2k^2\right)^3}$
Rolling	
$C_{Y_\beta}\sin\alpha - \left(a\frac{\tau_1^2k^2}{1+\tau_1^2k^2} + 2c_2\frac{\tau_1^4k^2\left(3-\tau_1^2k^2\right)}{\left(1+\tau_1^2k^2\right)^3}\right)\sin\alpha$	$C_{Y_p} - \left(a\frac{\tau_1}{1+\tau_1^2k^2} + 2c_2\frac{\tau_1^3\left(1-3\tau_1^2k^2\right)}{\left(1+\tau_1^2k^2\right)^3}\right)\sin\alpha$
$C_{n_\beta}\sin\alpha - \left(a\frac{\tau_1^2k^2}{1+\tau_1^2k^2} + 2c_2\frac{\tau_1^4k^2\left(3-\tau_1^2k^2\right)}{\left(1+\tau_1^2k^2\right)^3}\right)\sin\alpha$	$C_{n_p} - \left(a\frac{\tau_1}{1+\tau_1^2k^2} + 2c_2\frac{\tau_1^3\left(1-3\tau_1^2k^2\right)}{\left(1+\tau_1^2k^2\right)^3}\right)\sin\alpha$
$C_{l_\beta}\sin\alpha - \left(a\frac{\tau_1^2k^2}{1+\tau_1^2k^2} + 2c_2\frac{\tau_1^4k^2\left(3-\tau_1^2k^2\right)}{\left(1+\tau_1^2k^2\right)^3}\right)\sin\alpha$	$C_{l_p} - \left(a\frac{\tau_1}{1+\tau_1^2k^2} + 2c_2\frac{\tau_1^3\left(1-3\tau_1^2k^2\right)}{\left(1+\tau_1^2k^2\right)^3}\right)\sin\alpha$
Yawing	
$C_{Y_\beta}\cos\alpha - \left(a\frac{\tau_1^2k^2}{1+\tau_1^2k^2} + 2c_2\frac{\tau_1^4k^2\left(3-\tau_1^2k^2\right)}{\left(1+\tau_1^2k^2\right)^3}\right)\cos\alpha$	$C_{Y_r} + \left(a\frac{\tau_1}{1+\tau_1^2k^2} + 2c_2\frac{\tau_1^3\left(1-3\tau_1^2k^2\right)}{\left(1+\tau_1^2k^2\right)^3}\right)\cos\alpha$
$C_{n_\beta}\cos\alpha - \left(a\frac{\tau_1^2k^2}{1+\tau_1^2k^2} + 2c_2\frac{\tau_1^4k^2\left(3-\tau_1^2k^2\right)}{\left(1+\tau_1^2k^2\right)^3}\right)\cos\alpha$	$C_{n_r} + \left(a\frac{\tau_1}{1+\tau_1^2k^2} + 2c_2\frac{\tau_1^3\left(1-3\tau_1^2k^2\right)}{\left(1+\tau_1^2k^2\right)^3}\right)\cos\alpha$
$C_{l_\beta}\cos\alpha - \left(a\frac{\tau_1^2k^2}{1+\tau_1^2k^2} + 2c_2\frac{\tau_1^4k^2\left(3-\tau_1^2k^2\right)}{\left(1+\tau_1^2k^2\right)^3}\right)\cos\alpha$	$C_{l_r} + \left(a\frac{\tau_1}{1+\tau_1^2k^2} + 2c_2\frac{\tau_1^3\left(1-3\tau_1^2k^2\right)}{\left(1+\tau_1^2k^2\right)^3}\right)\cos\alpha$

Table 16a. Comparison of model costs and variances. Pitch-axis oscillations.

Measured Data	s^2_I	s^2_{II}	J_I	J_{II}
$\overline{C}_{N_\alpha}, \overline{C}_{N_q}$	0.1685	0.0447	26.955	6.1227
$\overline{C}_{m_\alpha}, \overline{C}_{m_q}$	0.0091	0.0029	1.4487	0.4298
$\overline{C}_{a_\alpha}, \overline{C}_{a_q}$	0.0054	0.0031	0.8564	0.3994

Table 16b. Comparison of model costs and variances. Roll-axis oscillations.

Measured Data	s^2_I	s^2_{II}	J_I	J_{II}
$\overline{C}_{y_\beta}, \overline{C}_{y_p}$	0.0282	0.0180	3.9242	2.1477
$\overline{C}_{n_\beta}, \overline{C}_{n_p}$	0.0033	0.0016	0.4561	0.1899
$\overline{C}_{l_\beta}, \overline{C}_{l_p}$	0.0012	0.0005	0.1619	0.0629

Table 16c. Comparison of model costs and variances. Yaw-axis oscillations.

Measured Data	s^2_I	s^2_{II}	J_I	J_{II}
$\overline{C}_{y_\beta}, \overline{C}_{y_r}$	0.0216	0.0129	3.3053	1.6480
$\overline{C}_{n_\beta}, \overline{C}_{n_r}$	0.0035	0.0012	0.3846	0.1070
$\overline{C}_{l_\beta}, \overline{C}_{l_r}$	0.0011	0.0003	0.1707	0.0379

Table 17a. Comparison of model prediction residuals. Pitch-axis oscillations, k=0.0483.

Measured Data	r^2_I	r^2_{II}
$\overline{C}_{a_\alpha}$	0.0050	0.0061
$\overline{C}_{a_q}$	0.4179	0.4488
$\overline{C}_{N_\alpha}$	0.0636	0.0656
$\overline{C}_{N_q}$	6.5379	7.3098
$\overline{C}_{m_\alpha}$	0.0030	0.0031
$\overline{C}_{m_q}$	0.6608	0.8721

Table 17b. Comparison of model prediction residuals. Roll-axis oscillations, k=0.089.

Measured Data	r^2_I	r^2_{II}
$\overline{C}_{n_\beta}$	0.0079	0.0078
$\overline{C}_{n_p}$	0.1298	0.2046
$\overline{C}_{l_\beta}$	0.0008	0.0015
$\overline{C}_{l_p}$	0.0969	0.1146
$\overline{C}_{y_\beta}$	0.0204	0.0390
$\overline{C}_{y_p}$	0.6384	1.1930

Table 17c. Comparison of model prediction residuals. Yaw-axis oscillations, k=0.089.

Measured Data	r^2_I	r^2_{II}
$\overline{C}_{n_\beta}$	0.0059	0.0046
$\overline{C}_{n_r}$	0.2999	0.5145
$\overline{C}_{l_\beta}$	0.0012	0.0010
$\overline{C}_{l_r}$	0.1005	0.0942
$\overline{C}_{y_\beta}$	0.0099	0.0095
$\overline{C}_{y_r}$	1.2003	1.4700

Table 18. Estimated model parameters. Model I.

Measured Data	Parameter		
	τ_1	b_1, sec^{-1}	T_1, sec
	Pitching		
$\overline{C}_{N_\alpha}, \overline{C}_{N_q}$	18.5 ± 0.46	4.22 ± 0.11	0.24 ± 0.01
$\overline{C}_{m_\alpha}, \overline{C}_{m_q}$	21.3 ± 0.81	3.67 ± 0.14	0.27 ± 0.01
$\overline{C}_{A_\alpha}, \overline{C}_{A_q}$	18.1 ± 0.42	4.33 ± 0.10	0.23 ± 0.01
	Rolling		
$\overline{C}_{Y_\beta}, \overline{C}_{Y_p}$	7.54 ± 1.13	5.62 ± 0.84	0.18 ± 0.03
$\overline{C}_{n_\beta}, \overline{C}_{n_p}$	13.7 ± 1.43	3.09 ± 0.32	0.32 ± 0.03
$\overline{C}_{l_\beta}, \overline{C}_{l_p}$	12.0 ± 0.80	3.54 ± 0.24	0.28 ± 0.02
	Yawing		
$\overline{C}_{Y_\beta}, \overline{C}_{Y_r}$	9.96 ± 0.98	4.25 ± 0.42	0.24 ± 0.02
$\overline{C}_{n_\beta}, \overline{C}_{n_r}$	12.7 ± 1.24	3.35 ± 0.33	0.30 ± 0.03
$\overline{C}_{l_\beta}, \overline{C}_{l_r}$	12.3 ± 0.55	3.46 ± 0.16	0.29 ± 0.01

Table 19. Estimated model parameters. Model II.

Measured Data	Parameter		
	τ_1	b_1, sec^{-1}	T_1, sec
	Pitching		
$\overline{C}_{N_\alpha}, \overline{C}_{N_q}$	19.75 ± 0.58	3.96 ± 0.12	0.25 ± 0.01
$\overline{C}_{m_\alpha}, \overline{C}_{m_q}$	22.35 ± 0.96	3.50 ± 0.15	0.29 ± 0.01
$\overline{C}_{A_\alpha}, \overline{C}_{A_q}$	19.92 ± 0.84	3.92 ± 0.17	0.25 ± 0.01
	Rolling		
$\overline{C}_{Y_\beta}, \overline{C}_{Y_p}$	17.81 ± 1.73	2.38 ± 0.23	0.42 ± 0.04
$\overline{C}_{n_\beta}, \overline{C}_{n_p}$	15.25 ± 1.34	2.78 ± 0.24	0.36 ± 0.03
$\overline{C}_{l_\beta}, \overline{C}_{l_p}$	16.96 ± 1.11	2.50 ± 0.16	0.40 ± 0.03
	Yawing		
$\overline{C}_{Y_\beta}, \overline{C}_{Y_r}$	16.27 ± 1.38	2.60 ± 0.22	0.38 ± 0.03
$\overline{C}_{n_\beta}, \overline{C}_{n_r}$	10.61 ± 0.83	3.99 ± 0.31	0.25 ± 0.02
$\overline{C}_{l_\beta}, \overline{C}_{l_r}$	13.21 ± 0.52	3.21 ± 0.13	0.31 ± 0.01

Table 20. Minimum and maximum values of standard errors of estimated parameters. Model I.

Measured Data	$s(\hat{a})$		$s\left(C_{\xi_x}(\infty)\right)^*$	
	min	**max**	**min**	**max**
			Pitching	
$\overline{C}_{a_\alpha}$	0.0073	0.0133	0.0329	0.0330
$\overline{C}_{a_q}$			0.0769	0.1122
$\overline{C}_{N_\alpha}$	0.0399	0.0765	0.1846	0.1849
$\overline{C}_{N_q}$			0.4232	0.6461
$\overline{C}_{m_\alpha}$	0.0079	0.0167	0.0428	0.0429
$\overline{C}_{m_q}$			0.0886	0.1478
			Rolling	
$\overline{C}_{n_\beta}$	0.0075	0.0425	0.0260	0.1497
$\overline{C}_{n_p}$			0.0480	0.0695
$\overline{C}_{l_\beta}$	0.0050	0.0287	0.0155	0.0893
$\overline{C}_{l_p}$			0.0309	0.0513
$\overline{C}_{y_\beta}$	0.0454	0.2583	0.0778	0.4435
$\overline{C}_{y_p}$			0.2233	0.4501
			Yawing	
$\overline{C}_{n_\beta}$	0.0085	0.1034	0.0300	0.3448
$\overline{C}_{n_r}$			0.0576	0.0903
$\overline{C}_{l_\beta}$	0.0048	0.0548	0.0152	0.1741
$\overline{C}_{l_r}$			0.0298	0.0491
$\overline{C}_{y_\beta}$	0.0287	0.3259	0.0670	0.7685
$\overline{C}_{y_r}$			0.1515	0.2406

*where ξ_x=A_α,A_q,N_α,N_q,m_α,m_q,n_β,n_p,l_β,l_p,Y_β,Y_p,n_r,l_r, or Y_r

Table 21. Minimum and maximum values of standard errors of estimated parameters. Model II.

Measured Data	$s(\hat{a})$		$s(\hat{c}_2)\mathbf{x10^3}$		$s\left(C_{\xi_x}(\infty)\right)^*$	
	min	**max**	**min**	**max**	**min**	**max**
	Pitching					
$\overline{C}_{a_\alpha}$	0.0078	0.0198	0.0257	0.0351	0.0252	0.0256
$\overline{C}_{a_q}$					0.0863	0.1523
$\overline{C}_{N_\alpha}$	0.0301	0.0776	0.0991	0.1749	0.0952	0.0956
$\overline{C}_{N_q}$					0.3308	0.5903
$\overline{C}_{m_\alpha}$	0.0055	0.0135	0.0188	0.0364	0.0243	0.0245
$\overline{C}_{m_q}$					0.0676	0.1106
	Rolling					
$\overline{C}_{n_\beta}$	0.0051	0.0280	0.0582	0.3285	0.0186	0.1048
$\overline{C}_{n_p}$					0.0361	0.0586
$\overline{C}_{l_\beta}$	0.0029	0.0251	0.0293	0.1713	0.0106	0.0623
$\overline{C}_{l_p}$					0.0187	0.0397
$\overline{C}_{y_\beta}$	0.0188	0.1068	0.1699	0.9533	0.0625	0.3581
$\overline{C}_{y_p}$					0.1047	0.2027
	Yawing					
$\overline{C}_{n_\beta}$	0.0095	0.1308	0.1000	1.4000	0.0178	0.2052
$\overline{C}_{n_r}$					0.0546	0.0965
$\overline{C}_{l_\beta}$	0.0026	0.0378	0.0307	0.3718	0.0077	0.0893
$\overline{C}_{l_r}$					0.0184	0.0371
$\overline{C}_{y_\beta}$	0.0141	0.4504	0.1000	1.9000	0.0526	0.6524
$\overline{C}_{y_r}$					0.0956	0.1420

*where ξ_x=A_α,A_q,N_α,N_q,m_α,m_q,n_β,n_p,l_β,l_p,Y_β,Y_p,n_r,l_r, or Y_r

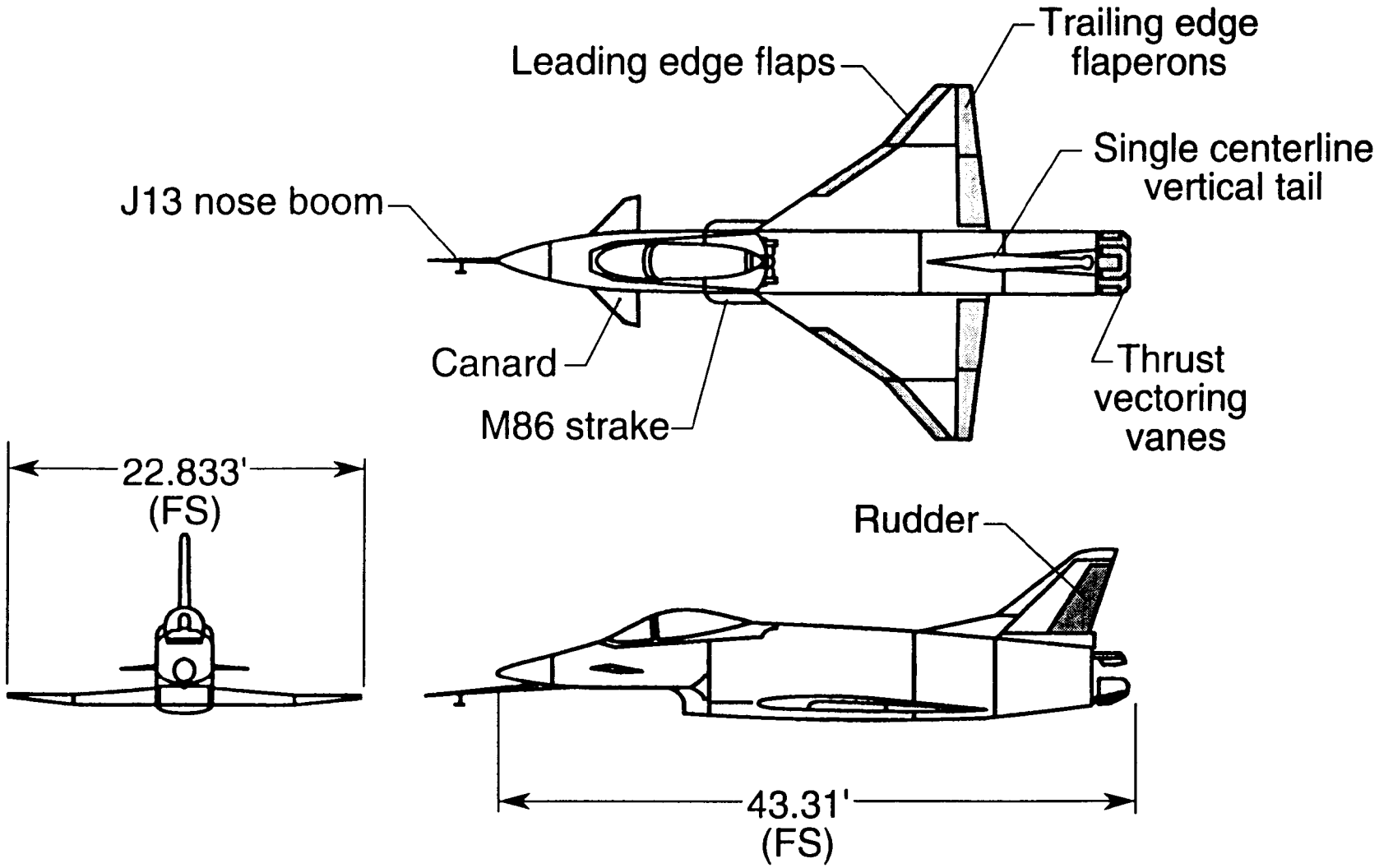

Figure 1. Three-view of the X-31A aircraft. (Ref. 5)

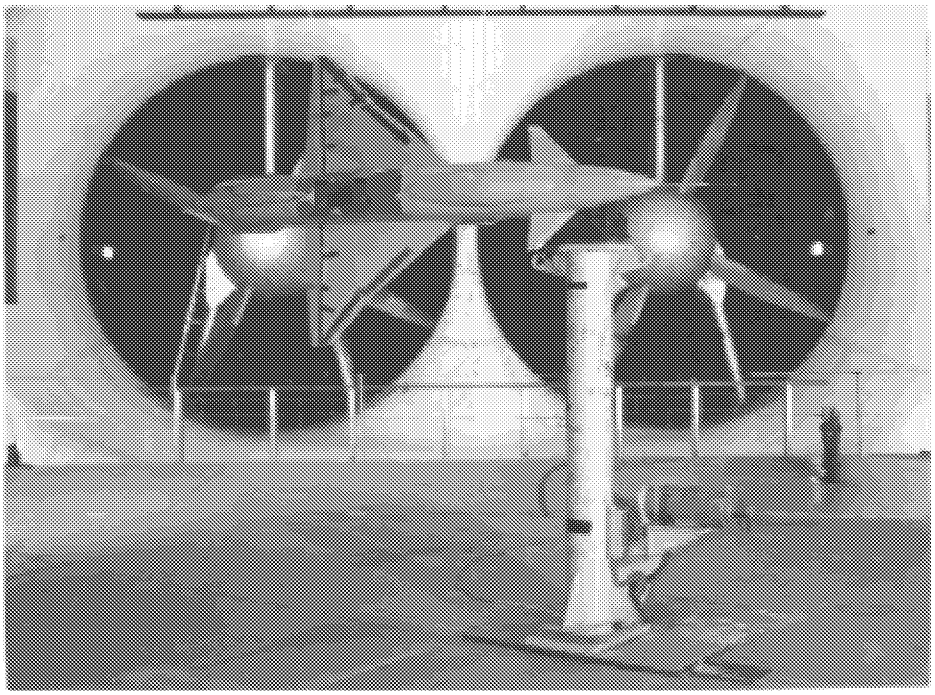

Figure 2. 19%-scale X-31 model (with reduced vertical tail) mounted on forced-oscillation test rig in the NASA Langley 30x60-Ft. wind tunnel. (NASA L-94-08995)

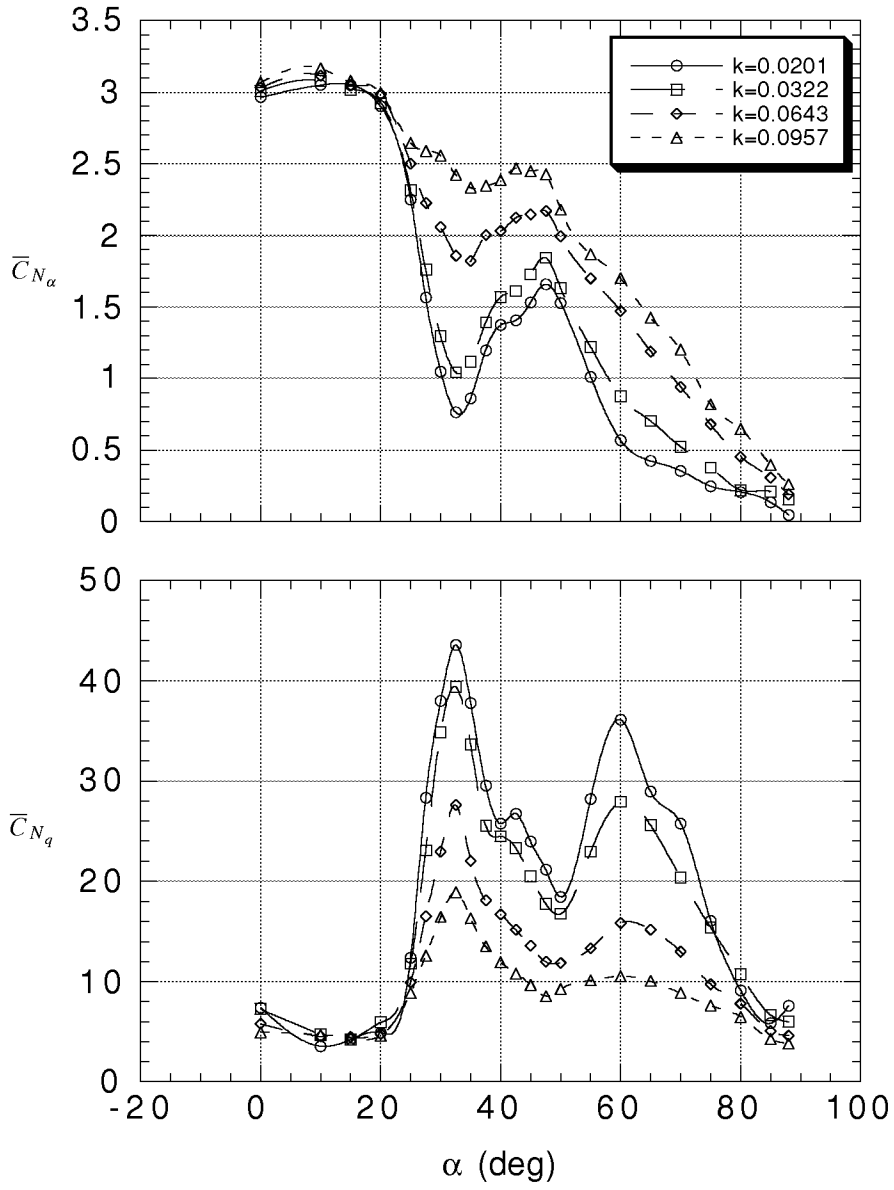

Figure 3. Measured in-phase and out-of-phase components of normal-force coefficient. Pitch oscillations.

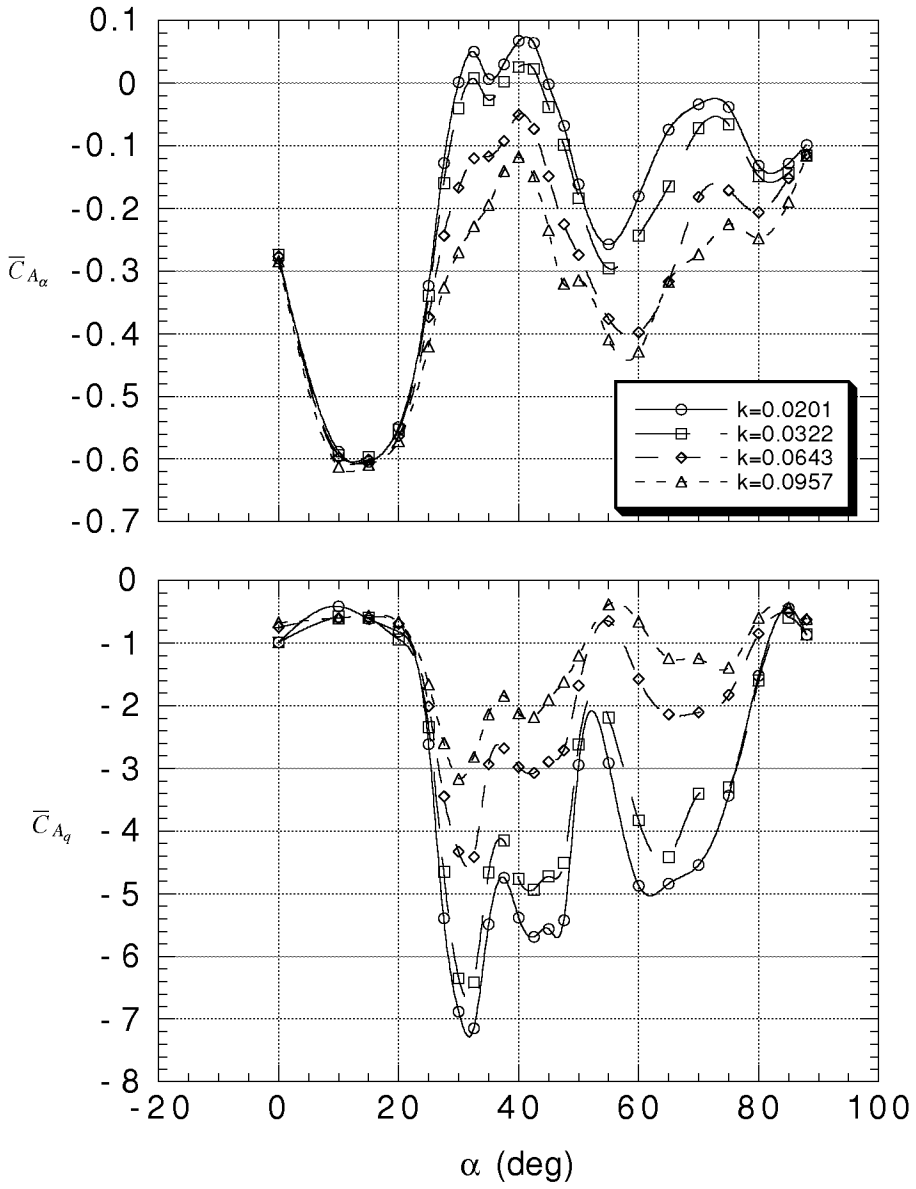

Figure 4. Measured in-phase and out-of-phase components of axial-force coefficient. Pitch oscillations.

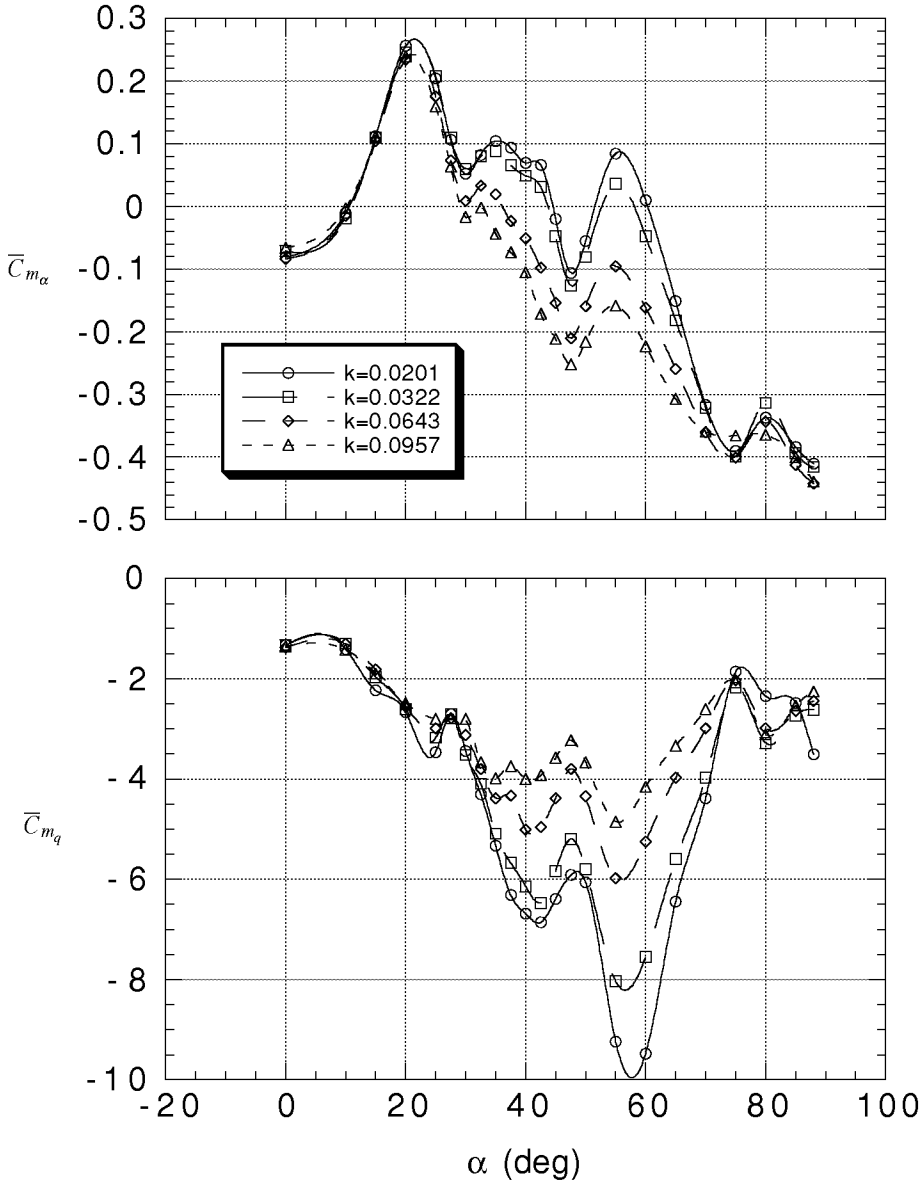

Figure 5. Measured in-phase and out-of-phase components of pitching-moment coefficient. Pitch oscillations.

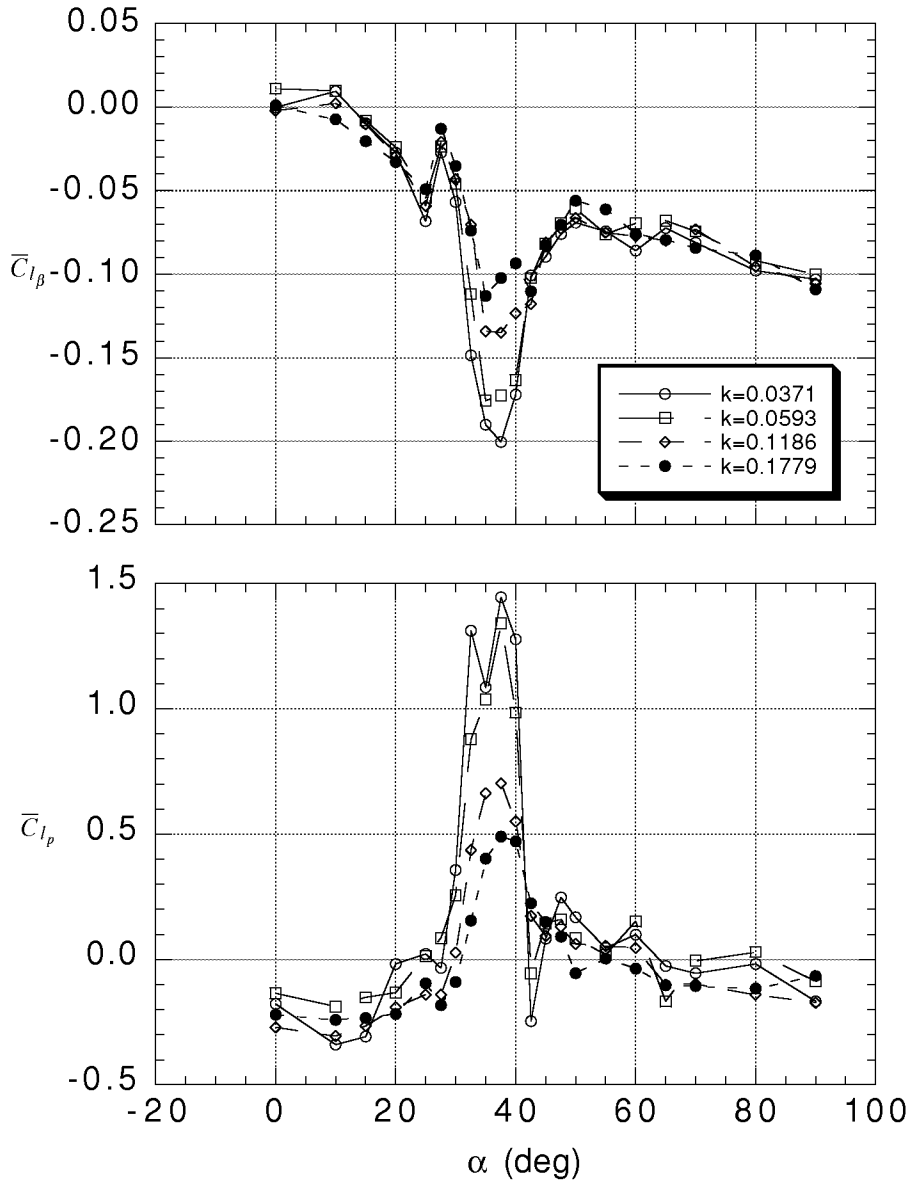

Figure 6. Measured in-phase and out-of-phase components of rolling-moment coefficient. Roll oscillations.

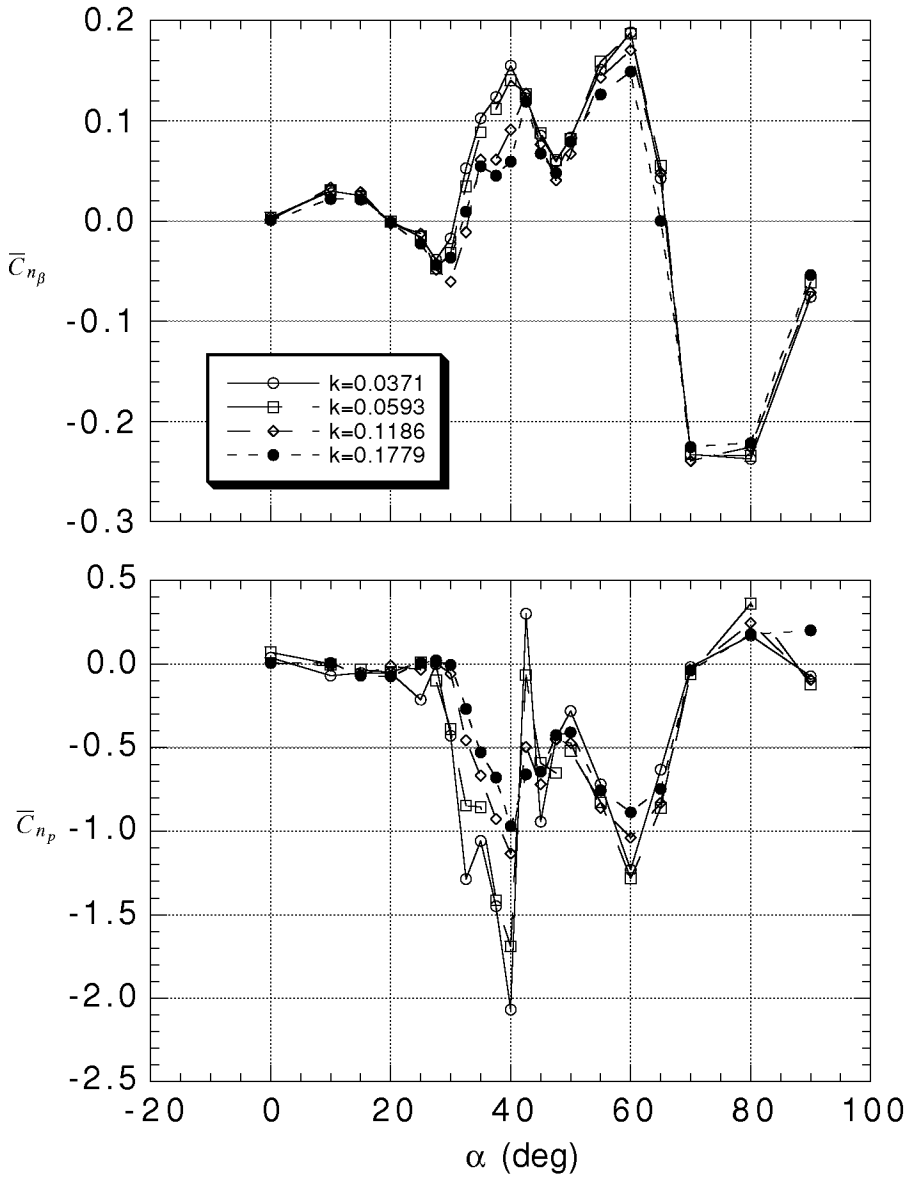

Figure 7. Measured in-phase and out-of-phase components of yawing-moment coefficient. Roll oscillations.

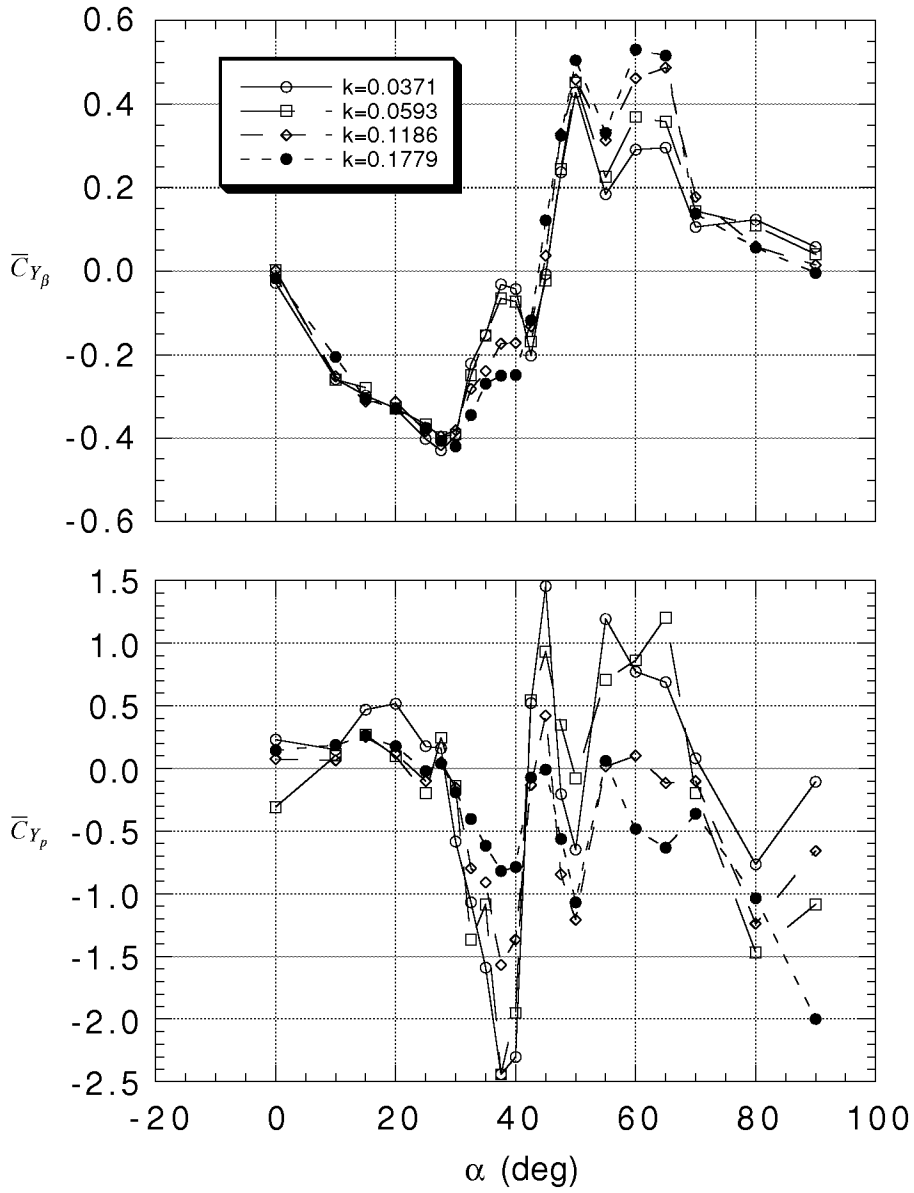

Figure 8. Measured in-phase and out-of-phase components of side-force coefficient. Roll oscillations.

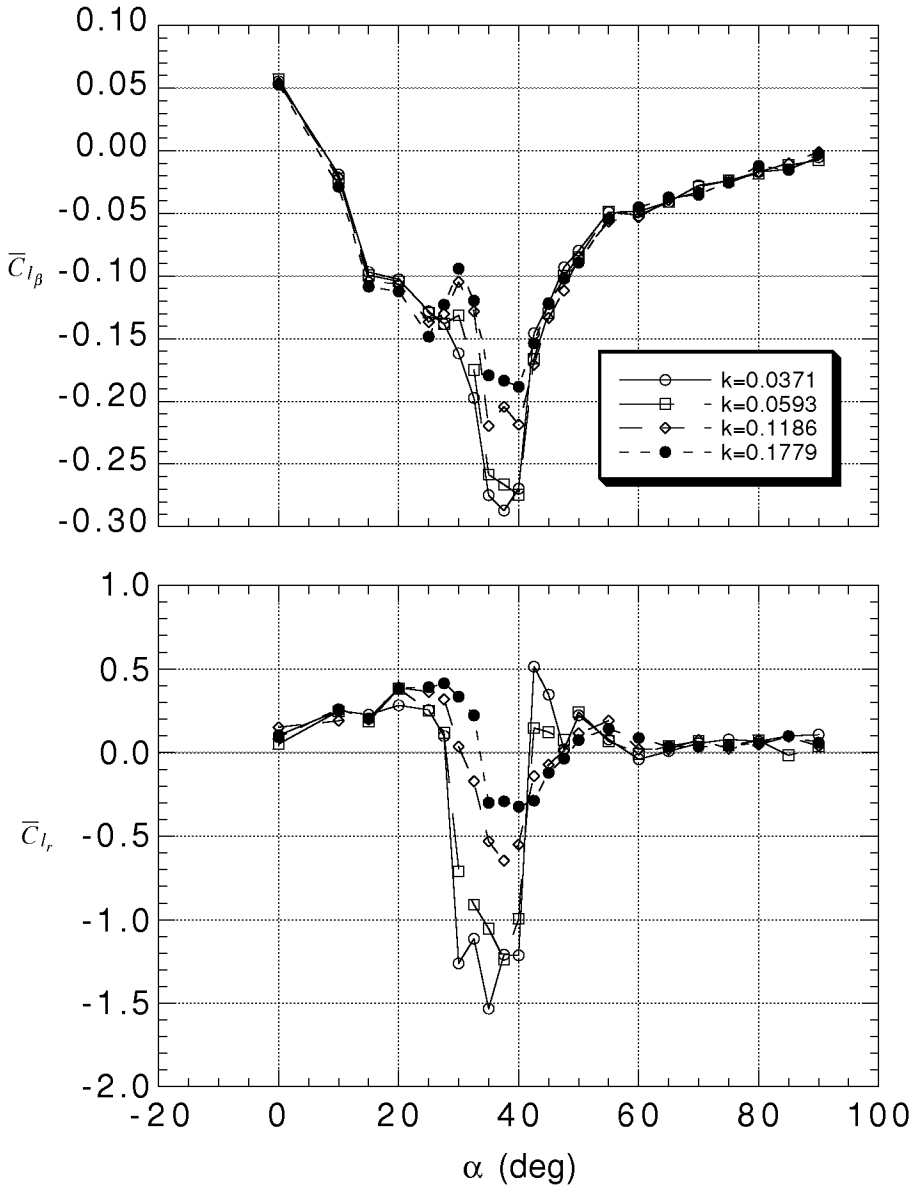

Figure 9. Measured in-phase and out-of-phase components of rolling-moment coefficient. Yaw oscillations.

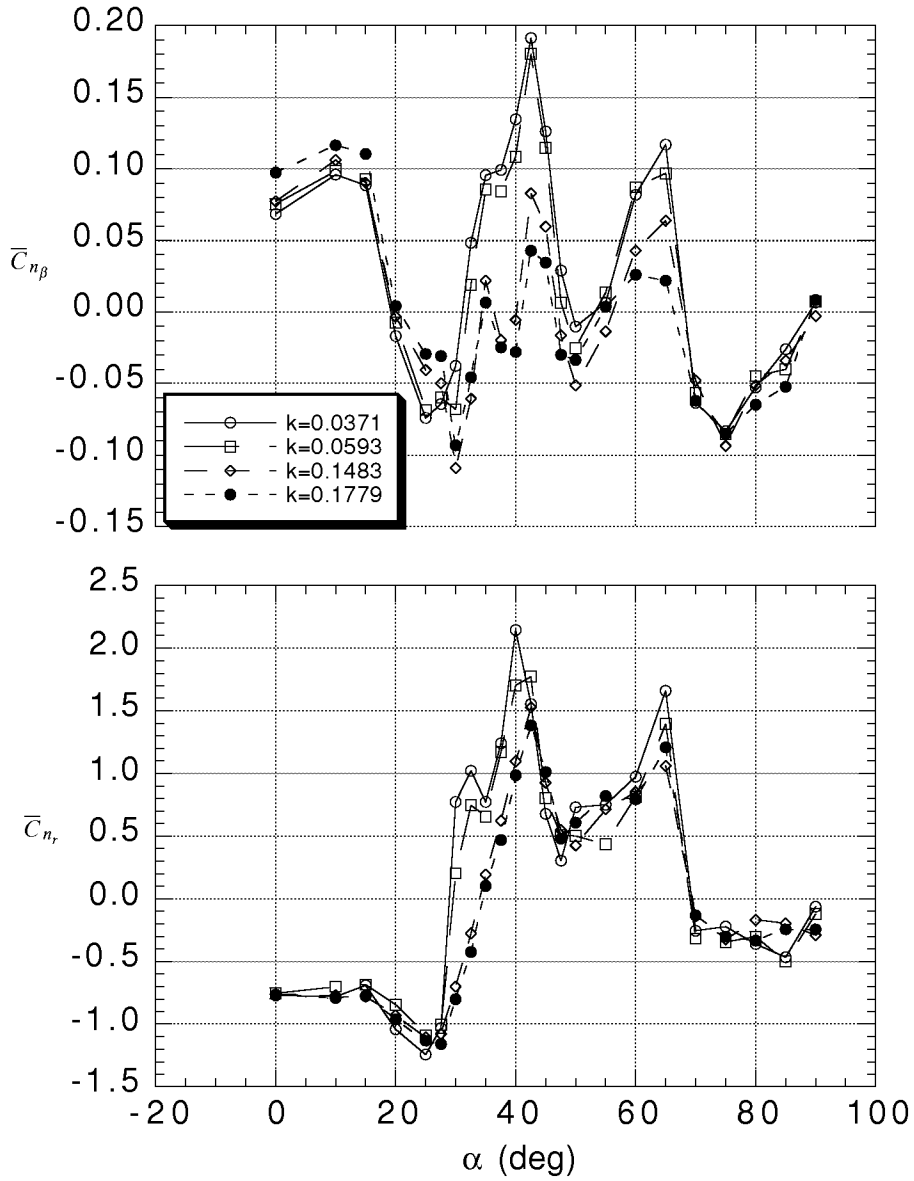

Figure 10. Measured in-phase and out-of-phase components of yawing-moment coefficient. Yaw oscillations.

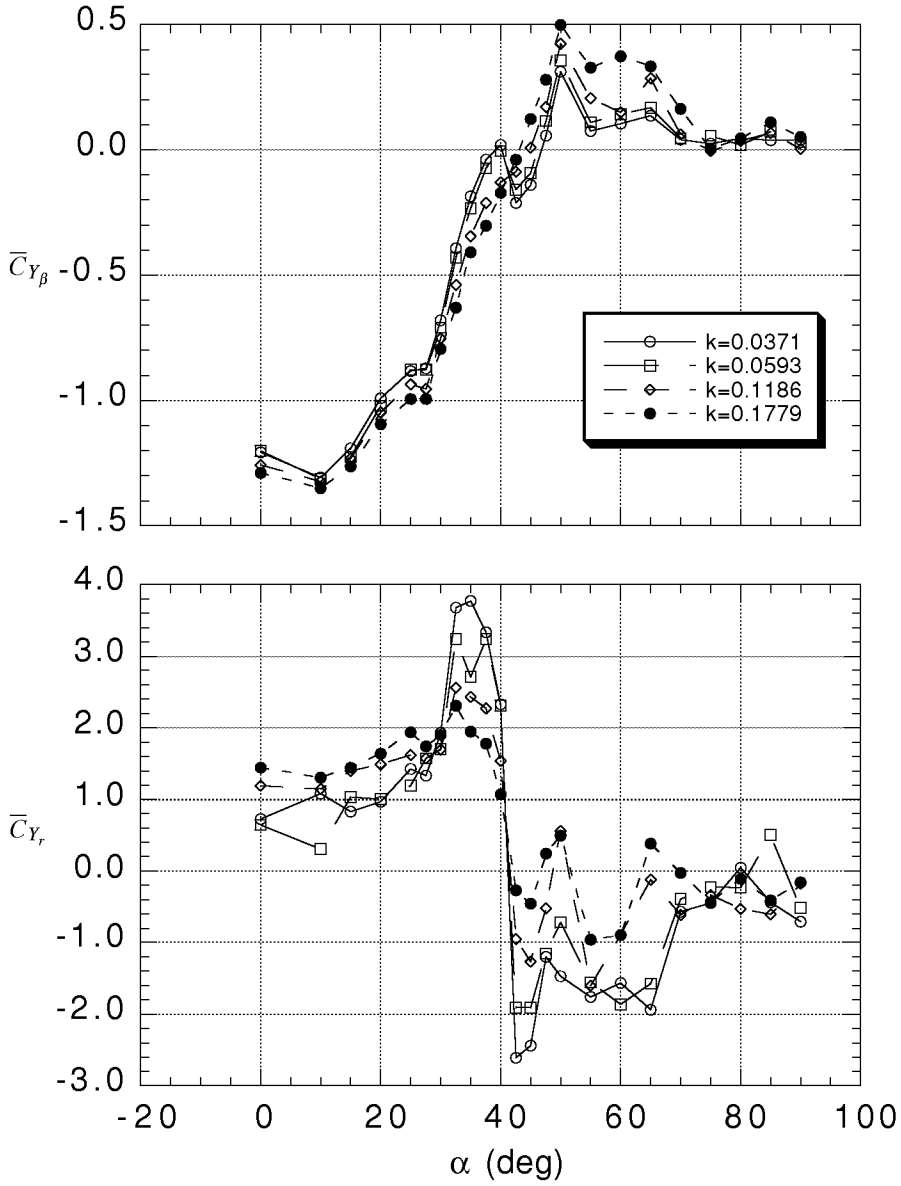

Figure 11. Measured in-phase and out-of-phase components of side-force coefficient. Yaw oscillations.

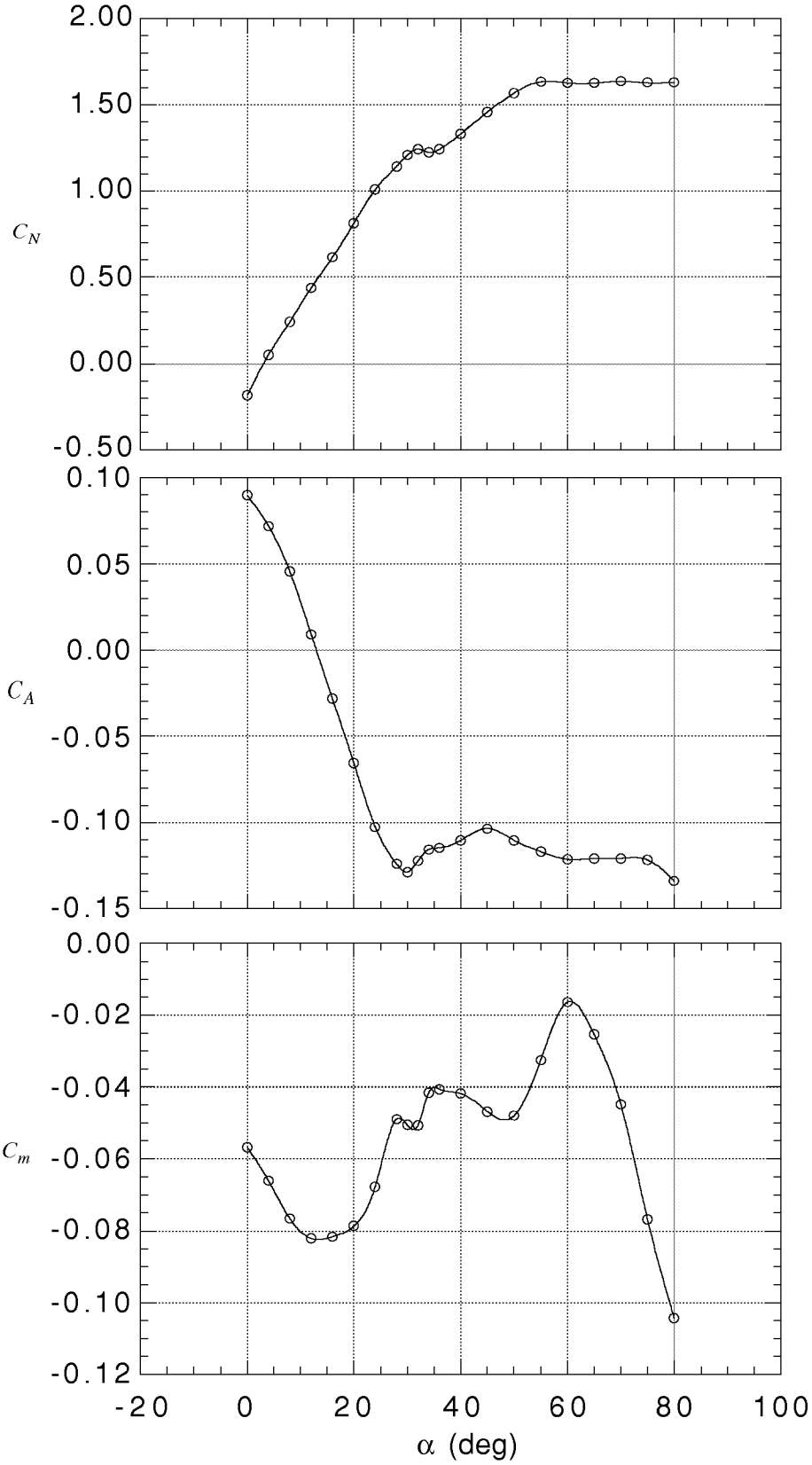

Figure 12. Variation of longitudinal coefficients with angle of attack. Static data.

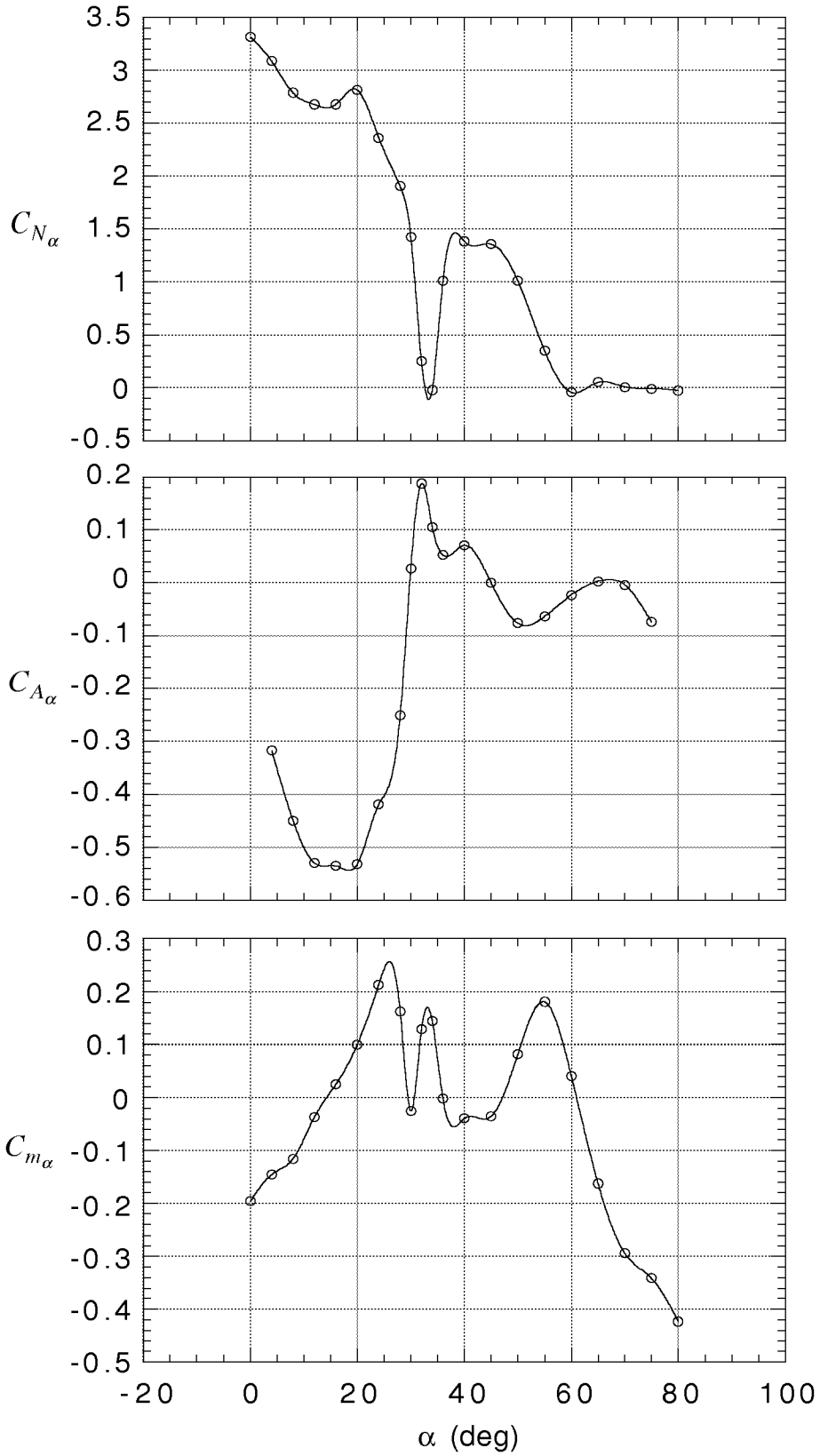

Figure 13. Variation of longitudinal stability parameters with angle of attack. Static data.

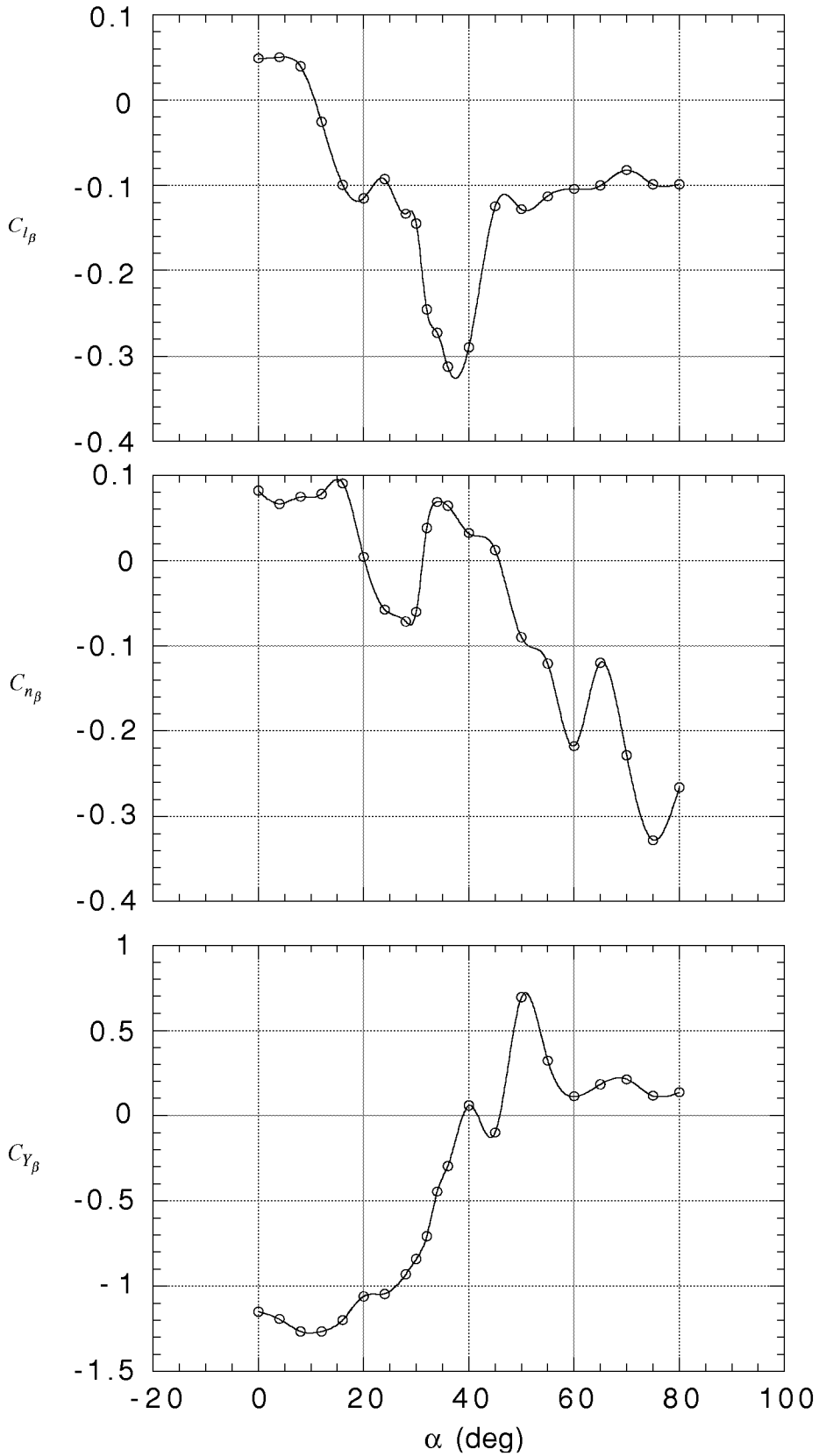

Figure 14. Variation of lateral stability parameters with angle of attack. Static data.

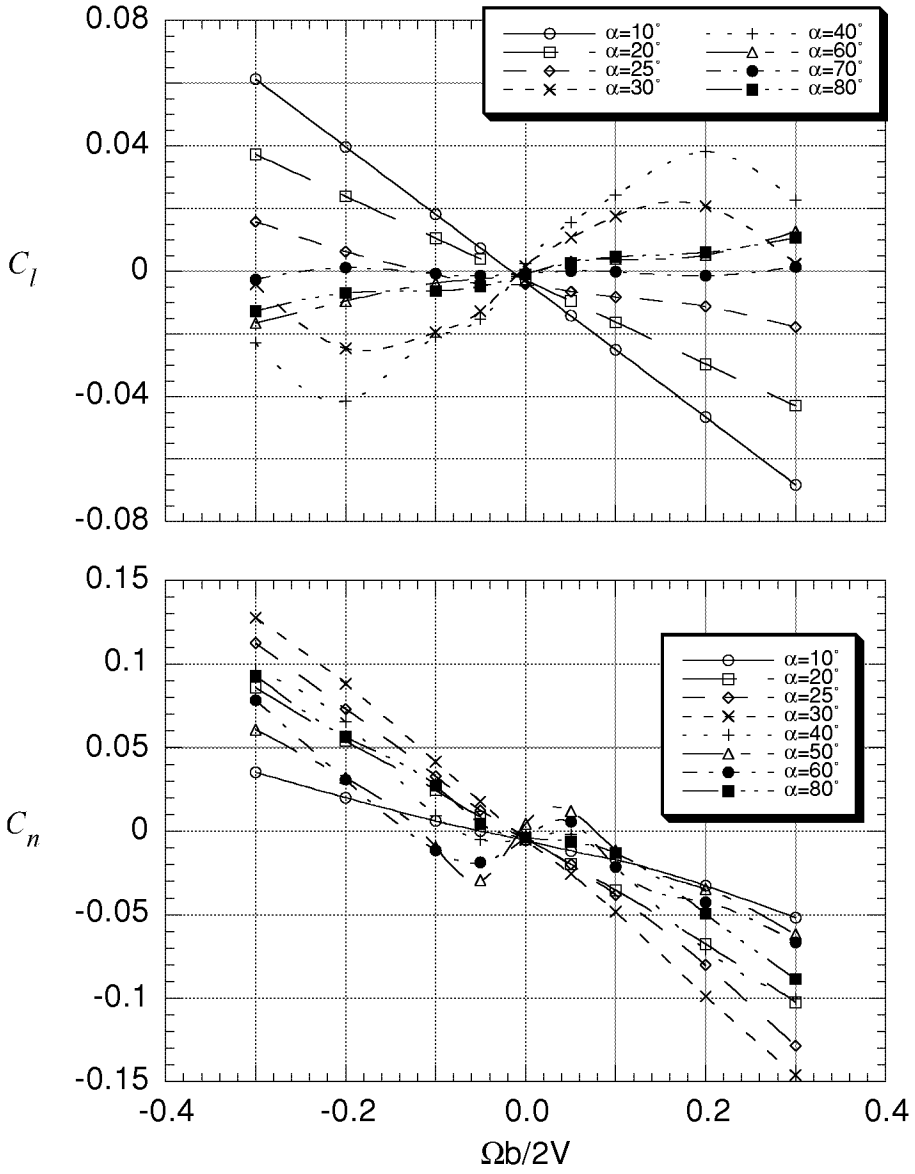

Figure 15. Measured rolling and yawing-moment coefficients from rotary-balance test. (Ref. 8)

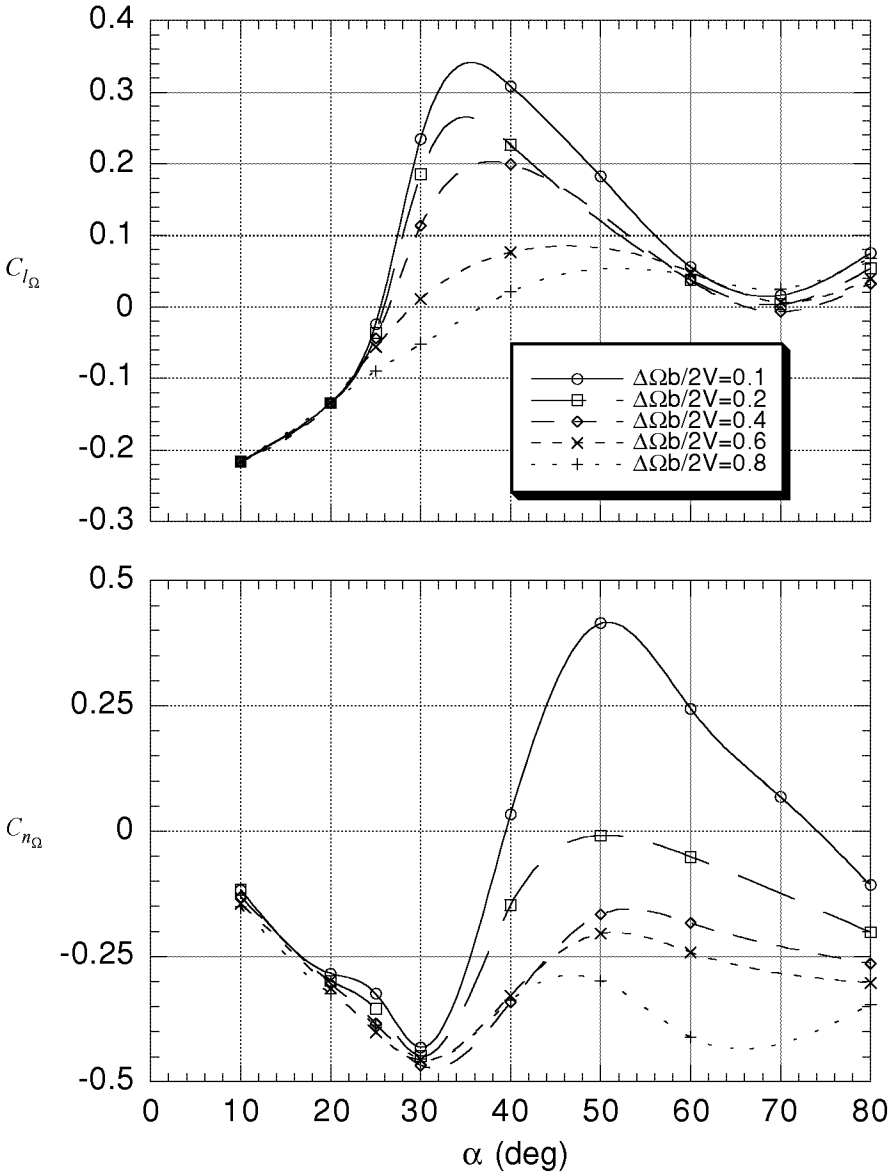

Figure 16. Rate derivatives estimated from rotary-balance test.

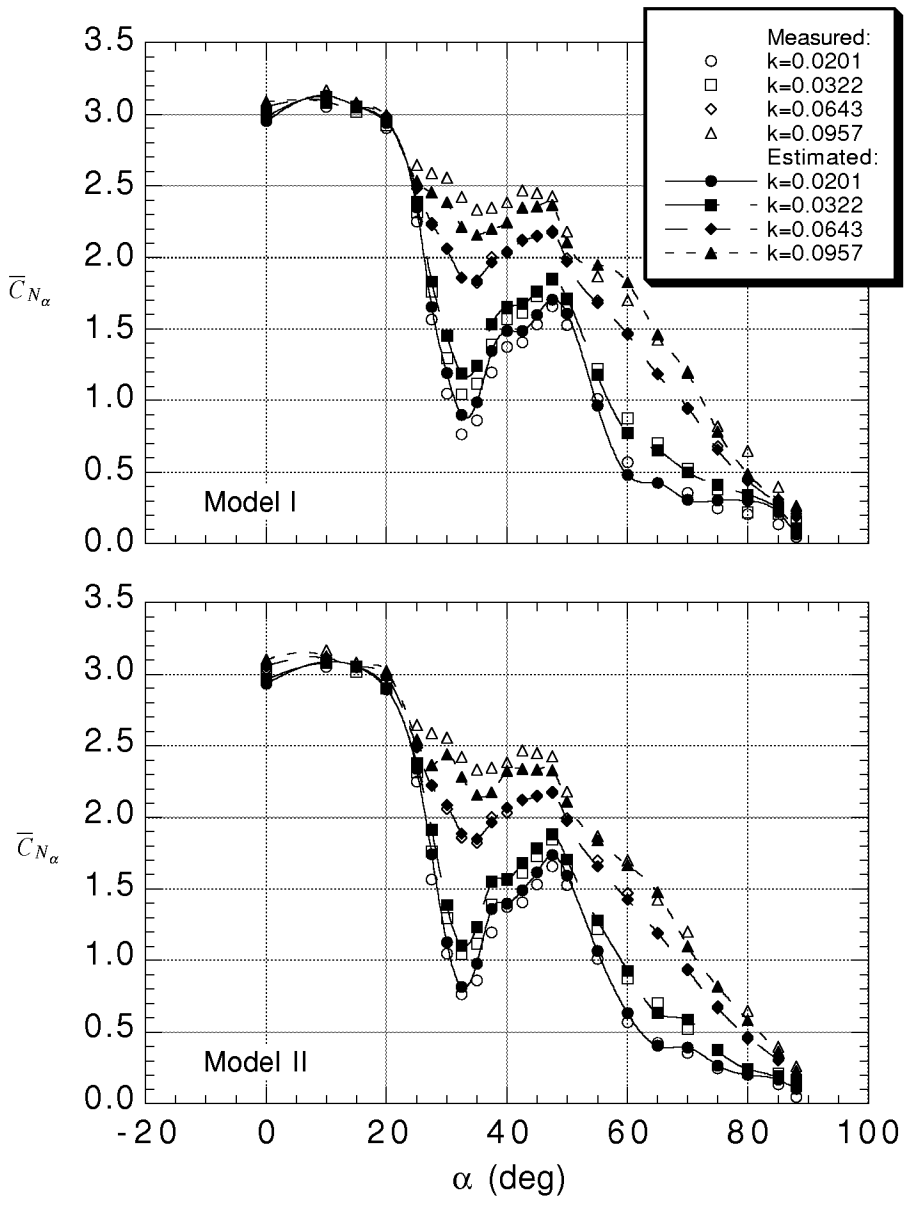

Figure 17. Measured and estimated in-phase component of normal-force coefficient. Pitch oscillations.

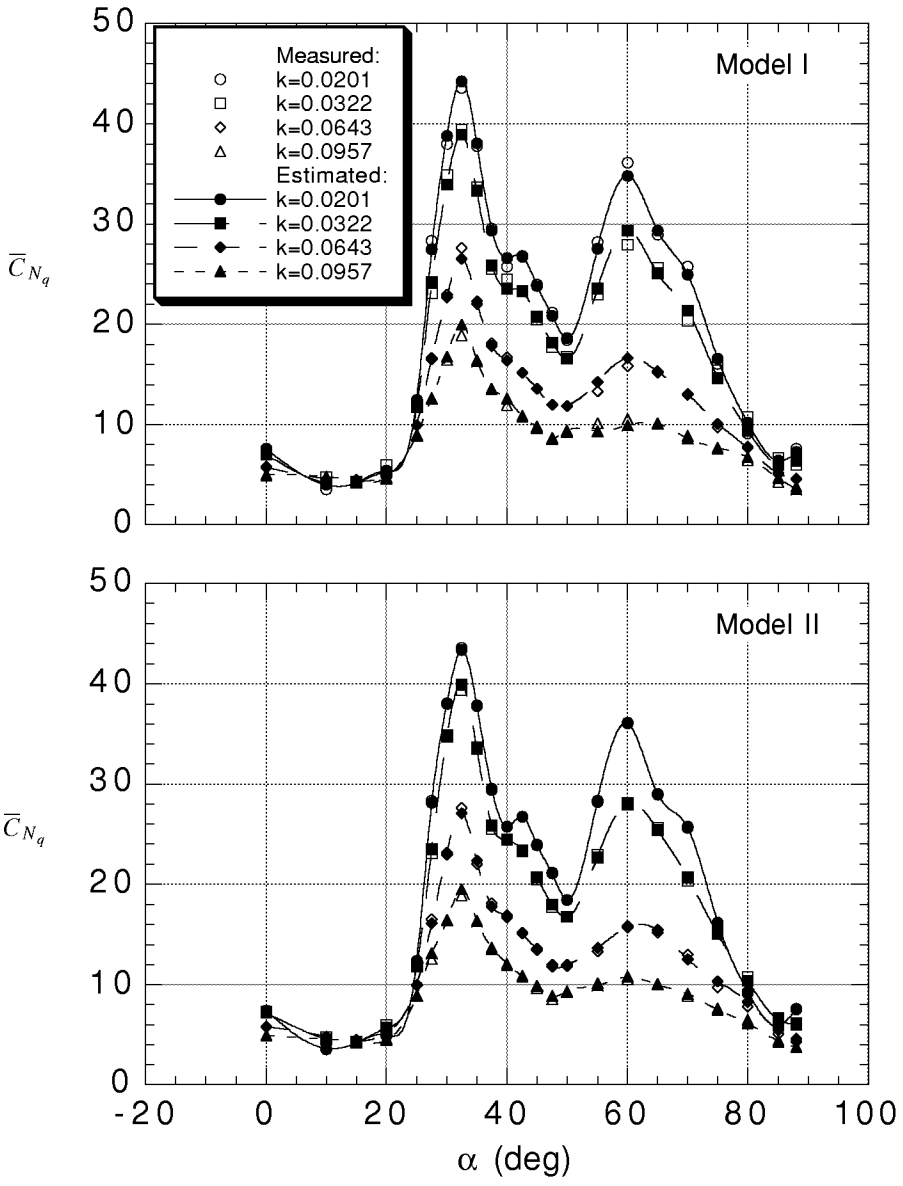

Figure 18. Measured and estimated out-of-phase component of normal-force coefficient. Pitch oscillations.

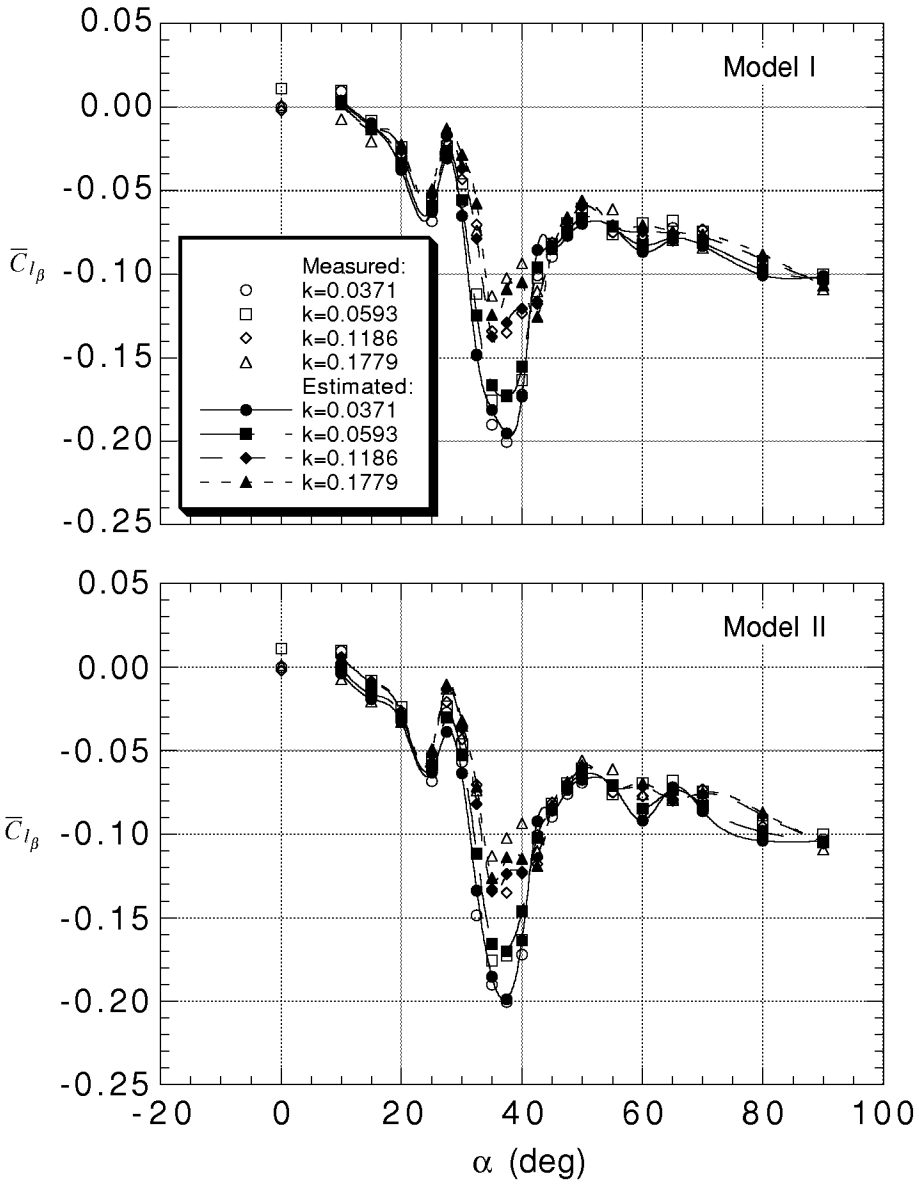

Figure 19. Measured and estimated in-phase component of rolling-moment coefficient. Roll oscillations.

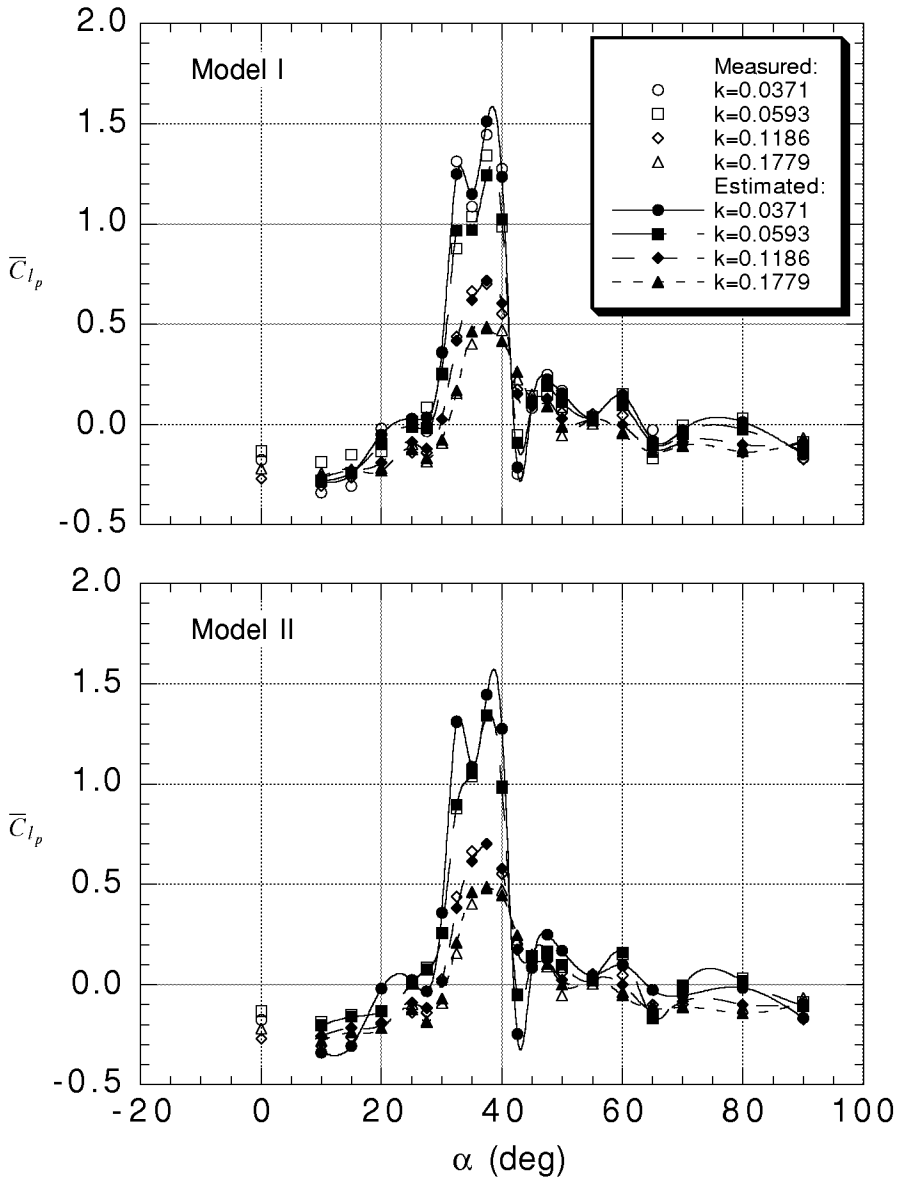

Figure 20. Measured and estimated out-of-phase component of rolling-moment coefficient. Roll oscillations.

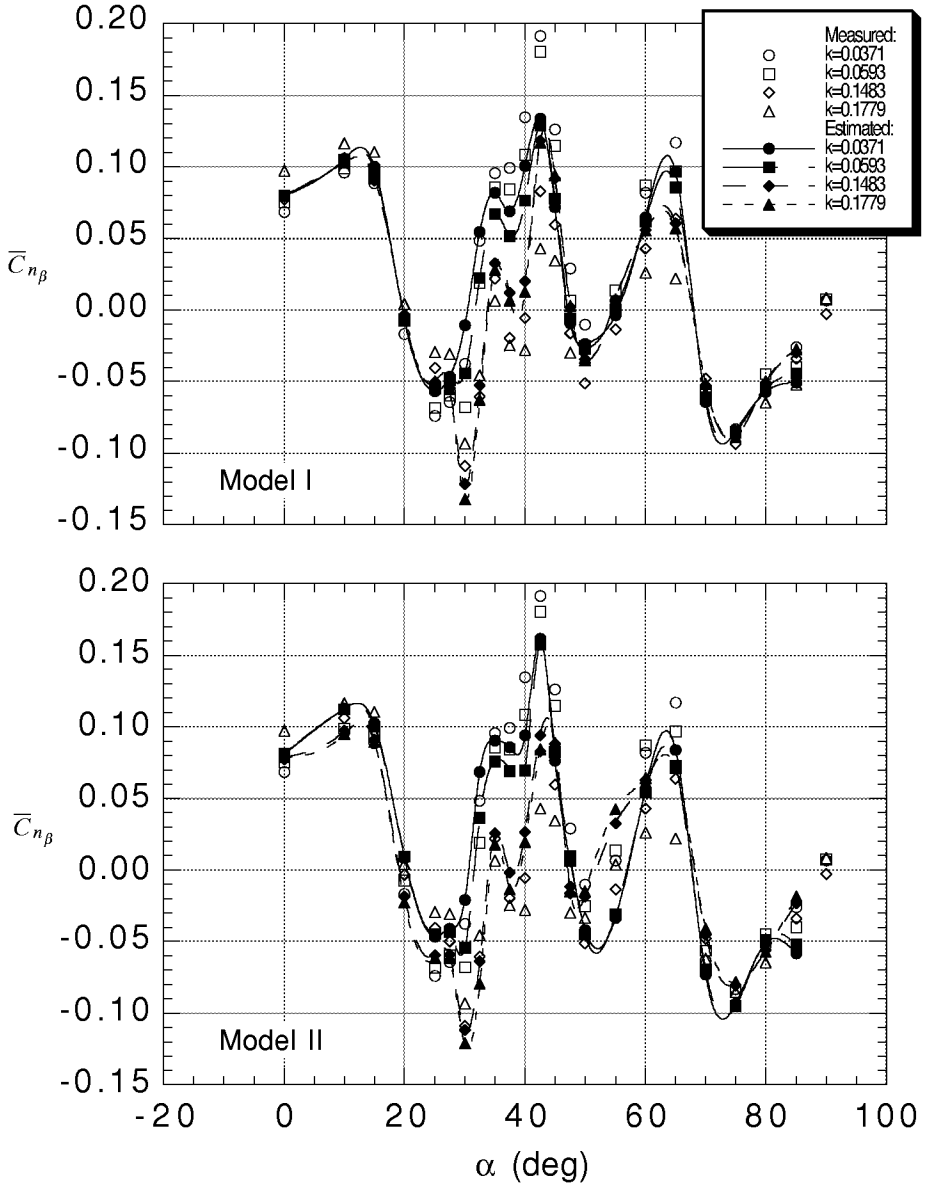

Figure 21. Measured and estimated in-phase component of yawing-moment coefficient. Yaw oscillations.

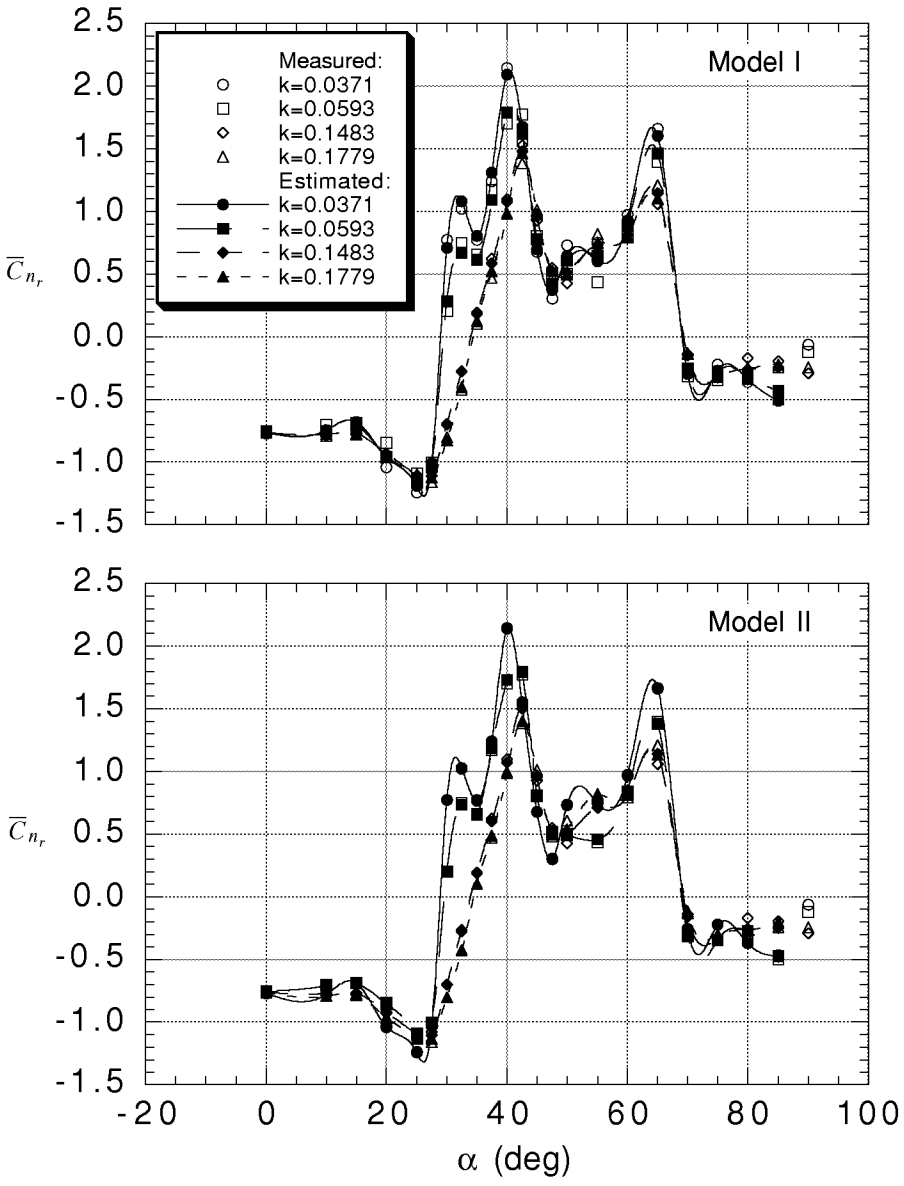

Figure 22. Measured and estimated out-of-phase component of yawing-moment coefficient. Yaw oscillations.

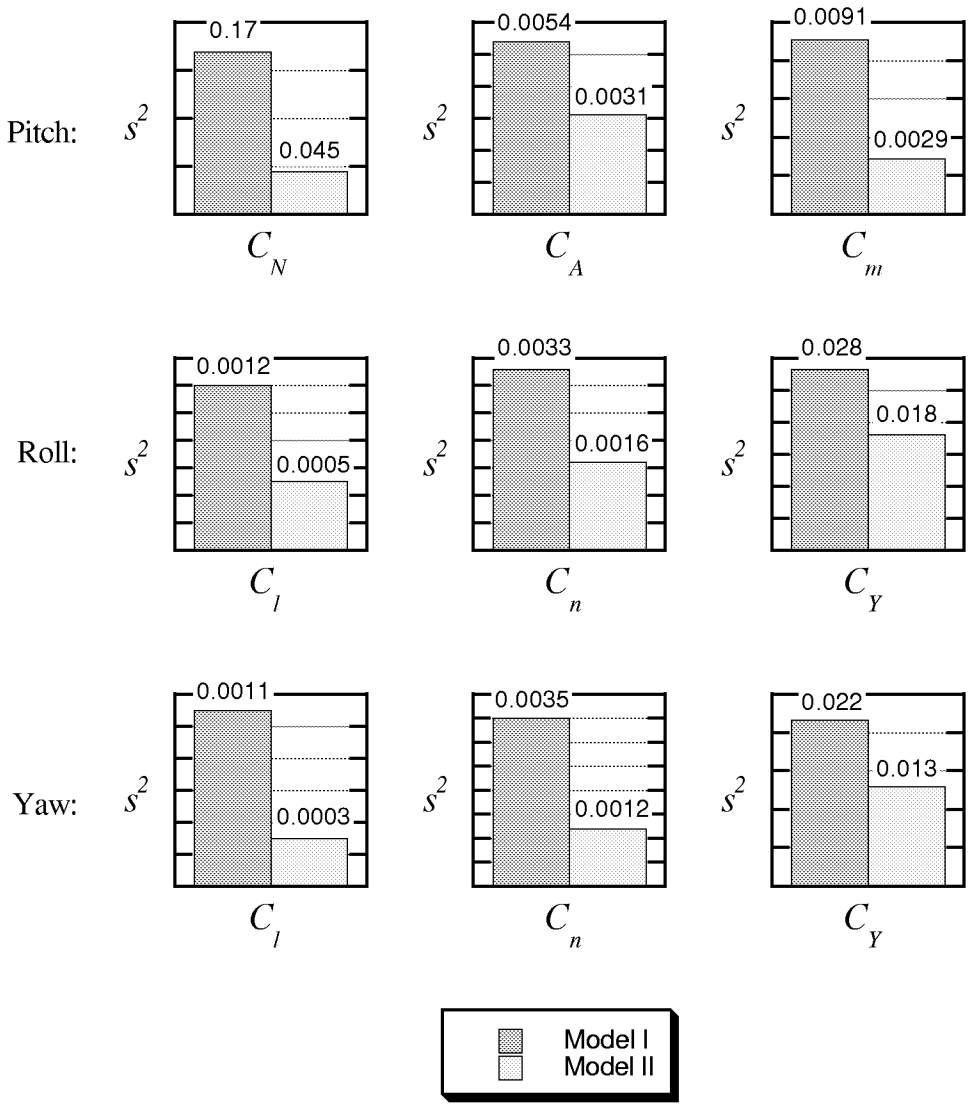

Figure 23. Comparison of mathematical model estimated variances.

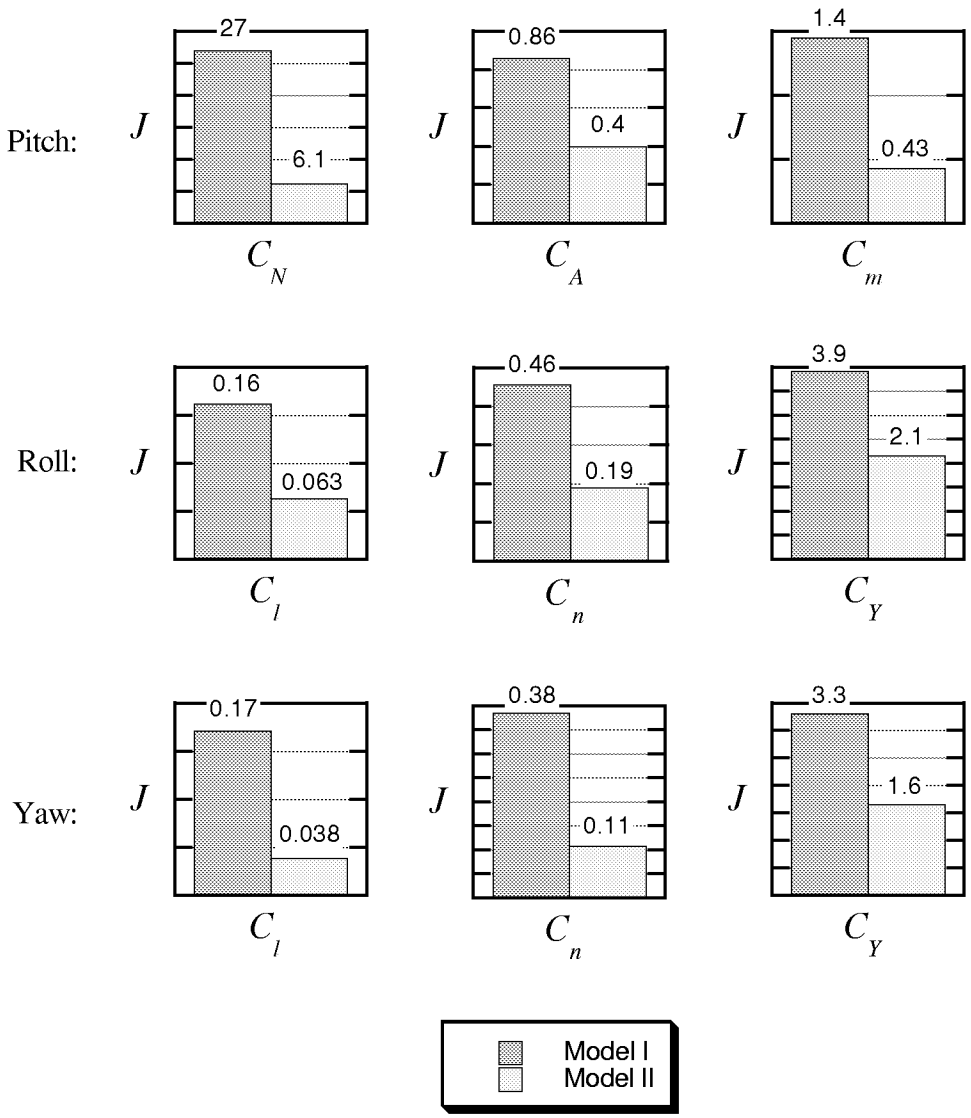

Figure 24. Comparison of mathematical model costs.

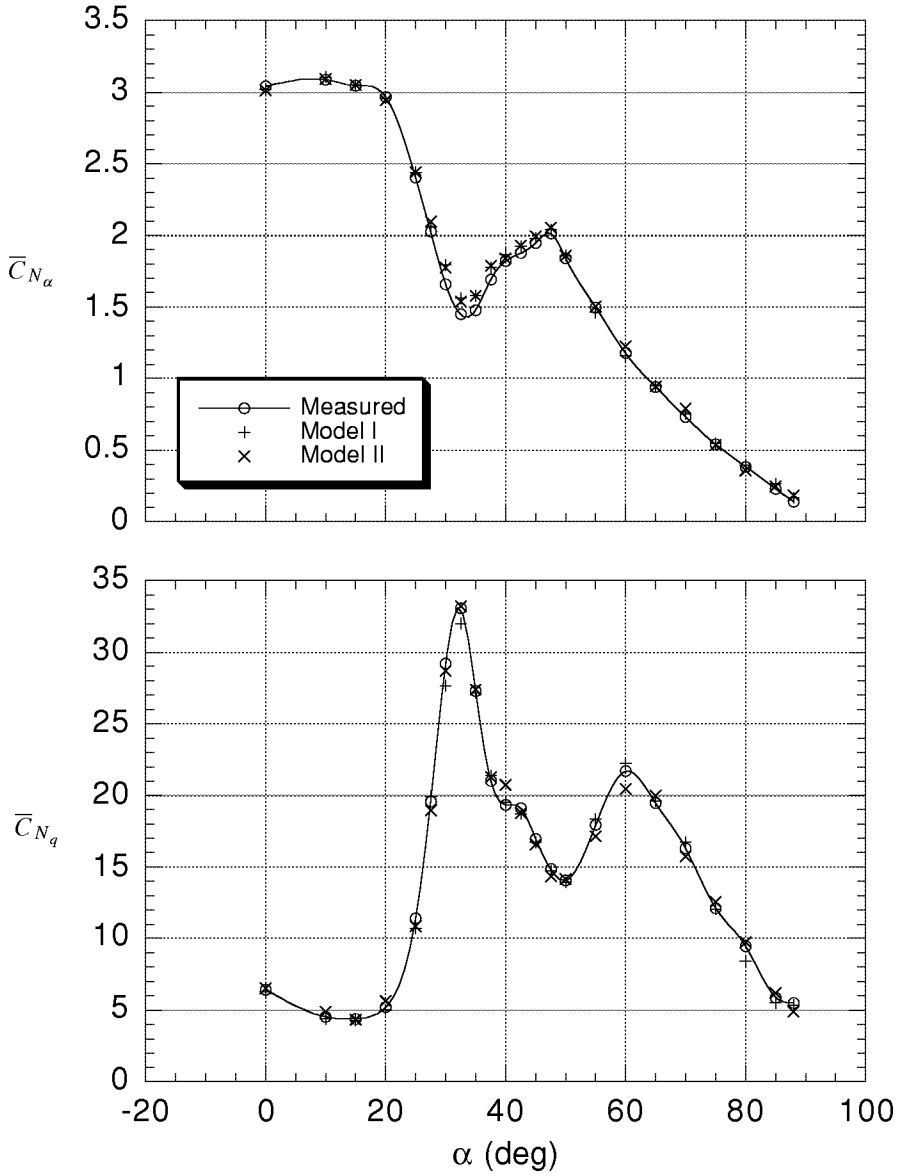

Figure 25. Measured and predicted in-phase and out-of-phase components of normal-force coefficient. Pitch oscillations, k=0.0483.

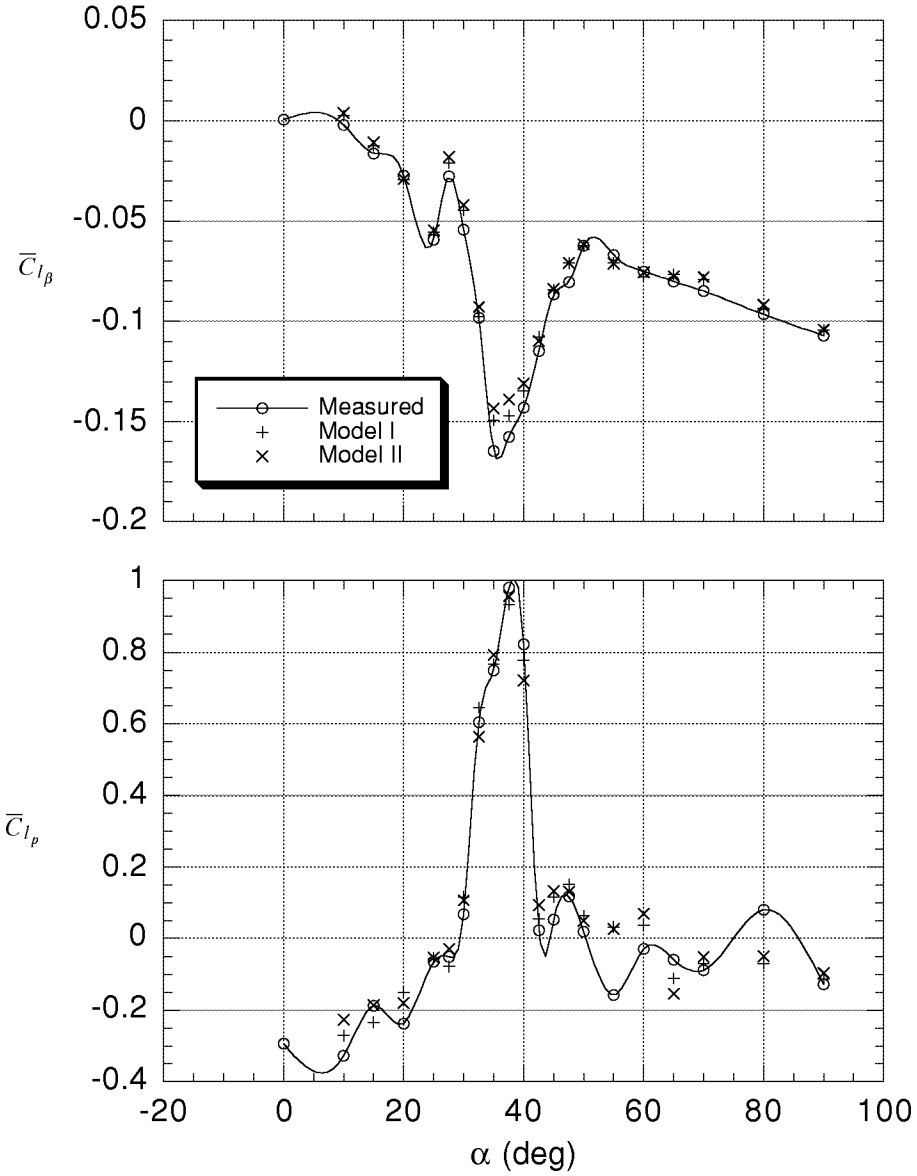

Figure 26. Measured and predicted in-phase and out-of-phase components of rolling-moment coefficient. Roll oscillations, k=0.089.

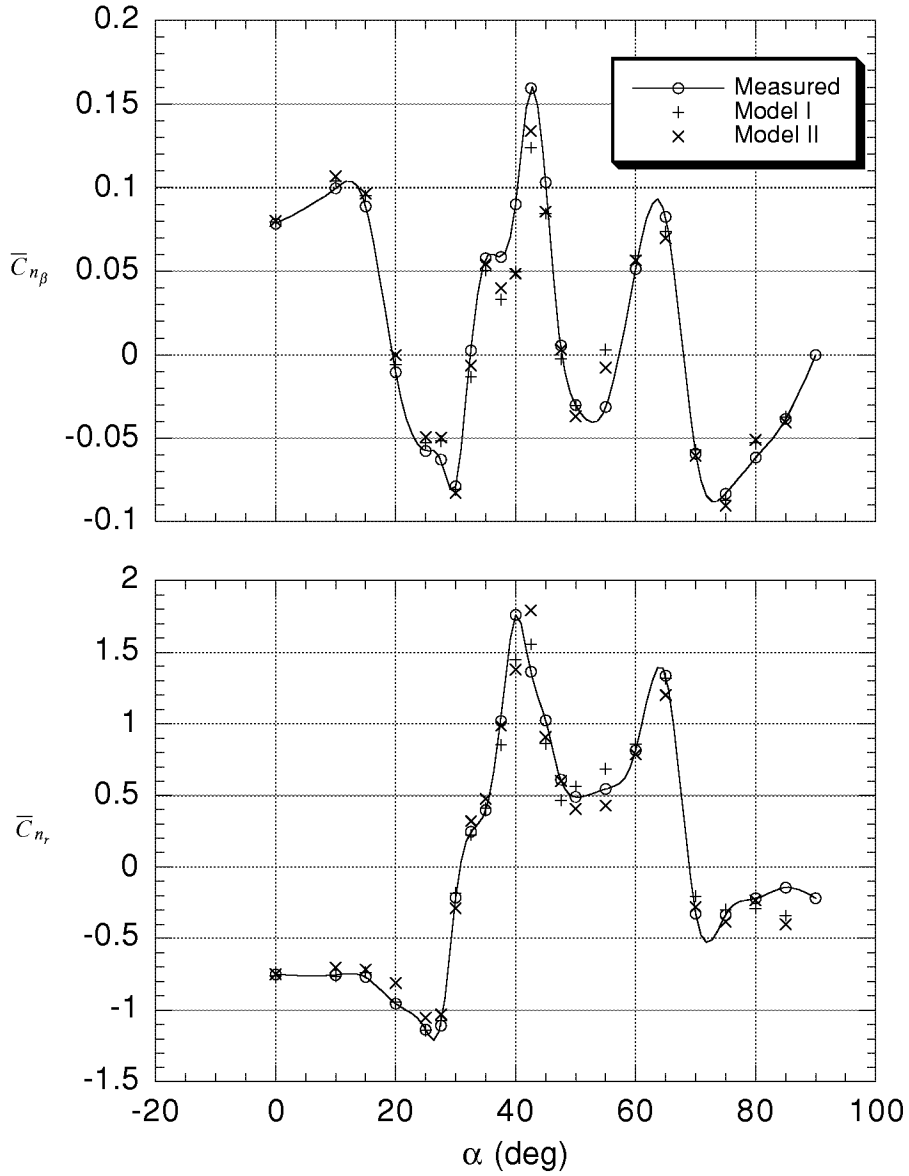

Figure 27. Measured and predicted in-phase and out-of-phase components of yawing-moment coefficient. Yaw oscillations, k=0.089.

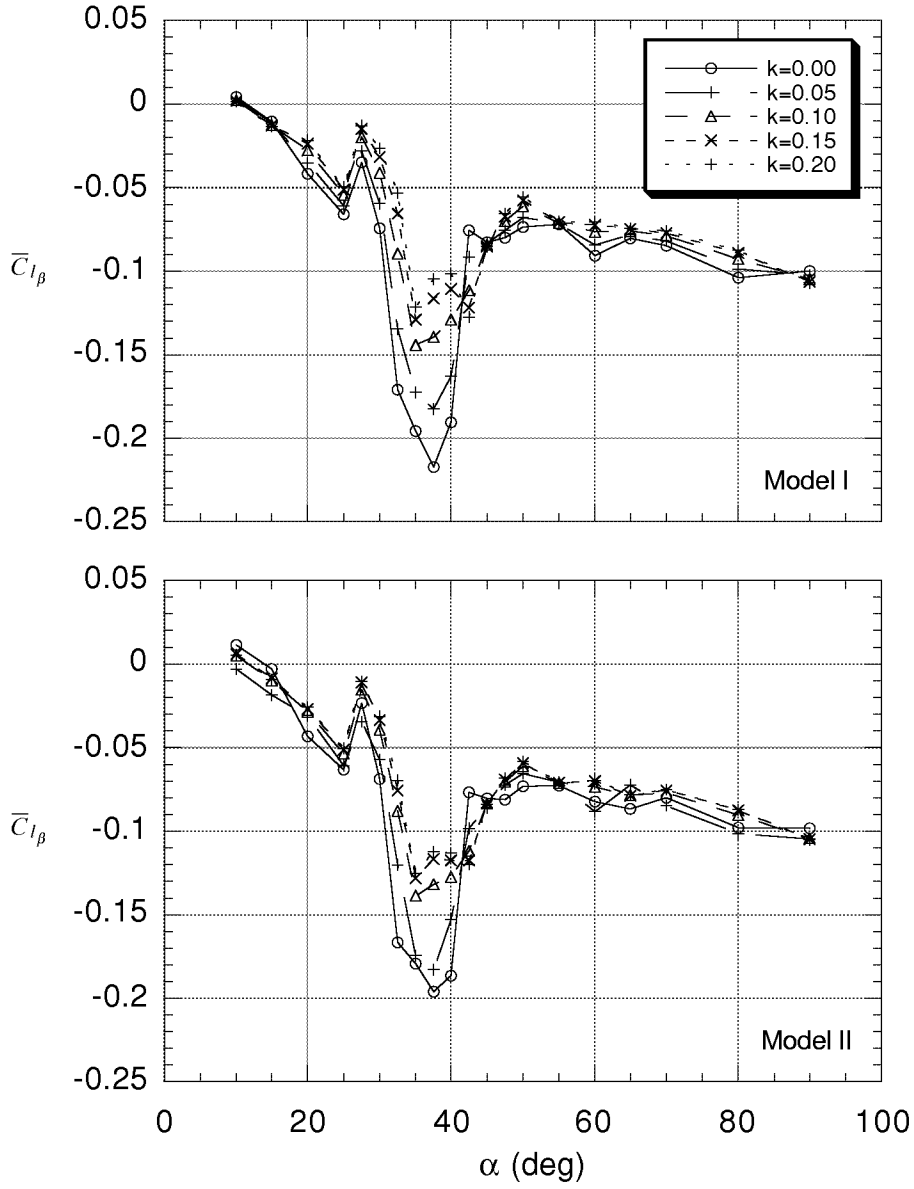

Figure 28. Predicted in-phase component of rolling-moment coefficient using roll oscillation models.

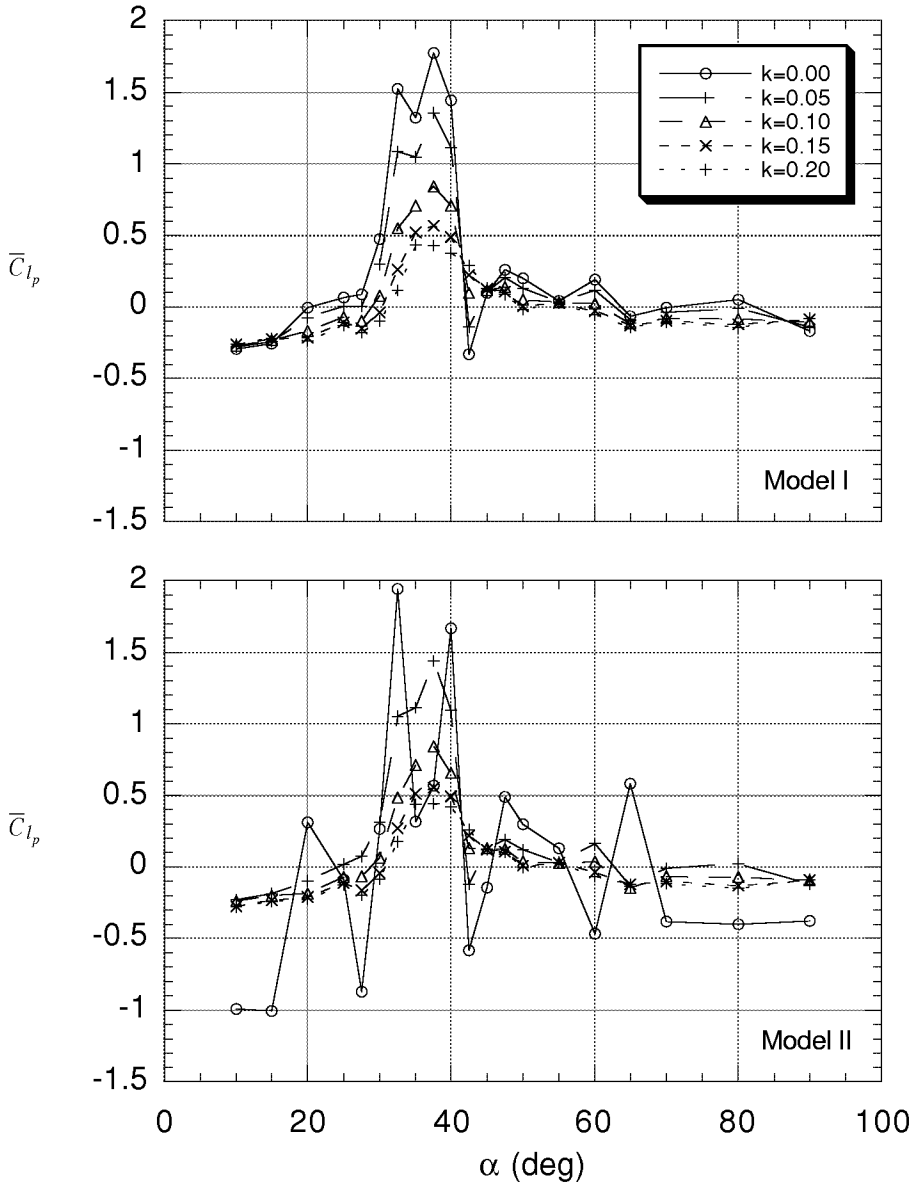

Figure 29. Predicted out-of-phase component of rolling-moment coefficient using roll oscillation models.

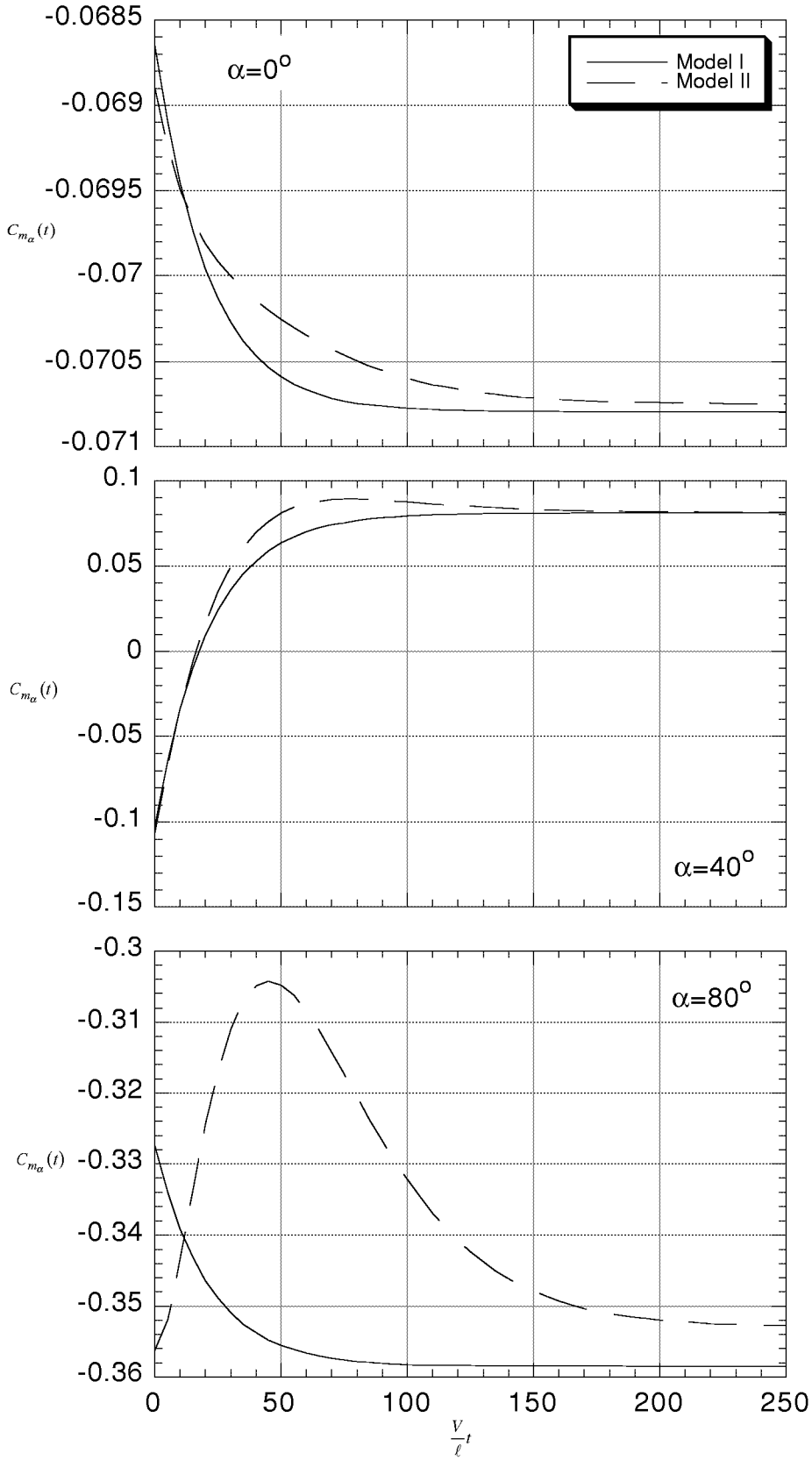

Figure 30. Comparison of indicial responses of Models I and II.

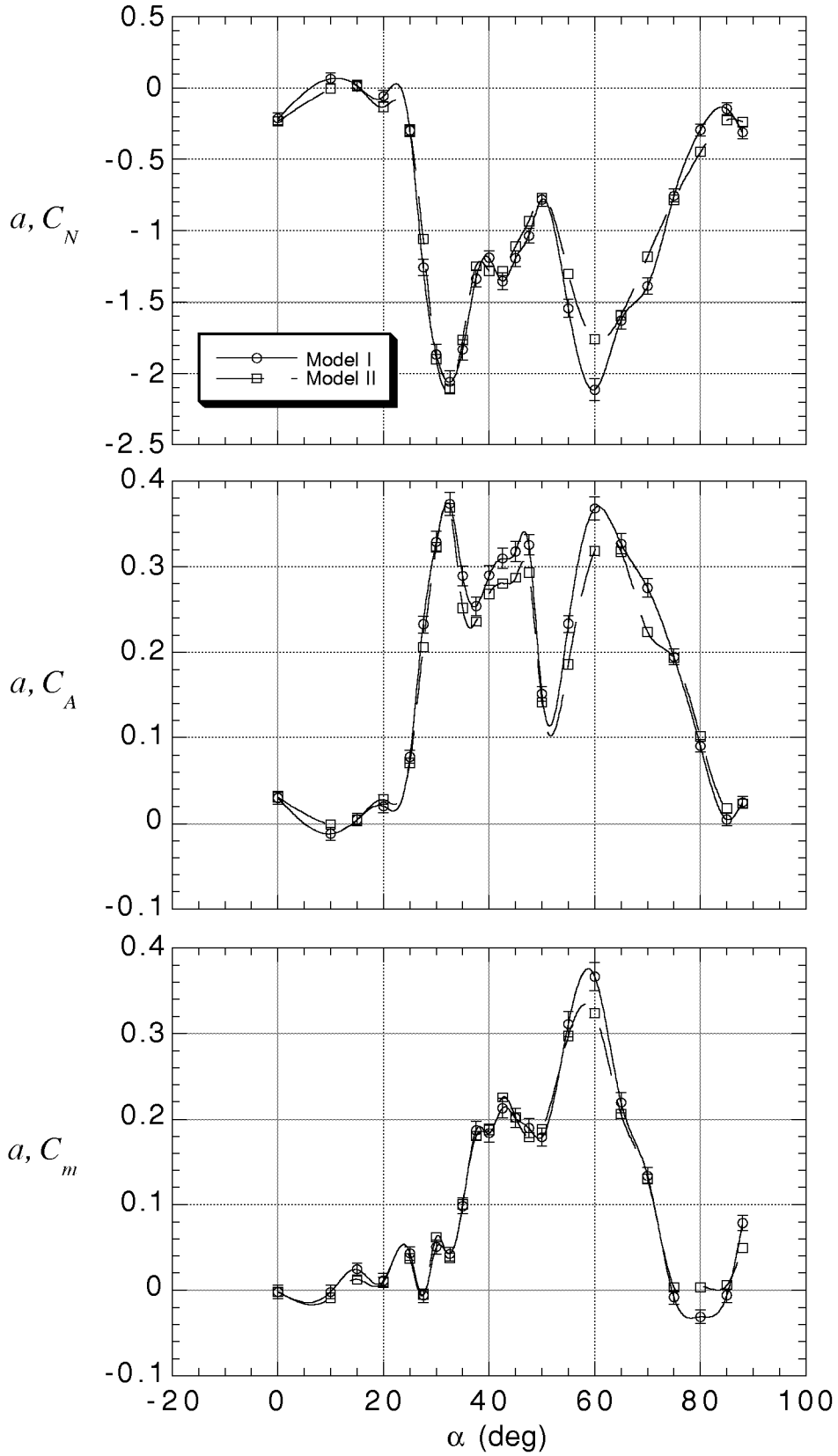

Figure 31. Comparison of estimated "a" vectors from Models I and II. Pitch oscillations.

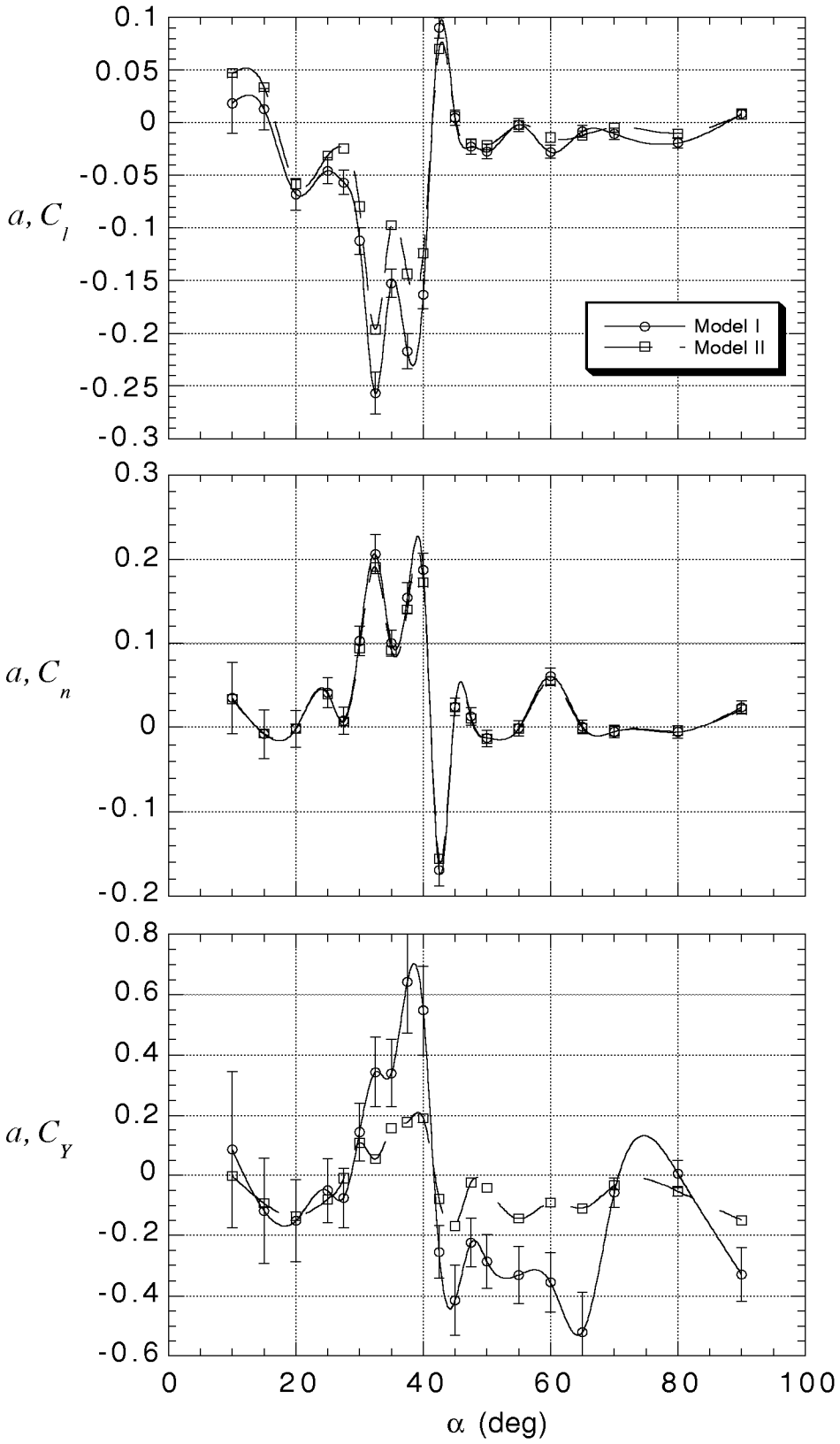

Figure 32. Comparison of estimated "a" vectors from Models I and II. Roll oscillations.

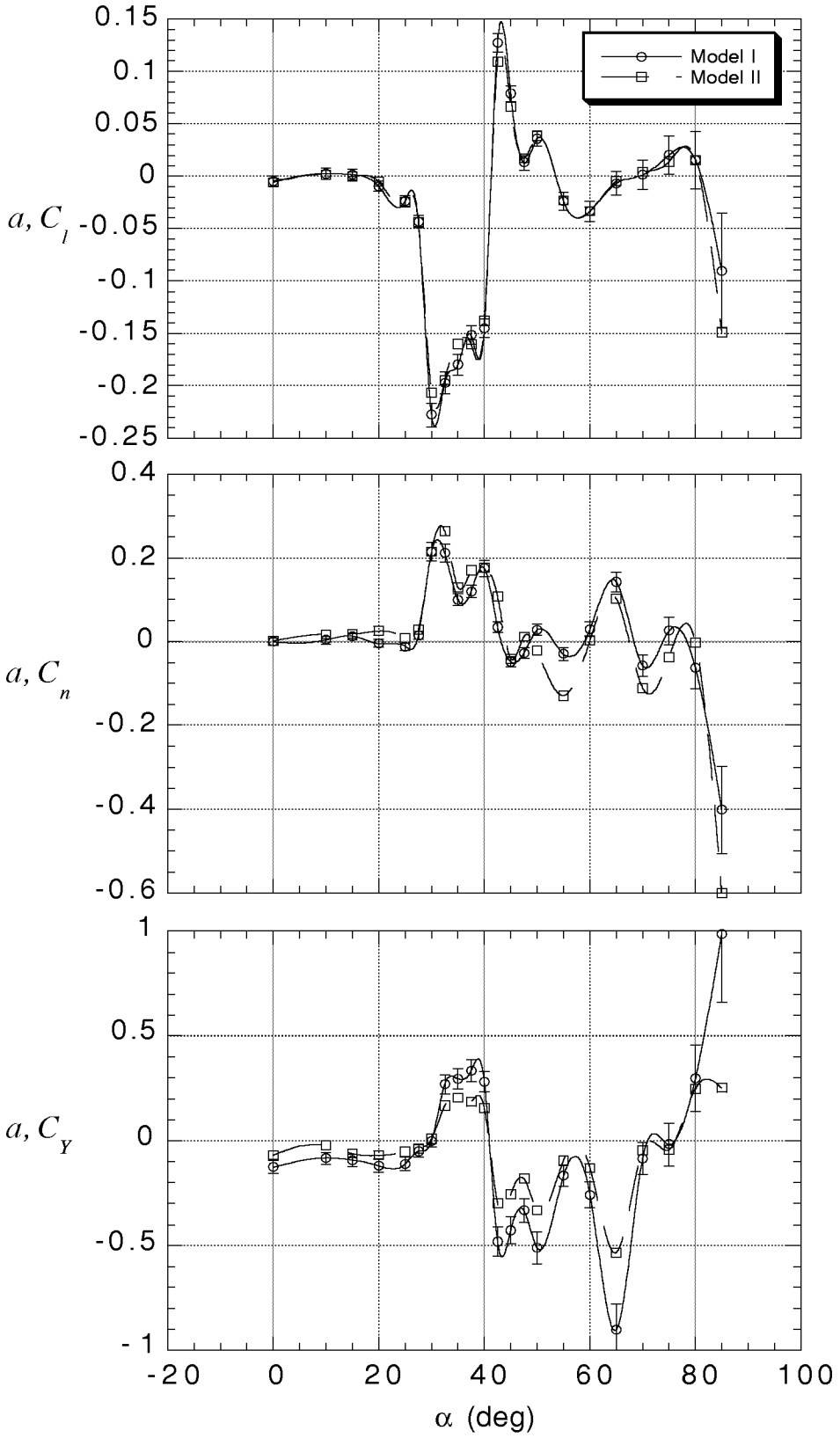

Figure 33. Comparison of estimated "a" vectors from Models I and II. Yaw oscillations.

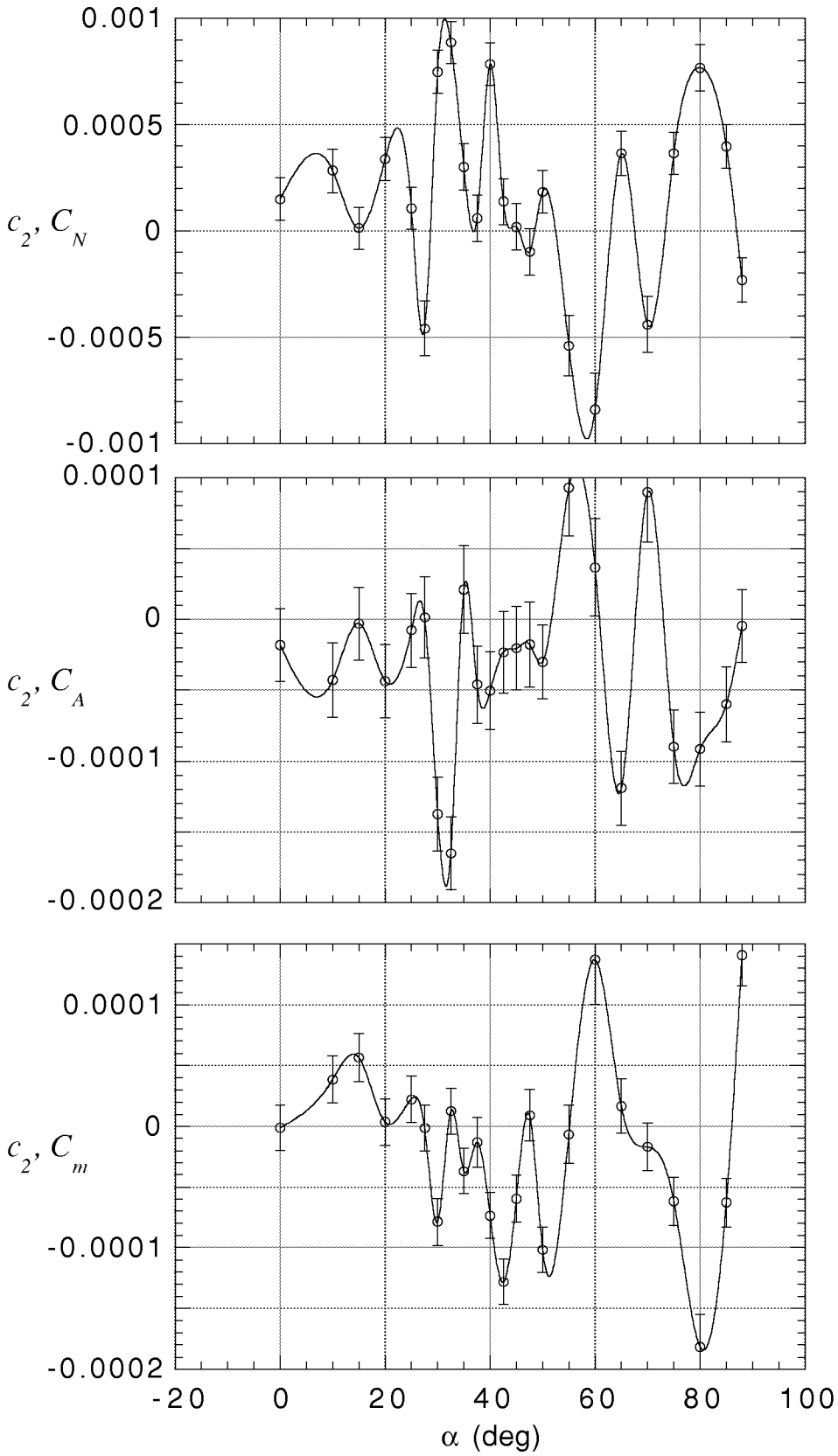

Figure 34. Estimated "c_2" vectors from Model II. Pitch oscillations.

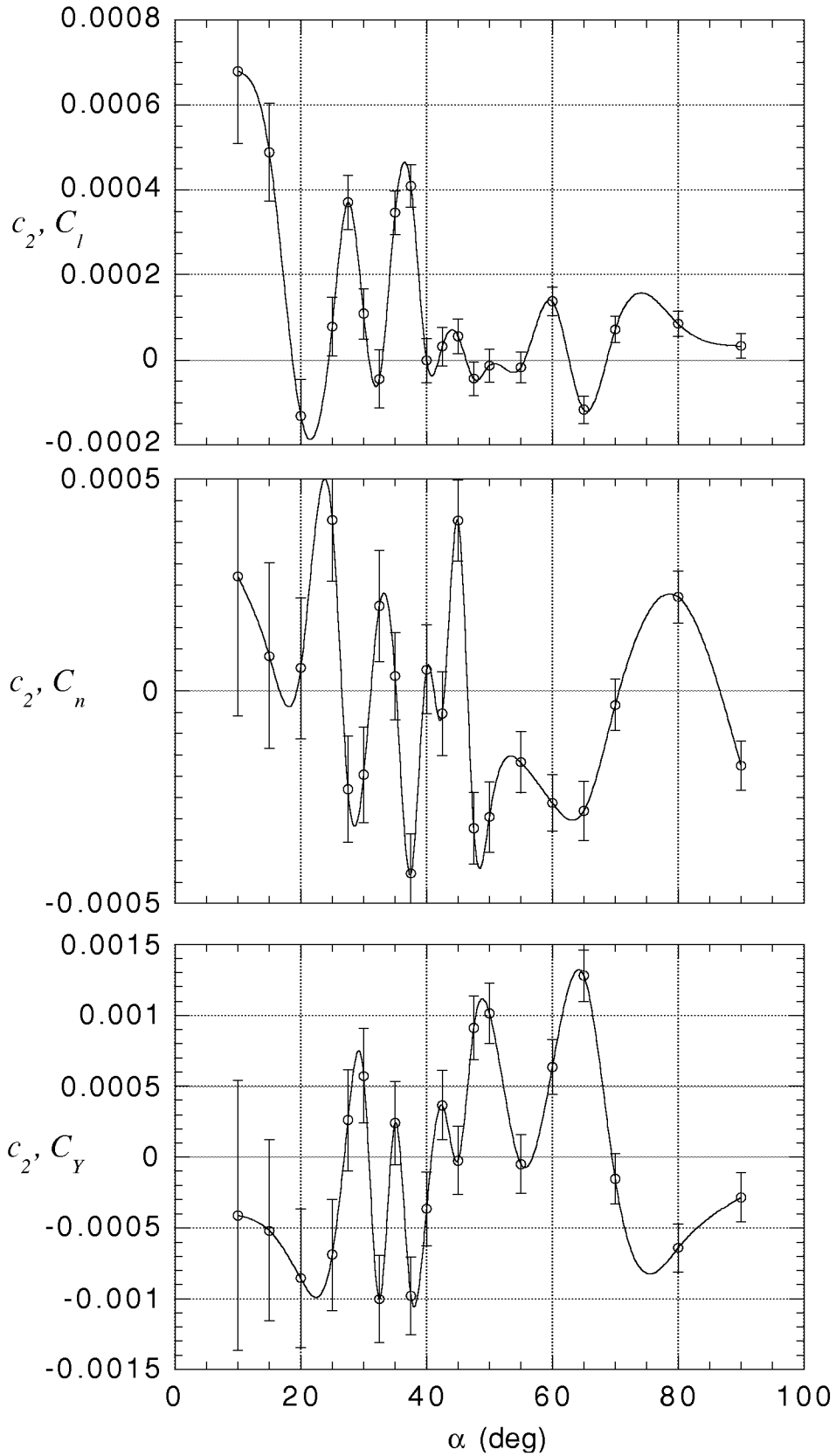

Figure 35. Estimated "c_2" vectors from Model II. Roll oscillations.

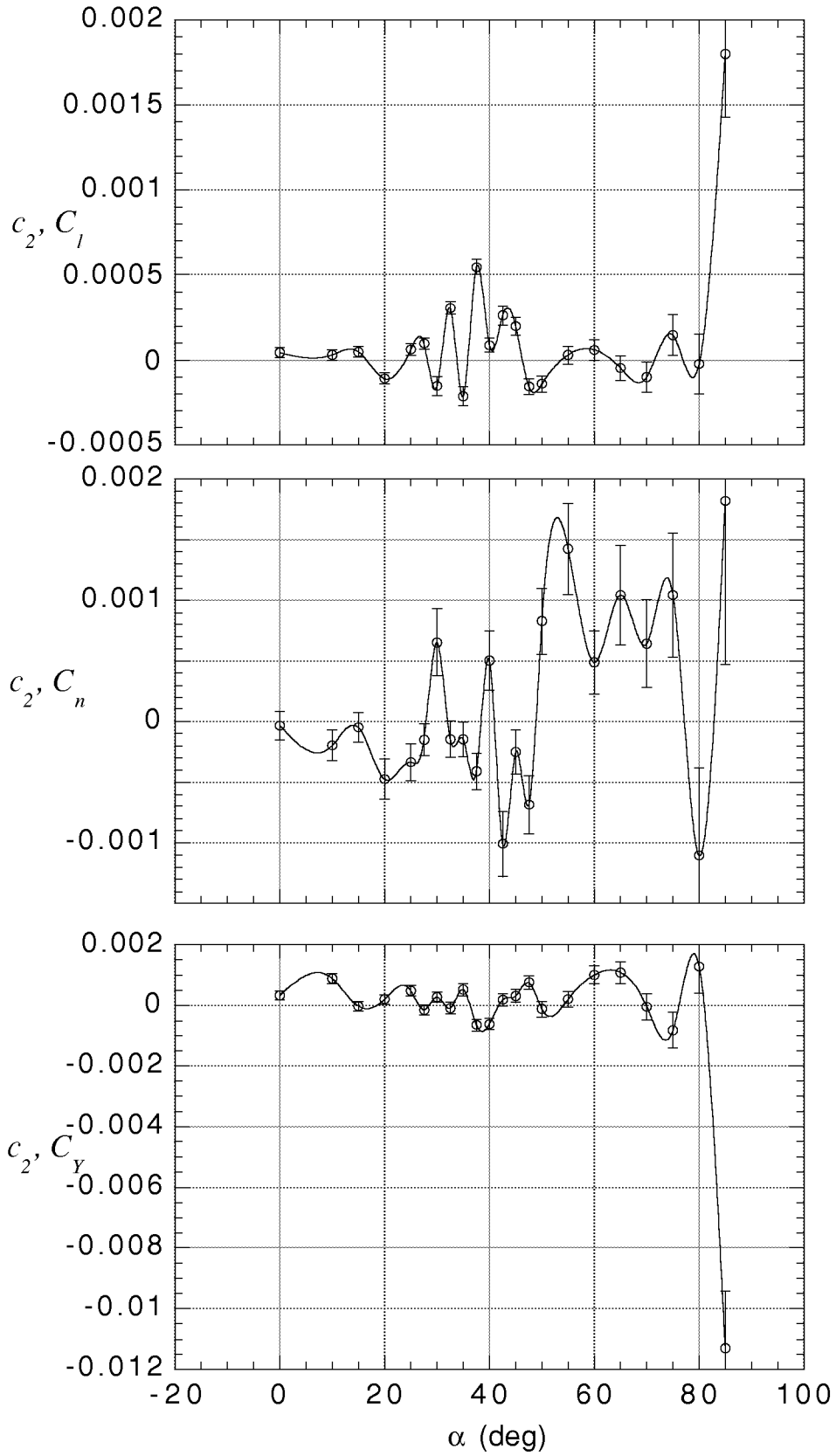

Figure 36. Estimated "c_2" vectors from Model II. Yaw oscillations.

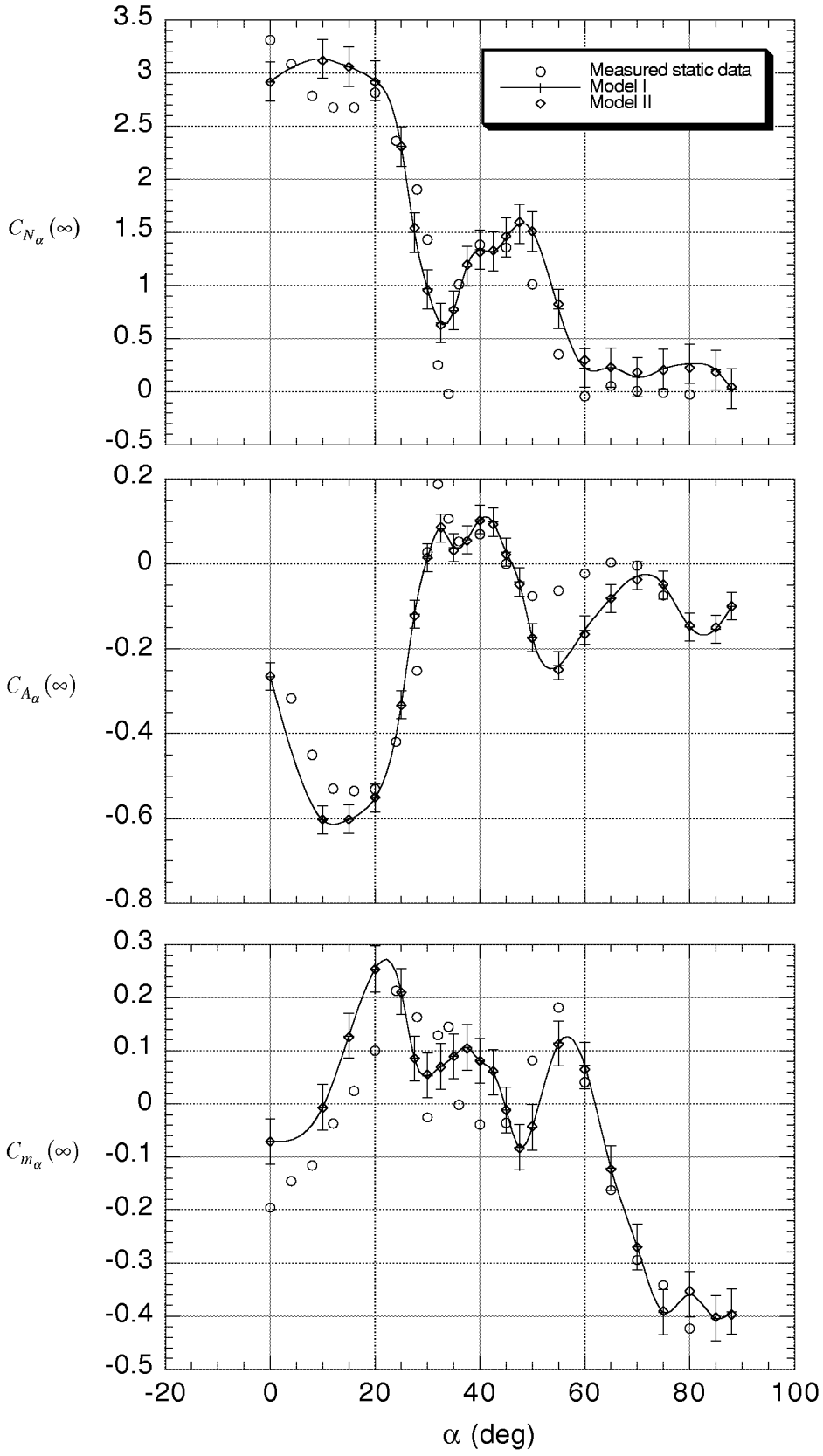

Figure 37. Comparison of longitudinal stability parameters from static data with estimates from Models I and II using pitch oscillation data.

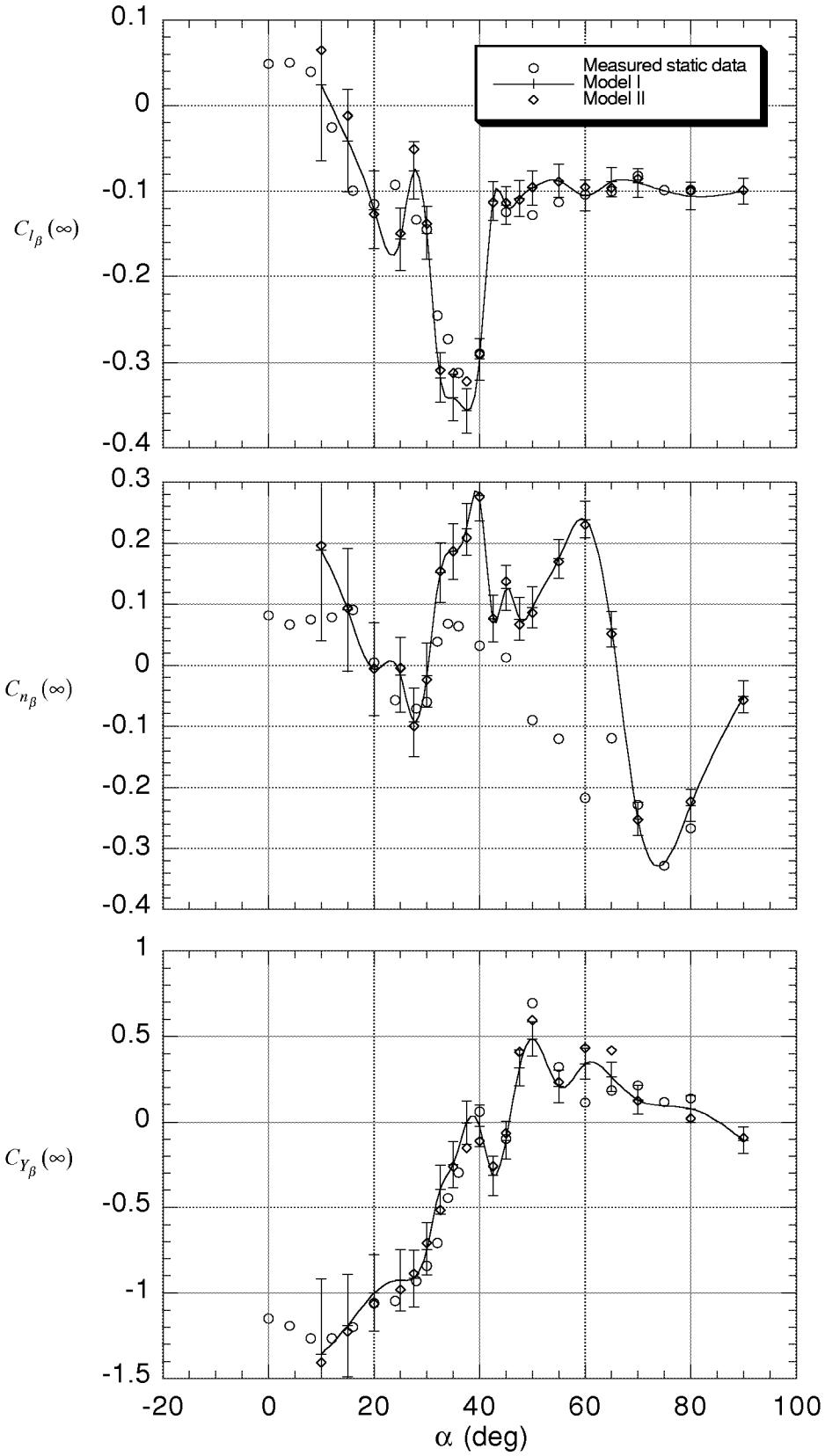

Figure 38. Comparison of lateral stability parameters from static data with estimates from Models I and II using roll oscillation data.

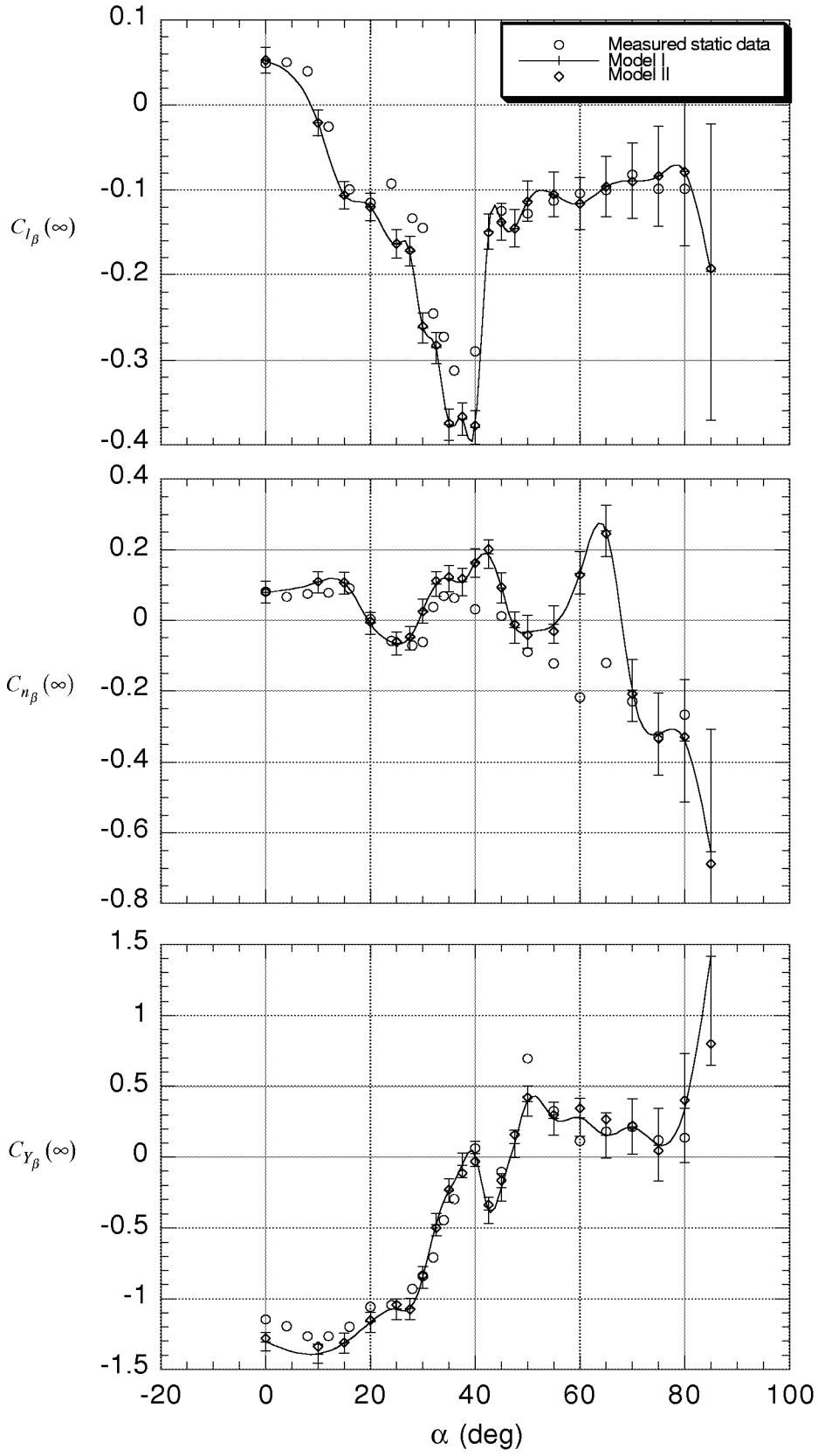

Figure 39. Comparison of lateral stability parameters from static data with estimates from Models I and II using yaw oscillation data.

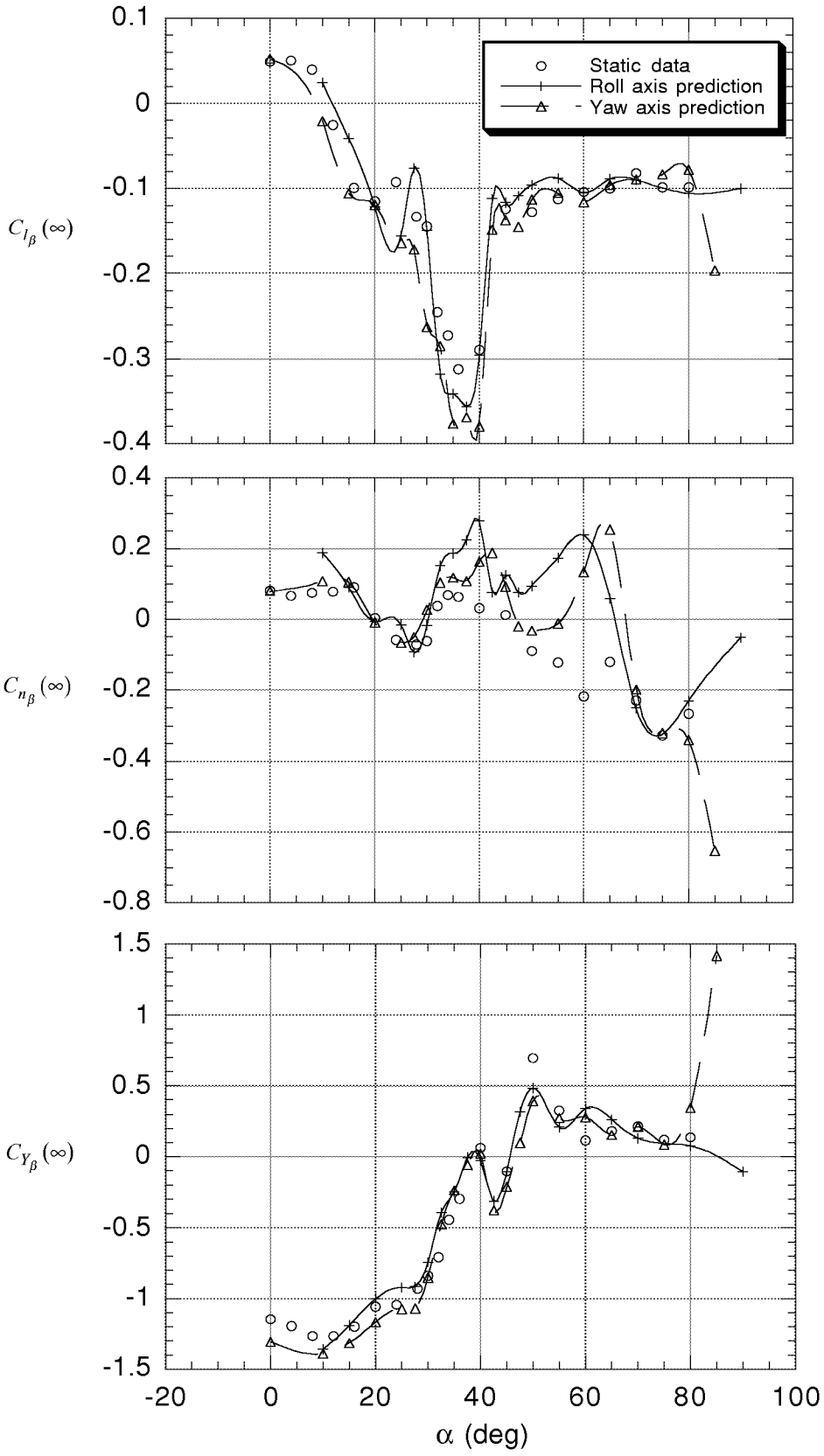

Figure 40. Comparison of lateral stability parameters estimated from roll and yaw axis oscillation data. Model I.

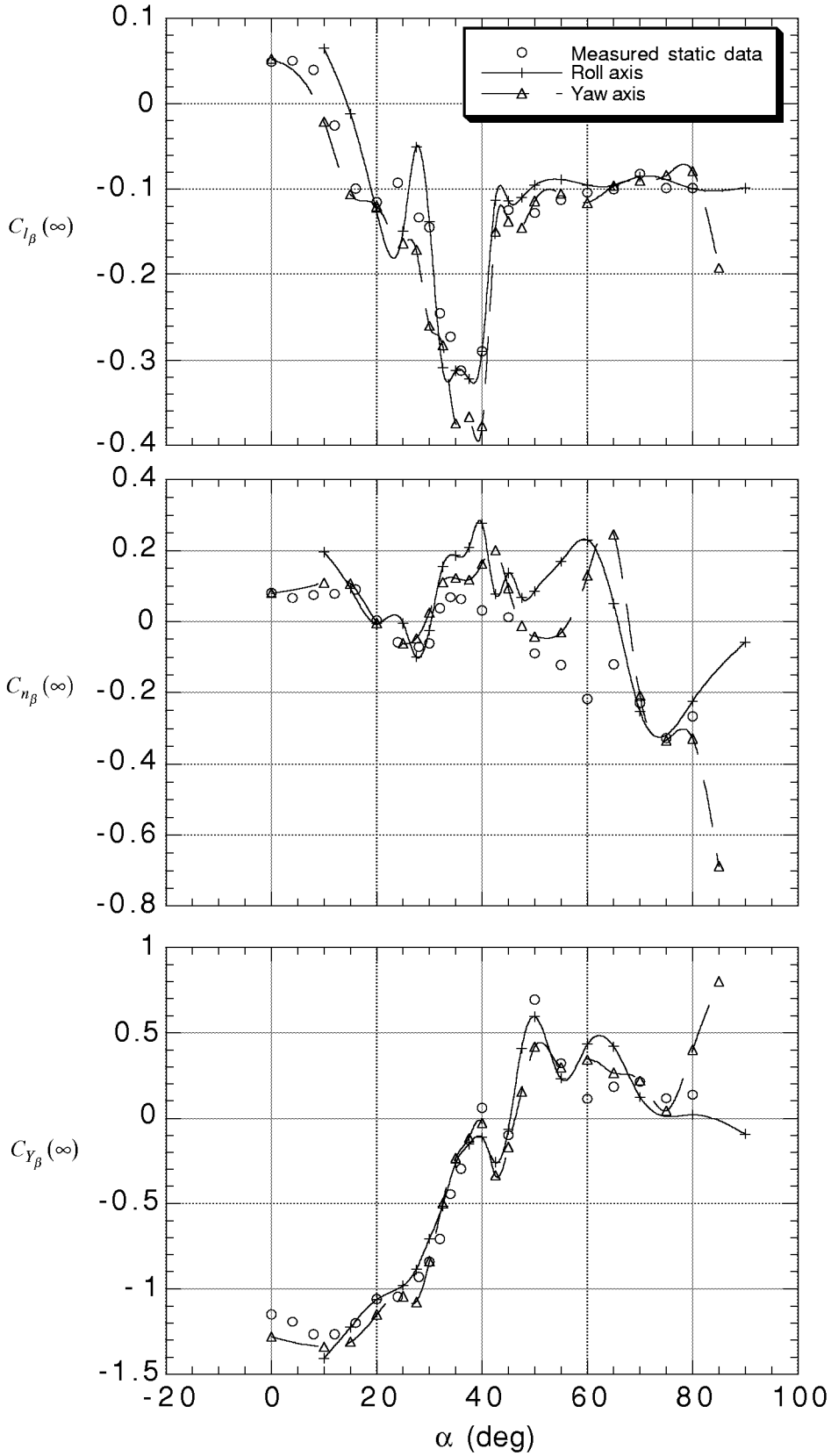

Figure 41. Comparison of lateral stability parameters estimated using roll and yaw axis oscillation data. Model II.

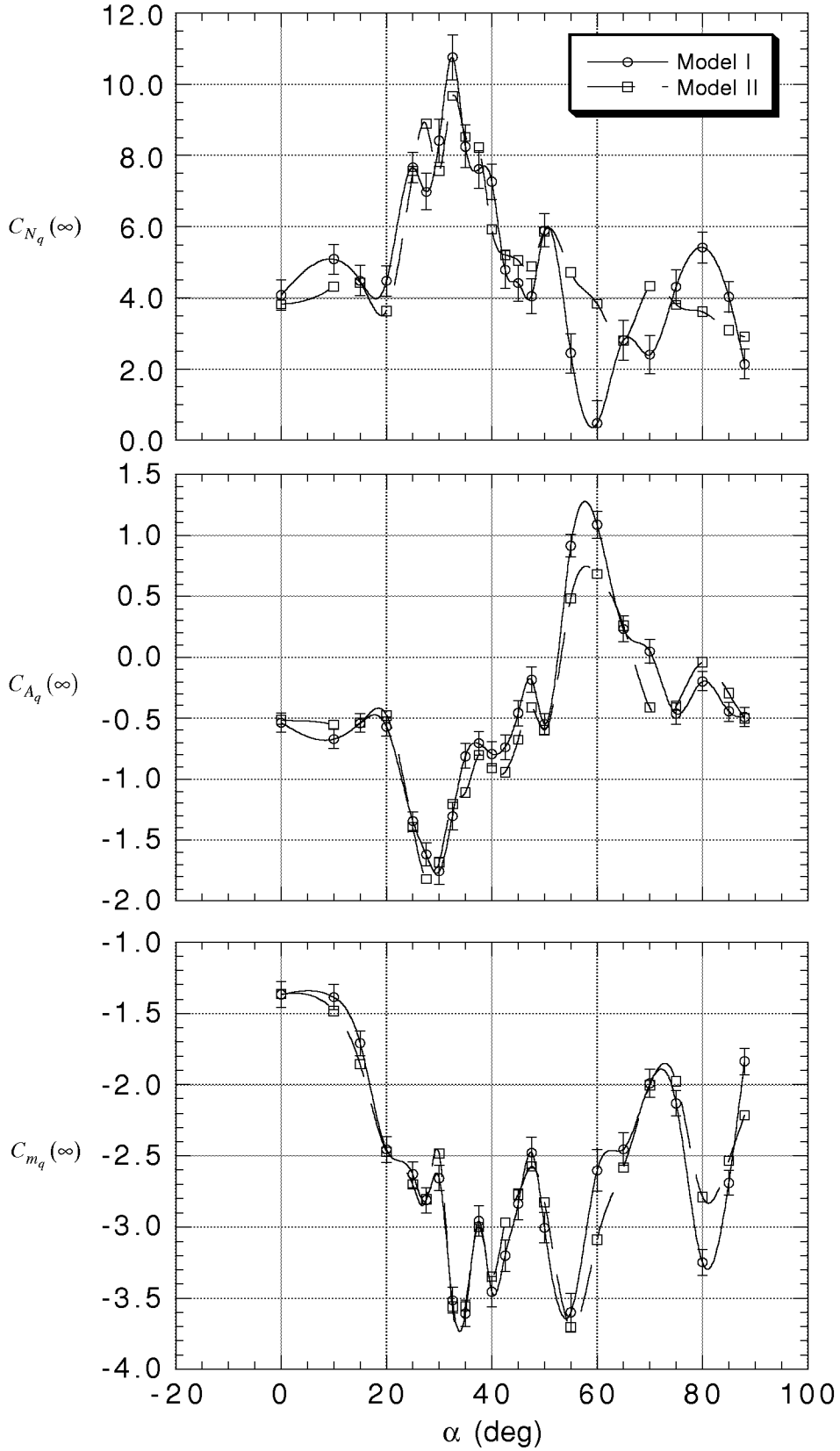

Figure 42. Estimated pitch rate stability derivatives.

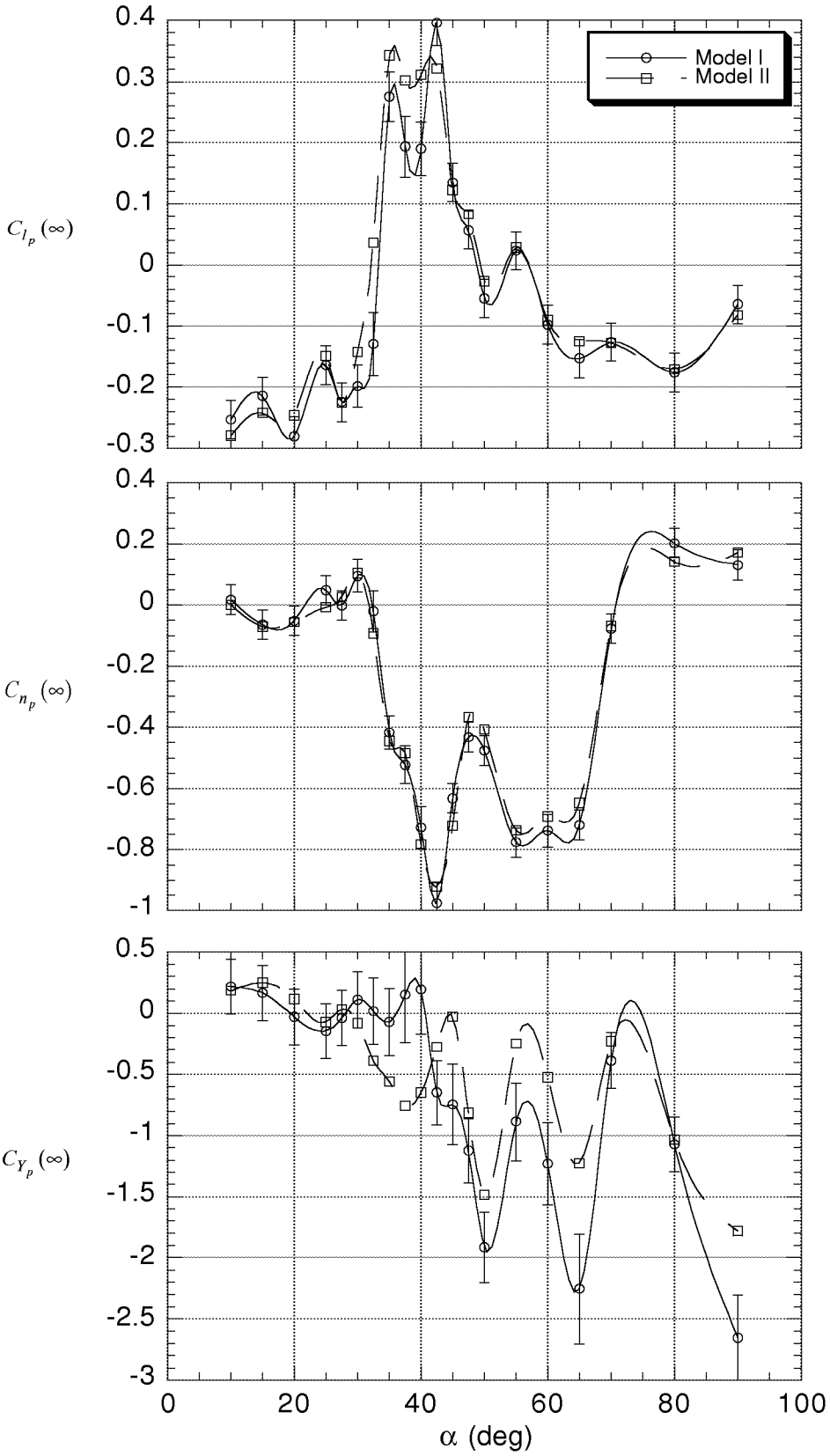

Figure 43. Estimated roll rate stability derivatives.

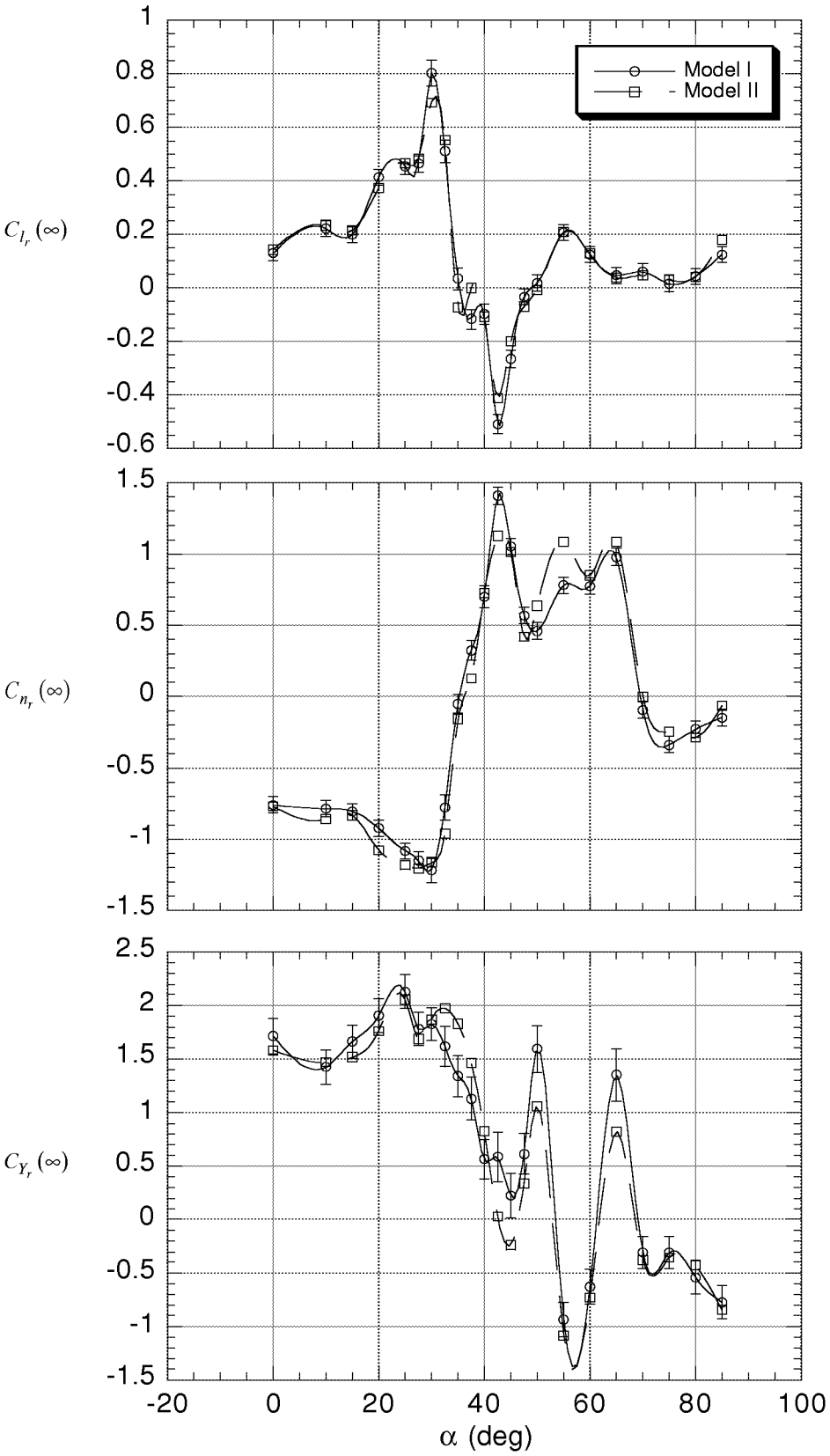

Figure 44. Estimated yaw rate stability derivatives.

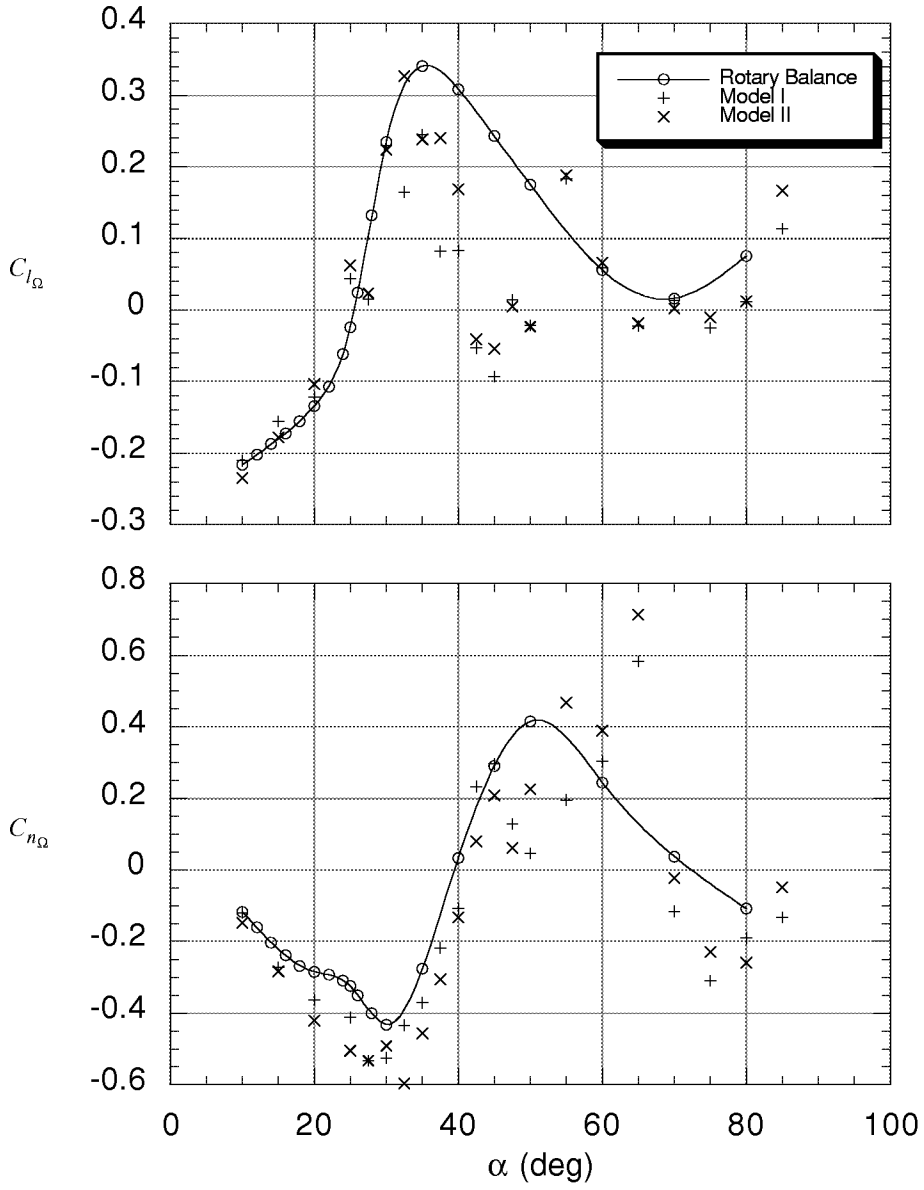

Figure 45. Comparison of rotary derivatives estimated from rotary-balance data with estimates using steady-state parameters from Models I and II.

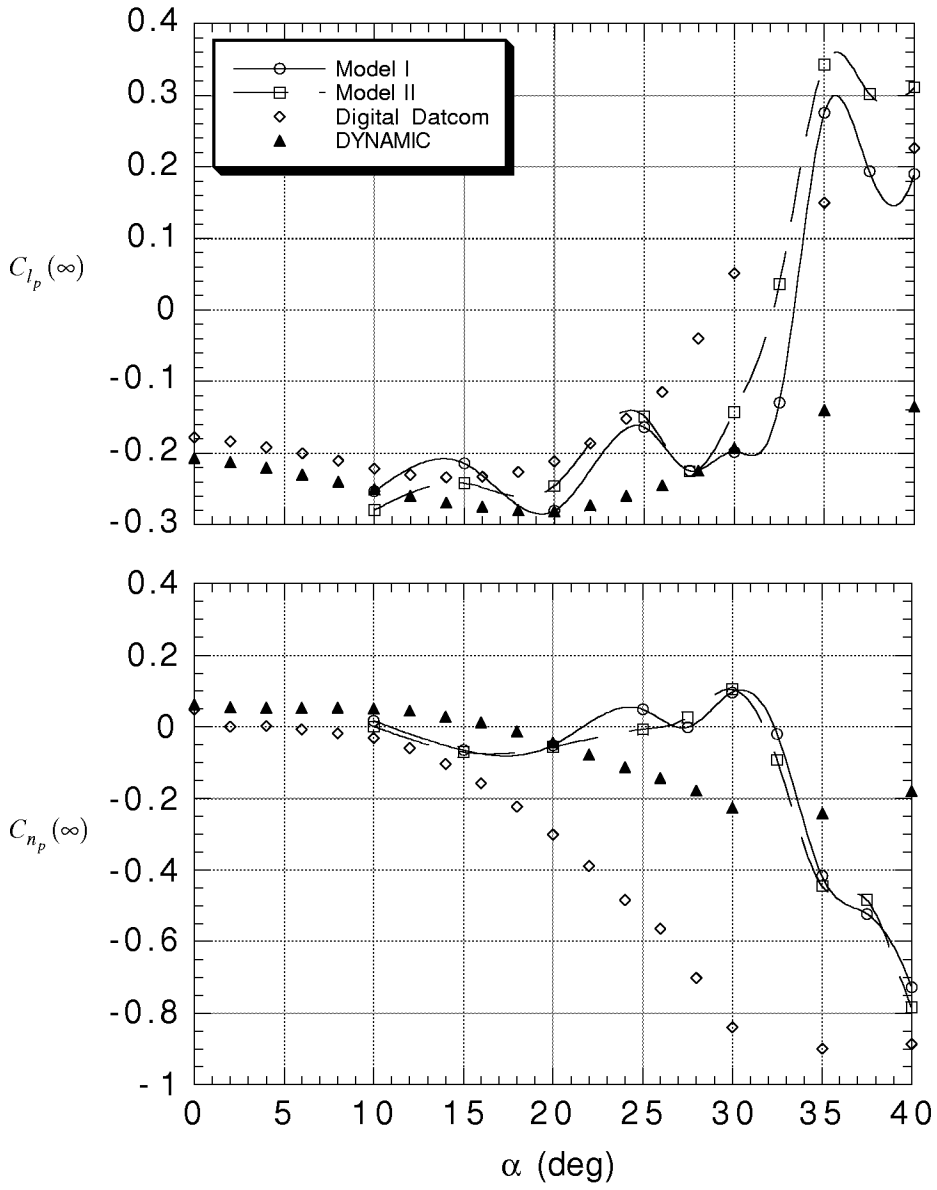

Figure 46. Comparison of estimated roll rate derivatives with theoretical predictions.

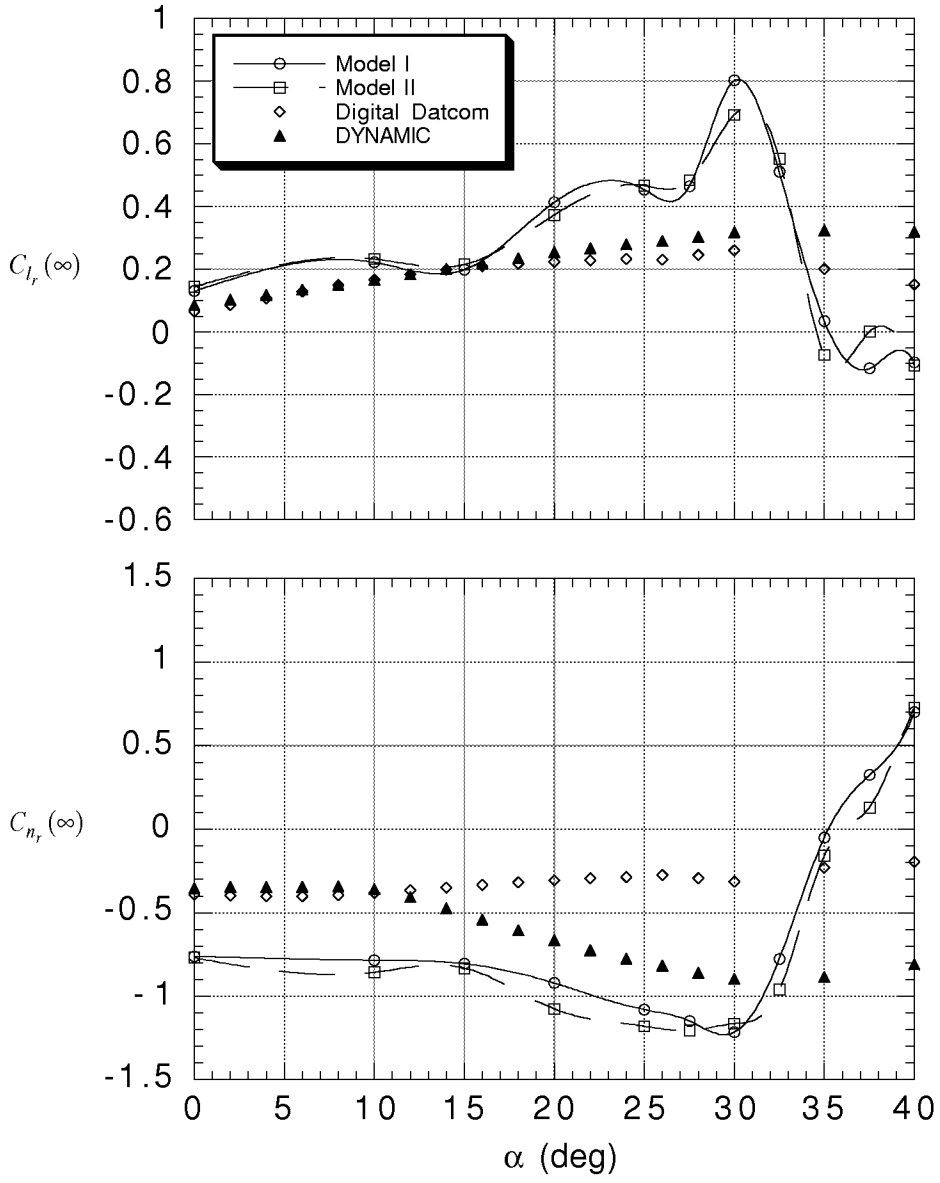

Figure 47. Comparison of estimated yaw rate derivatives with theoretical predictions.

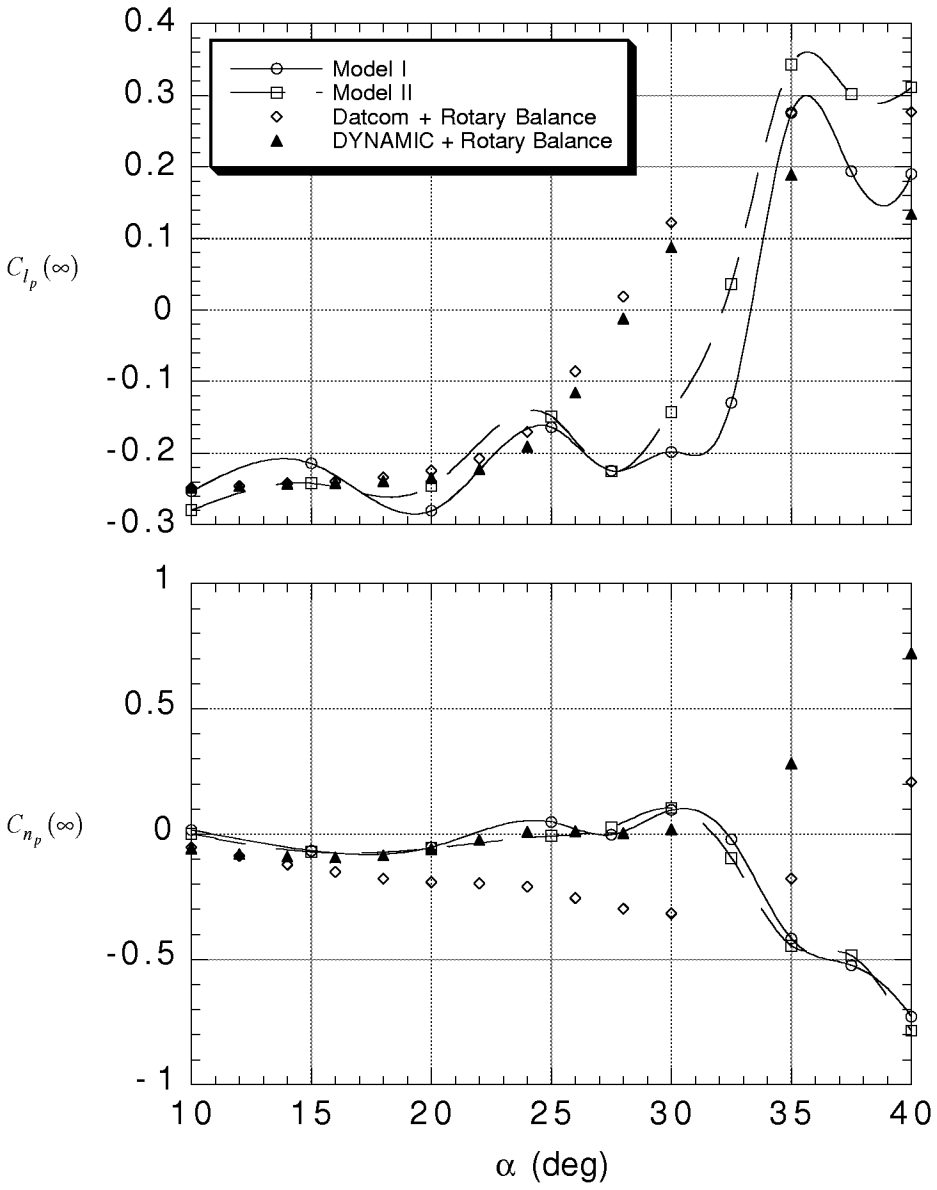

Figure 48. Comparison of estimated roll rate derivatives with combined predictions.

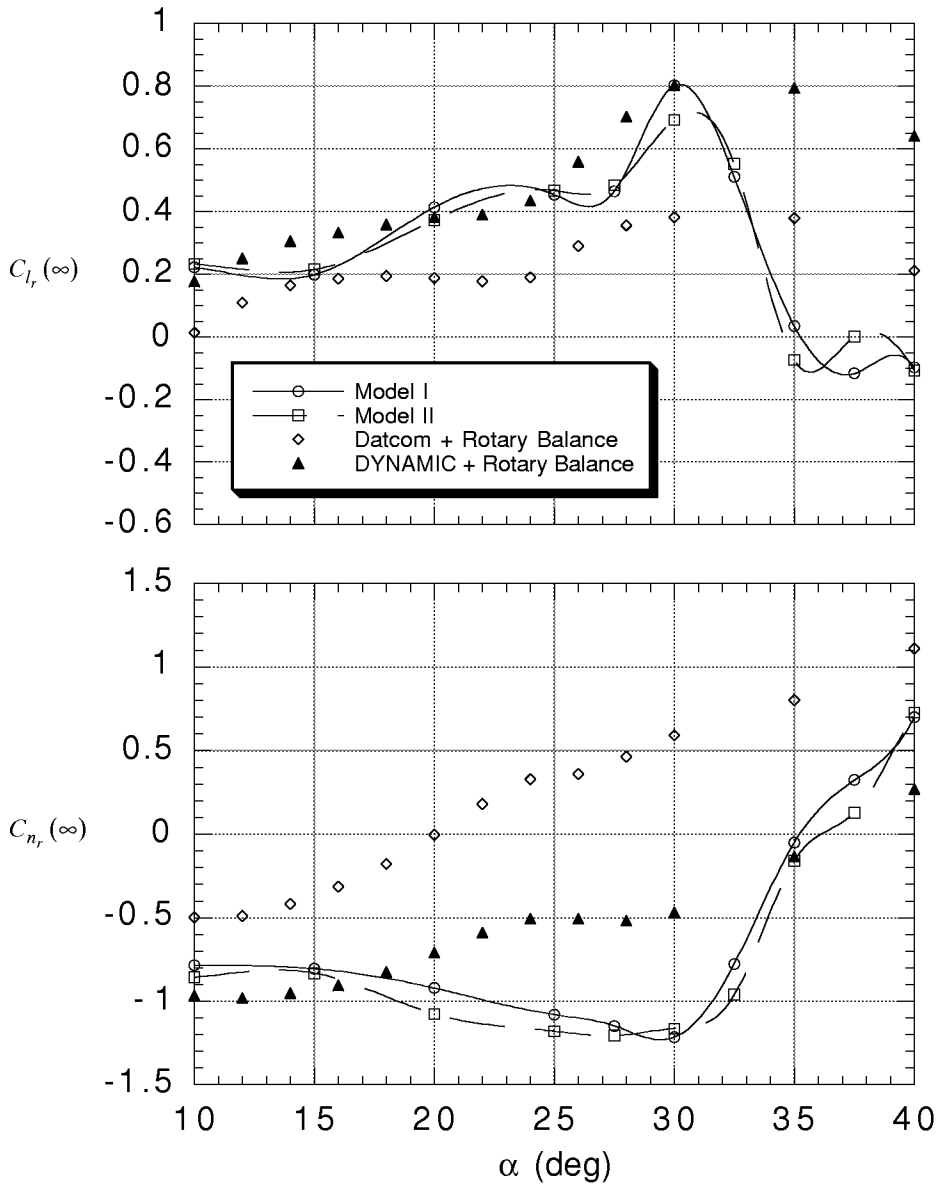

Figure 49. Comparison of estimated yaw rate derivatives with combined predictions.

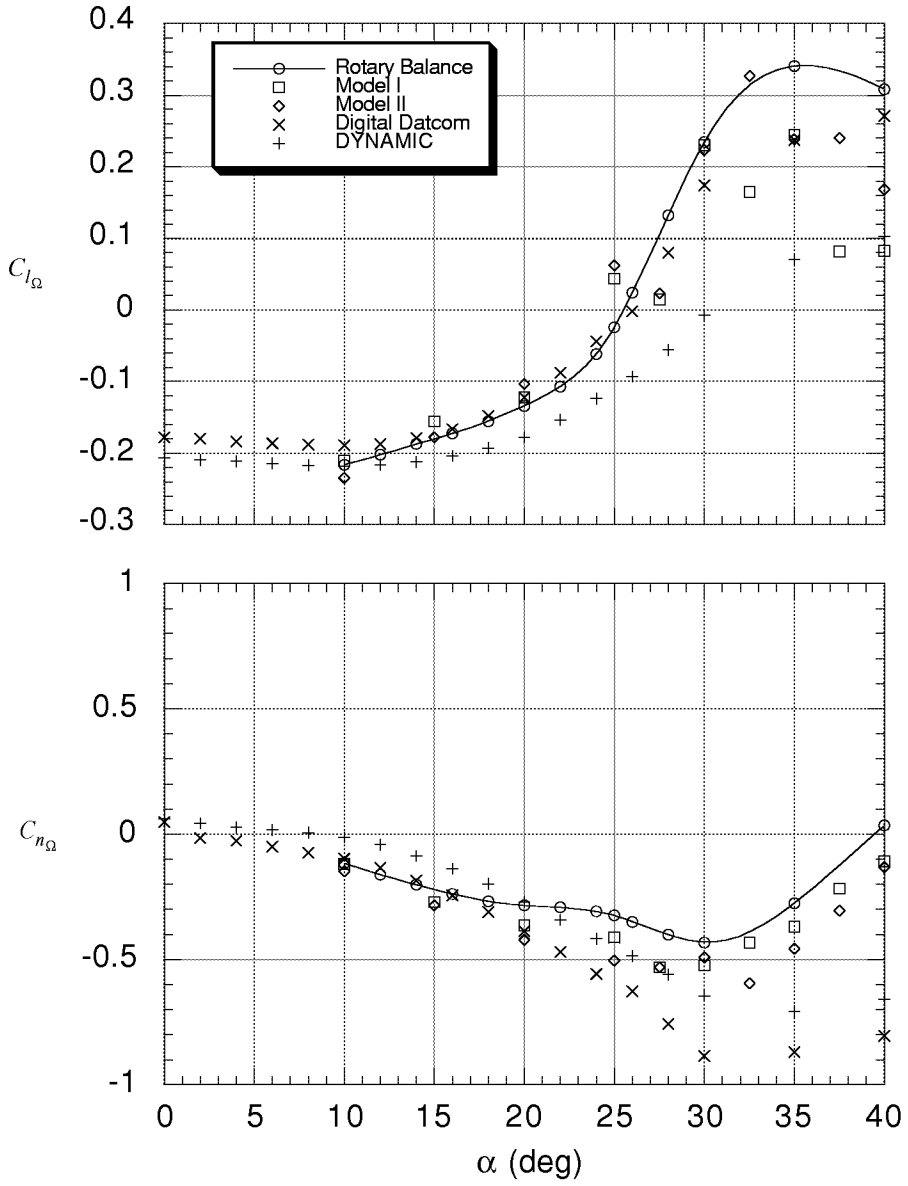

Figure 50. Comparison of estimated rotary derivatives with theoretical predictions.

REPORT DOCUMENTATION PAGE

Form Approved
OMB No. 07704-0188

1. AGENCY USE ONLY *(Leave blank)*	2. REPORT DATE	3. REPORT TYPE AND DATES COVERED
	February 1999	Contractor Report

4. TITLE AND SUBTITLE
Analysis of Wind Tunnel Oscillatory Data of the X-31A Aircraft

5. FUNDING NUMBERS
WU 522-25-21-07

NCC1-24

6. AUTHOR(S)
Mark S. Smith

7. PERFORMING ORGANIZATION NAME(S) AND ADDRESS(ES)
The George Washington University
Joint Institute for Advancement of Flight Sciences
Langley Research Center
Hampton, VA 23681

8. PERFORMING ORGANIZATION REPORT NUMBER

9. SPONSORING/MONITORING AGENCY NAME(S) AND ADDRESS(ES)
National Aeronautics and Space Administration
Langley Research Center
Hampton, VA 23681-2199

10. SPONSORING/MONITORING AGENCY REPORT NUMBER
NASA/CR-1999-208725

11. SUPPLEMENTARY NOTES
Langley Technical Monitor: Mark A. Croom

12a. DISTRIBUTION/AVAILABILITY STATEMENT
Unclassified–Unlimited
Subject Category 08 Distribution: Standard
Availability: NASA CASI (301) 621-0390

12b. DISTRIBUTION CODE

13. ABSTRACT ***(Maximum 200 words)***

Wind tunnel oscillatory tests in pitch, roll, and yaw were performed on a 19%-scale model of the X-31A aircraft. These tests were used to study the aerodynamic characteristics of the X-31A in response to harmonic oscillations at six frequencies. In-phase and out-of-phase components of the aerodynamic coefficients were obtained over a range of angles of attack from 0° to 90°. To account for the effect of frequency on the data, mathematical models with unsteady terms were formulated by use of two different indicial functions. Data from a reduced set of frequencies were used to estimate model parameters, including steady-state static and dynamic stability derivatives. Both models showed good prediction capability and the ability to accurately fit the measured data. Estimated static stability derivatives compared well with those obtained from static wind tunnel tests. The roll and yaw rate derivative estimates were compared with rotary-balanced wind tunnel data and theoretical predictions. The estimates and theoretical predictions were in agreement at small angles of attack. The rotary-balance data showed, in general, acceptable agreement with the steady-state derivative estimates.

14. SUBJECT TERMS	15. NUMBER OF PAGES
Wind Tunnel Testing; Static and Oscillatory data, Unsteady Aerodynamics; Indicial Functions	126
	16. PRICE CODE: A07

17. SECURITY CLASSIFICATION OF REPORT	18. SECURITY CLASSIFICATION OF THIS PAGE	19. SECURITY CLASSIFICATION OF ABSTRACT	20. LIMITATION OF ABSTRACT
Unclassified	Unclassified	Unclassified	UL